BILINGUAL PUBLISHING CO.
Pioneer of Global Academics Since 1984

Journal of Geological Research

Volume 3 · Issue 3 · July 2021 ISSN 2630-4961(Online)

BILINGUAL PUBLISHING CO.
Pioneer of Global Academics Since 1984

Editor-in-Chief

Editorial Board Members

Volume 3 Issue 3 • July 2021 • ISSN 2630-4961 (Online)

Journal of Geological Research

BILINGUAL PUBLISHING CO.
Pioneer of Global Academics Since 1984

BILINGUAL PUBLISHING CO.
Pioneer of Global Academics Since 1984

Volume 3 | Issue 3 | July 2021 | Page1-51
Journal of Geological Research

Contents

Editorial

1 **Climate Change and Natural Disasters: Are they linked?**
Ramesh Man Tuladhar

Articles

3 **The Horizontal Loop Electromagnetic (HLEM) Response of Ifewara Transcurrent Fault, Southwestern Nigeria: A Computational Results**
A.A. Adepelumi O.B. Olayiwola D.E. Falebita O.Afolabi B.O Soyinka J. Obokoh

14 **Integrated Geophysical and Hydrogeochemical Characterization and Assessment of Groundwater Studies in Adum West Area of Benue State, Nigeria**
Moses Oghenenyoreme Eyankware Christopher Ogwah Umayah Otitie Star

28 **Geochemistry of Volcanic Rocks of Beka, North East of Ngaoundéré (Adamawa Plateau, Cameroon): Petrogenesis and Geodynamic Context**
Pauline Wokwenmendam Nguet Benjamin Ntieche Joseph Legrand Tchop Bouba Christian Mana Eddy Ferdinand Mbossi

44 **Structural Exploration of Aeromagnetic Data over Part of Gwagwalada, Abuja for Potential Mineral Targets Using Derivatives Filters**
Priscillia Egbelehulu Abu Mallam Abel U. Osagie Adewumi taiwo

BILINGUAL PUBLISHING CO.
Pioneer of Global Academics Since 1984

Journal of Geological Research
http://ojs.bilpublishing.com/index.php/jgr-a

EDITORIAL

Climate Change and Natural Disasters: Are they linked?

Ramesh Man Tuladhar*

Disaster Preparedness Network, Nepal

ARTICLE INFO

Article history
Received: 17 August 2021
Accepted: 19 August 2021
Published Online: 23 August 2021

Geology, the science of earth – rocks, minerals, soils, and water within atmosphere and lithosphere encompasses a number of geological phenomena evolved over the geological time. Key components include sedimentation, stratification, volcanism, magmatism, metamorphism, weathering and erosion when reinforced by tectonic deformation episodes results in natural disasters such as earthquakes and tsunami among others. Subsequently when these geological processes get exposed to extreme climate, natural disasters such as landslide and flood or wildfire are inevitable. In recent years, frequency as well as intensity of such disaster events is increasing across the globe notably with the onset of global climate change having severe socioeconomic impacts particularly in the underdeveloped and/or developing countries. Realizing these facts, the *Journal of Geological Research* (JGR-A) is being continued by placing towards supporting the research community at the heart of everything we do, we strive for a future where researchers are motivated to work together, empowered with the tools and services they need to do so, and freed from any barriers that stand in their way. We aim to maximize the impact of scientific research through openness and global collaboration as we truly believe that science works best when research is open. In line with this strategic policy guideline, JGR-A calls to all contributors for a more innovative geological research in the backdrop of recent global climate change scenario triggering severe natural disasters across the globe.

This Vol 3 Issue 3 focuses on to publish three papers from Nigeria within underdeveloped African continent. It includes: a) innovative research towards developing a computer program to calculate the horizon loop electromagnetic (HLEM) method responses for optimal conductor model with known values of coil separations (L), depth of burial (z) and angle of dip of the target for different geological scenarios in the Ilesha area of Osun State in the southwestern part of Nigeria. This will contribute to enhance further computer program in delineating the geometry and position of the causative body precisely [1]; b) detailed study on mineralogy and petro-genesis of Beka basaltic lava situated in the Adamaoua Plateau of Cameroon in central Africa for the first time. This contributes to understand the mineral assemblage, geochemistry and geodynamics of central Africa leading towards discovery of new mineral prospects in future [2]; c) evaluate the quality of aquifer located at Adum West Area of Benue State, Nigeria. Important information emerged from this paper is extremely useful for the local community people. They

**Corresponding Author:*
Ramesh Man Tuladhar,
Disaster Preparedness Network, Nepal;
Email: r.tula1950@gmail.com

 DOI: https://doi.org/10.30564/jgr.v3i3.3596

are: i) aquifer is considered vulnerable to contamination from the surface and aquifer protective capacity fell within poor to moderate category"; ii) the pH values were below WHO permissible limit and at some sampling points TDS values above WHO limit; and iii) groundwater is characterized to be temporary to permanent hard [3].

All these published papers from the geological research community of African continent are apparently contributing towards overall socioeconomic development and humankind across the globe - a strategic policy of JGR platform.

References

[1] Adepelumi, A., Olayiwola, O., Falebita, D., Falebita, D., Afolabi, O., Soyinka, B., & Obokoh, J. (2021). The Horizontal Loop Electromagnetic (HLEM) Response of Ifewara Transcurrent Fault,Southwestern Nigeria: A Computational Results. Journal of Geological Research, 3(3).
DOI: https://doi.org/10.30564/jgr.v3i3.3146.

[2] Wokwenmendam Nguet, P., Ntieche, B., Legrand Tchop, J., Christian Mana, B., & Mbossi, E. (2021). Geochemistry of Volcanic Rocks of Beka, North East of Ngaoundéré (Adamawa Plateau, Cameroon): Petrogenesis and Geodynamic Context. Journal of Geological Research, 3(3).
DOI: https://doi.org/10.30564/jgr.v3i3.3325.

[3] Eyankware, M., Ogwah, C., & Star, U. (2021). Integrated Geophysical and Hydrogeochemical Characterization and Assessment of Groundwater Studies in Adum West Area of Benue State,Nigeria. Journal of Geological Research, 3(3).
DOI: https://doi.org/10.30564/jgr.v3i3.3197.

DOI: https://doi.org/10.30564/jgr.v3i3.3596

BILINGUAL PUBLISHING CO.
Pioneer of Global Academics Since 1984

Journal of Geological Research
http://ojs.bilpublishing.com/index.php/jgr-a

ARTICLE

The Horizontal Loop Electromagnetic (HLEM) Response of Ifewara Transcurrent Fault, Southwestern Nigeria: A Computational Results

A.A. Adepelumi[1*] O.B. Olayiwola[2] D.E. Falebita[1] O.Afolabi[1] B.O Soyinka[3] J. Obokoh[4]

1.Department of Geology, Obafemi Awolowo University, Ile-Ife, Nigeria
2.Nigerian Defence Academy, Kaduna, Nigeria
3.Terracon, Seattle, Washington DC, USA
4.Sam Houston State University, Spring, Texas, USA

ARTICLE INFO

Article history
Received: 25 April 2021
Accepted: 25 May 2021
Published Online: 4 June 2021

Keywords:
Mineralized
Conductor
Overburden
HLEM
Modeling
Basement complex

ABSTRACT

The need to accurately interpret geological models that approximate mineralized zones in a Basement Complex terrain necessitate the development of horizon loop electromagnetic method (HLEM) forward modeling solutions for such scenarios. The focus of the present work is on finding rapid forward modeling solutions for synthetic HLEM data as an aid in exploration for moderate to deep conductive mineral exploration targets. The main thrust is obtaining idealized HLEM models that are required for geological interpretation of the subsurface in such environment. The original HLEM equations developed by Wesley were extended to represent a horizontally stratified earth with a conductive approximated by shear zone. From these equations a computer program was written to calculate the HLEM responses for optimal conductor model with known values of coil separations (L), depth of burial (z) and angle of dip of the target. The thin conductive model was used because it is simple and suitable for different geological scenarios. The accuracy of the approximate forward solution has been confirmed for HLEM systems with various geometric ranges, frequencies and conductivities. Three models having varying overburden thickness, dip angle of target and source-receiver separation were used in the forward modeling. The effect of varying the dip angle, overburden thickness and coil separation was studied in all the three models used. The result obtained from the forward modeling showed that variation of the dip angle gave rise to changes in the amplitudes of the anomalies generated, while that of overburden and coil separation gave rise to changes in anomaly shape. Also, the geometry and position of the causative body were precisely delineated.

1. Introduction

The main thrust of this works is the application of numeral electromagnetic forward modeling [1-16] in the mapping of geologic structure called the Ifewara transcurrent fault system (ITFS) in a study area located between 7^0 25' N - 7^0 27' N and 4^0 41' E - $4^0$42' E (Figure 1). The ITFS is situated in Ilesha area of Osun State in the southwestern

**Corresponding Author:*
A.A. Adepelumi,
Department of Geology, Obafemi Awolowo University, Ile-Ife, Nigeria;
Email: aadepelu@oauife.edu.ng

 DOI: https://doi.org/10.30564/jgr.v3i3.3146

part of Nigeria. It extends from Iwara through Aiyetoro to Ifewara. Three different geologic models with varying properties were used to determine the effects of conductive overburden, conductive host rock, coil separations and angle of dip on the pre-supposed fault and/or shear zone. The forward modeling code developed for this purpose is the localized, non-linear Born approximations of the 2.5D integrals of EM scattering problems [16]. Its application is based on the assumption of a wholly conductive thin conductor, whereby the HLEM anomalies are considered to be completely in-phase without a quadrature component [17].

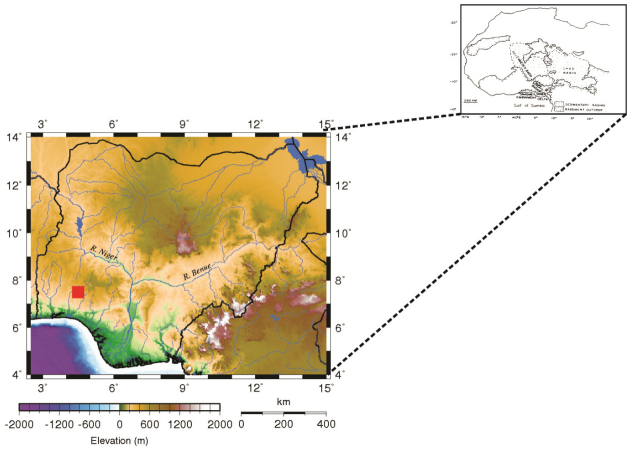

Figure 1. The location of Ifewara southwestern Nigeria inserted in the digital elevation map

The forward modelling of a thin bedrock conductor gives a trough-like HLEM anomaly whose width at the zero level equals the coil separation and the thickness of the conductor [18]. This is because there is a relationship between the geometry, depth of the conductor and the source-receiver distance of the measurement system [18]. For example, [19] has shown that clay-filled shear zones can produce spiky trough-like HLEM anomalies. However, regarding the ITFS, [20] successfully mapped the imprint of the Ifewara transcurrent fault system (ITFS), using integrated geophysical mapping methods that involved the magnetic and dipole-dipole resistivity. While [21] found extensive mylonite associated with the location of the (ITFS). They adduced the presence of this rock type is indicative of a possible fault or shear zone presence. They reported that the anomalies observed in the generated magnetic profiles correlated with the shear zones. The anomalous zone is structurally low that is gently dipping. Also, the resistivity responses obtained by [21] showed that the ITFS or shear zone is covered by thin overburden thickness, producing distinct anomaly responses. They noted that there is an inverse relationship between overburden thickness and the resolution of the resistivity images. The results of [20,21] corroborated the earlier work of [22] that employed the electrical resistivity and electromagnetic method for the detection of the ITFS and its associated possible sulphide mineralization that were earlier reported by [23].

2. Regional Geology and Tectonic Settings

The survey area falls within a region underlain by crystalline rocks that belong to the basement complex of Nigeria which forms part of the Pan-African mobile belt, east of the West African craton [20]. The common features of the Nigerian Basement Complex are polycyclicity in evolution and structural complexity due to multiple metamorphism and igneous intrusions. The earliest geologic cycle through which the rocks in this area evolved began with sedimentation [23]. This was followed by several periods of deformation that produced the gneisses and schists. The basic intrusive cycle preceded the granitic gneisses. During this cycle, a period of granitisation and deformation imparted secondary schistocity on the earlier rocks and the basic intrusives were amphibolites.

The survey area belongs to the Ife-Ilesha schist belt of southwestern Nigeria which has abundant mafic and ultramafic rocks and constitutes the upper Proterozoic schist belt of the basement complex [24,25]. Work by [26] shows that this area consists of two contrasting lithological rock association separated by a major fault called the "Ifewara fault". Detailed characteristics of the two major deformations (D1 and D2) associated with the Ifewara Shear Zone are described by [27].

3. Electromagnetic Method Overview

There are several electromagnetic techniques commonly used to delineate variations in conductivity of the earth. The conductivity is monitored on the basis of time-varying electric and magnetic fields. Maxwell's equations relate the distribution of physical property to the electromagnetic field which is a manifestation of the distribution of electric charge [16,28]. The Maxwell's equations are expressed in differential forms as equations 1 - 4.

The differential forms of the Maxwell's equations are

$$\text{rot}\,\mathrm{E} = \nabla \times \mathrm{E} = -\frac{\partial \mathrm{B}}{\partial \mathrm{t}} \quad (1)$$

$$\text{rot}\,\mathrm{H} = \nabla \times \mathrm{H} = \frac{\partial \mathrm{D}}{\partial \mathrm{t}} + \mathrm{J} \quad (2)$$

$$\text{div}\,\mathrm{B} = \nabla \cdot \mathrm{B} = 0 \quad (3)$$

$$\text{div}\,\mathrm{D} = \nabla \cdot \mathrm{D} = \mathrm{q} \quad (4)$$

Where E (V/m) is the electric field intensity vector, H (A/m) is the magnetic field intensity vector, D (C/m^2) is the electric flux density vector, B (Wb/m^2 or tesla) is the mag-

DOI: https://doi.org/10.30564/jgr.v3i3.3146

netic flux density vector, J (A/m²) is the electrical current density and q = C/m^3 is the electric charge. These fields are usually functions of space (x, y, z), time t (seconds), frequency f (hertz) and angular frequency ($\omega = 2\pi f$).

Equation (1) is the Faraday's law that relates time varying magnetic field to generation of electrical voltage; Equation (2) is the Ampere's law that relates how the passage of time varying electric field leads to generation of magnetic field; Equation (3) indicates that there are no single magnetic and that the lines of magnetic induction are continuous and Equation (4) shows that electrical fields can begin and end on electrical charges which are directly related to equations 5 - 7.

$$D = \varepsilon E \quad (5)$$

$$B = \mu H \quad (6)$$

$$J = \sigma E \quad (7)$$

Where ε = electrical permittivity; μ = magnetic permeability and σ = electrical conductivity.

The commonly used small-loop EM profiling technique is the Horizontal loop electromagnetic method (HLEM). It is also known as Ronka, or MaxMin. The horizontal loop, moving transmitter and receiver, system is very flexible and used in both classic mineral exploration geophysics and in environmental and engineering applications, although different approaches to measurement are taken. The system consists of two horizontal loops, in the exploration system the loops are about a meter in diameter. For small coil separations, the loops are very small and often iron cored to achieve a high magnetic moment. In the classic systems, the coil separation is typically variable at 25, 50 or 100 m. One loop is wired to a signal generator powered by a portable battery pack. In the mineral exploration mode the generator produces currents at several frequencies in the 300 Hz - 7000 Hz range. These currents flow through the horizontal transmitter coil, giving rise to time varying magnetic fields of the same frequency. A small coil is wound around the transmitter and connected to a wire which runs to the receiver. This wire enables the phase of the signal at the receiver to be determined and ensures the transmitters and receivers are kept a fixed distance apart. The same time varying magnetic field from the transmitter intersects any conductors in the subsurface and induces an emf which in turn causes a current in the conductor as we have noted earlier. This current then causes a secondary magnetic field which intersects the receiver and induces a secondary emf [28].

4. Numerical Forward Modeling of HLEM Data

The least square algorithm developed for this study was based on the numerical forward modelling theory [16]. It was applied based on the assumption of a wholly conductive thin conductor, whereby the HLEM anomalies are considered to be completely in-phase without a quadrature component [17]. Several researchers [29,30,31,32] have used the theory which suggested the expression of normalized secondary field at the receiver coil as a percentage of the secondary field [16] as:

$$H(x) = 100\left\{\frac{L^3}{\pi}\left[\frac{tan^{-1}\left(\frac{a}{L}\right)}{L^3} - \frac{\pi}{L^3} + \frac{a}{p^2L^2}\right] + \frac{L^3}{\pi}\left[\frac{\pi}{2q^3} + \frac{tan^{-1}\left(\frac{b}{q}\right)}{q^3} + \frac{b}{q^2p^2}\right]\right.$$

$$+ \frac{L^3(q^2-3L^2)sin^2\propto}{\pi}\left[\frac{\pi}{2q^5} + \frac{tan^{-1}\left(\frac{b}{q}\right)}{q^5} + \frac{b}{q^4p^2}\right] + \frac{2L^3bsin^2\propto}{\pi q^2p^4}$$

$$[(x_t + x_r)^2 - L^2cos^2\propto] + \frac{L^3}{4\pi r_r r_t p^2}[a + bcos\,2\propto - c\,sin2\propto] +$$

$$\frac{L^3sin\propto}{\pi p^4 r_r}\left[\left((x_t + x_r) + L\cos\propto\right) \times (d\sin\propto + a\cos\propto)\right]$$

$$-\frac{L^3sin\propto}{\pi p^4 r_t}\left[\left((x_t + x_r) - L\cos\propto\right) \times (d\sin\propto - a\cos\propto)\right]$$

$$\left. + \frac{L^3}{2\pi r_r r_t p^4}[(bd^2 - ac^2)\,sin^2\propto + abc\sin 2\propto - ab(a+b)\,cos^2\propto]\right\} \quad (8)$$

Where L is the coil separation and α is the dip angle of the conductor as shown in Figure 2. Other notations used for simplifying equation (8) are as follows:

$x_r = (x - x_o)\,cos\propto + z\,sin\propto + \frac{L}{2}\cos\propto$; $x_t = (x - x_o)\,cos\propto + z\,sin\propto - \frac{L}{2}\cos\propto$; $z_r = z\,cos\propto - (x - x_o)\,sin\propto - \frac{L}{2}sin\propto$; $z_t = z\,cos\propto - (x - x_o)\,sin\propto + \frac{L}{2}sin\propto$; $r_r = \sqrt{x_r^2 + z_r^2}$; $r_t = \sqrt{x_t^2 + z_t^2}$; $a = 2\sqrt{r_r r_t}\,cos\left(\frac{\emptyset_r - \emptyset_t}{2}\right)$; $b = 2\sqrt{r_r r_t}\,cos\left(\frac{\emptyset_r + \emptyset_t - 3\pi}{2}\right)$; $c = 2\sqrt{r_r r_t}\,cos\left(\frac{\emptyset_r + \emptyset_t}{2}\right)$; $d = 2\sqrt{r_r r_t}\,cos\left(\frac{\emptyset_r - \emptyset_t - 3\pi}{2}\right)$; $p = \sqrt{L^2 + a^2}$; $q = \sqrt{(x_t + x_r)^2 + (L\,sin\propto)^2}$; $z_r < 0 \Rightarrow \emptyset_r = -\frac{\pi}{2} - tan^{-1}\frac{x_r}{z_r}$; $z_r > 0 \Rightarrow \emptyset_r = \frac{\pi}{2} - tan^{-1}\frac{x_r}{z_r}$; $z_t < 0 \Rightarrow \emptyset_t = -\frac{\pi}{2} - tan^{-1}\frac{x_t}{z_t}$; $z_t > 0 \Rightarrow \emptyset_t = \frac{\pi}{2} - tan^{-1}\frac{x_t}{z_t}$;

where the dip angle of the conductor α should be in the range of 0^0 - 90^0 [16] and x is midpoint between transmitter and receiver coils.

DOI: https://doi.org/10.30564/jgr.v3i3.3146

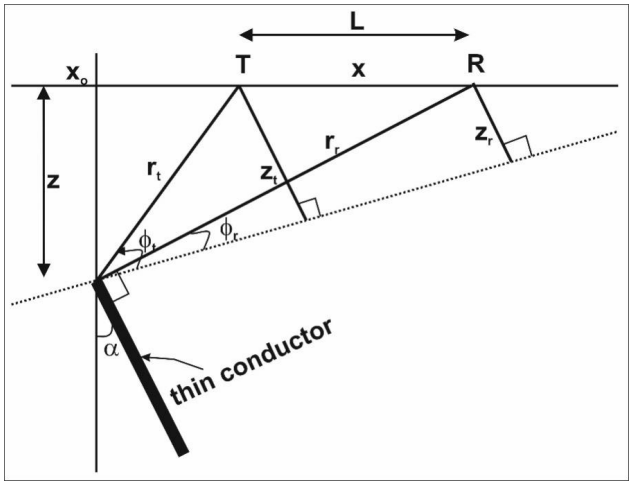

Figure 2. Geometrical relationship between transmitter T, receiver R and the thin conductor with infinite extent (modified after [29] and [30]). Optimized parameters are the burial depth (z), dip angle (α) and surface projection point (x_0)

4.1 The Models

In order to predict the characteristic response of the conductive target (Ifewara fault), theoretical anomalies were produced using equation 8 for coil separations of L = 50 m, 100 m, and 150 m (Table 1). The angle of dip of the target was varied from 0^0 to 90^0 with 5^0 increments. Forward modeling was carried out using five different overburden depth which are z = 10 m, 20 m, 30 m, 40 m and 50 m, while the projection point to the surface (x_o) was 225 m. The characteristics of the slingram (HLEM) profiles are determined by the geometry of the receiver and transmitter coils as well as geometry and attitude of the conductive source. It is expected that the response of a vertically oriented plate-like conductive body would appear as a negative peak, approximately 1.3 times the coil separation distance with two lower amplitude positive shoulders on either side [28].

Table 1. Model parameters

Parameters	Model	1	2	3
T - R coil separation (L)	A	50 m	100 m	150 m
Surface projection (x_o)	B	225 m	225 m	225 m
Profile length	C	500 m	500 m	500 m
Angle of dip (α)	D	0^o - 90^o step 5^o	0^o - 90^o step 5^o	0^o - 90^o step 5^o
Depth of burial (z)	E	10 - 50 m	10 - 50 m	10 - 50 m

5. Discussion of Results

5.1 Forward Modeling

The synthetic anomaly signatures obtained for Model 1 are shown in Figures 3 (a - e). It is obvious from the figures that the amplitudes of the anomaly changes with change in the angle of dip. As the angle of dip increases from 0^0 to 90^0, amplitudes of the anomaly is observed to be rising on the down dip side of the conductive target, while the amplitudes on the up dip side becomes flattened (decreased) gradually. At dip angle of 90^0, a vertically dipping target, the amplitudes of the anomaly curve are observed wide apart. While one arm has its maximum value to be positive, the other has it to be negative. It can be observed also, that with a change in the value of the overburden thickness but with the same coil spacing, the behaviour of the arms of the anomaly was observed to change compared to that of model 1A. This change in behaviour is deduced to be solely due to the change in the overburden thickness. From the figure, it is obvious that the change in behaviour is conspicuous when the conductive target is dipping at angle of 90^0 as one of the peak amplitudes of the anomaly for Model 1A (Figure 3a) is negative while both peak amplitudes in the case of Model 1B are positive. Furthermore, it is observed that the increase in overburden thickness from 10 m to 20 m significantly affected the anomaly response obtained. This shows that overburden thickness affects the amplitude of slingram responses. The interpretation of these anomalies are similar to those above except that the peak positive and negative amplitudes of the slingram response has reduce to as low as 10 and -5 respectively unlike in Model 1A (Figure 3a) where the overburden thickness is very shallow and the transmitted wave is able to induce substantial secondary signal in the conductor.

In Figure 3d (Model 1D), the effect of the overburden is further observed on the slingram response. As the overburden increases to 40 m, the peak negative response increases to -3, while that of positive response reduces to about 10. The effect of this is that transmitted signal getting to the conductor is small hence its response is also minute. The effect of increased overburden depth led to lower slingram response to about 4 and -1.5 (See Figure 3e, Model 1E) for peak positive and negative amplitudes respectively; this indicates that the conductor has been energized by small quantity of the signal. In this case the overburden depth is 50 m.

Similar interpretation can be given to Figure 4a just like in Model 1A (Figure 3a) interpretation except that the width of the anomaly is wider compared to the former. The slingram responses are high just as in the case of Model 1A

DOI: https://doi.org/10.30564/jgr.v3i3.3146

which shows that large quantity of the signal energized the conductor due to small overburden effect but larger width is attributed to increase in Transmitter - Receiver coil separation which is 100 m while that of Model 1A is 50 m both with overburden of 10 m. In Figure 4b, the effect of increased overburden depth and increased T - R coil separation is observed further and the width of the anomaly has reduced due to the increment in the overburden depth. The values of the response have also decreased implying that the conductor is being energized by lesser signal compared to that of Model 2A (Figure 4a). In Figure 4c, the width of the anomaly is further reduced as the overburden depth is increased. Just as in others, the amplitudes of the anomaly is symmetrical for a vertical conductor, while the amplitude increases on the down dip side and decreases on the up dip side showing an asymmetric shape. At 90^0, one of the amplitudes is negative while the other is positive. In Figure 4d, it is evident that the width of the anomaly is further reduced while other interpretations are similar to the above except that at 90^0, both amplitudes are positive. Similarly, the anomalies shown in Figure 4e shows a different signature compared to that of Model 1E above. The slingram responses are relatively higher. They range from -7 to - 10 for the peak negative, while those of peak positive ranges from 5 to 20; compared to that of Model 1E (Figure 3e) where we have peak negative to range from -0.5 to -1.5 and peak positive to range from 1 to 3. This shows that the coil separation influences the depth of penetration of the signal with the same frequency.

With increase in the Transmitter - Receiver coil separation to 150 m, and varying the overburden depth from 10 m to 50 m, EM response that is different from other models was observed (Figure 5a). The widths of the anomalies are observed to be wider compared to those of other two models connoting that the coil separation affect the shape of the anomaly and the longer the coil separation the wider the width of the anomaly for the same overburden depth. In Figure 5b, it is observed that increase in the overburden depth from 10 m to 20 m for the same coil separation led to decrease in the width of the anomaly. Also, the slingram (HLEM) responses are much higher than the previous models for the same overburden depth; the significant of this is that the increased coil separation enhanced energization of the conductor. This modeling result shown in Figure 5c is similar to those of Figure 5b except that the width of the anomaly is further reduced due to increase in the overburden depth and reduction in the slingram responses showing that, lesser signal energizes the conductor. The effect of varying the dip angle is observed as the symmetry of the anomaly changes from symmetrical for vertical conductor with dip angle of zero degree to asymmetrical as the angle increases from 0 to 90 degrees. The effect of increased coil separation on the slingram responses is worthy of note here (Figure 5d). The slingram responses obtained in Figure 5d compared moderately well to the previous models (Figure 5c) for the same overburden depth is observed to be increasing with increasing coil separation. This implies that the higher the coil separation, the higher the energization of conductors for the same value of frequency. Also the width of the anomaly is further increased. Reduction in the width of the anomaly as a result of increase in the coil separation observed in Figure 5e possibly lead to the deduction that the width of the anomaly is dependent on the energization of the conductor. With high energization of the conductor, the peak negative width of the anomaly is high, while it is low for low energization. Effect of coil separation is mainly in enhancement of depth of investigation while that of dip is observed in the symmetry of the anomaly.

5.2 Effect of Conductive Overburden

In our study, the effects of overburden on the buried conductors(s) are explained using the forward modeling results shown in Figure 6 (a - d) respectively. Overburden layer is that layer enclosing the conductor from the top whose thickness can either or not be in contact with the conductor. Conductively coupling occurs when an overburden is in galvanic contact with the conductor. While inductively coupling occurs when an overburden does not have any contact with the conductor [28,33].

Figure 6 (a - d) shows slingram (HLEM) curves for 0^o, 30^o, 60^o, and 90^o dips and the effect of overburden depths of 10, 20, 30, 40, and 50 m plotted for each dip angle. In all cases, the conductor is located directly below the peak negative of the anomaly. Also, it is apparent from the figures that the smaller the overburden thickness to the conductor, the higher the anomaly response and vice-versa. In contrast, the higher the dip angle, the greater the amplitude and the asymmetry of the anomaly curves are much more pronounced at shallower depths. For example, the updip peak and downdip trough are sharper and broader respectively at 10 m than at 50 m. According to [34], if an overburden of appreciable response parameter is present (although neglected) as one makes an interpretation for the depth of a conductor, it appears as if the target is deeply buried and a better conductor than it actually is. The results obtained in this research confirm the observations of [35] that an increase in the conductance of an inductively coupled overburden layer will lead to a decrease in the horizontal loop EM anomaly.

5.3 Effect of Conductive Host Rock

The typical model [36] of an EM response of a conductor

 DOI: https://doi.org/10.30564/jgr.v3i3.3146

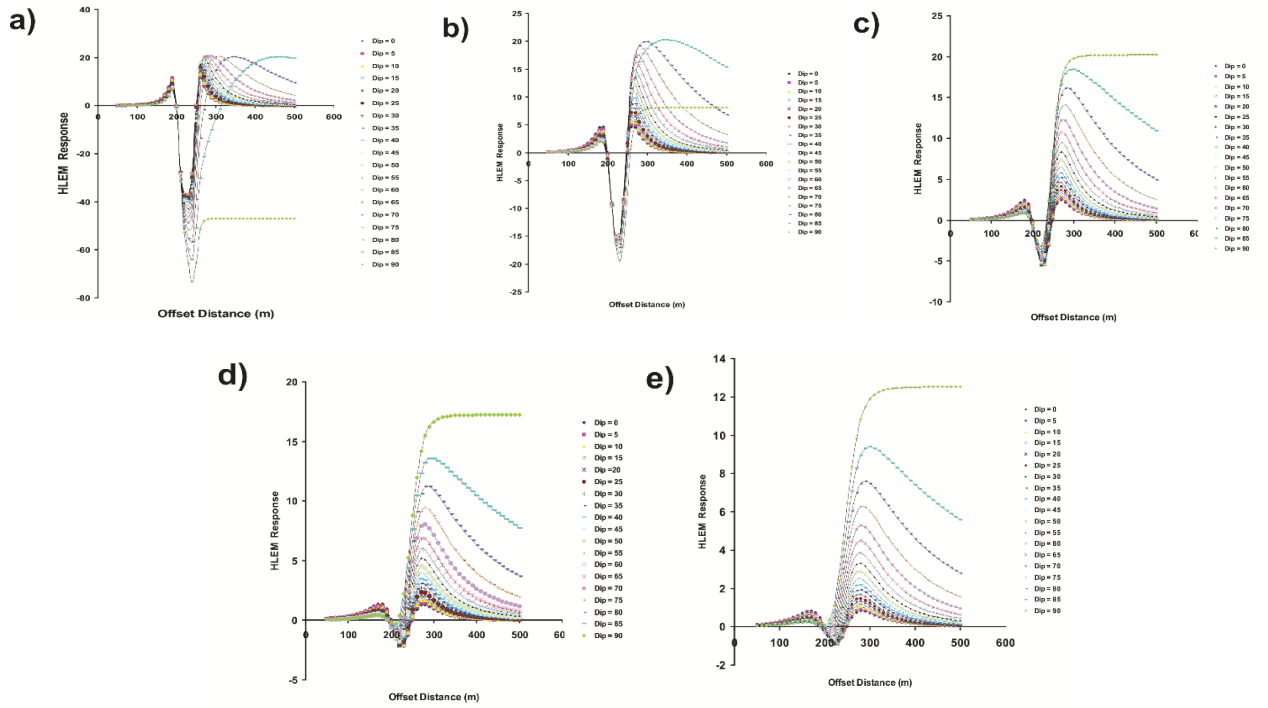

Figure 3. Superposition of HLEM anomaly responses for Model 1A (upper left panel), Model 1B (middle left panel), Model 1C (lower left panel), Model 1D (upper right panel) and Model 1E (middle right panel) with target dipping between 0 and 90 degrees, and depth of burial of 10 m, 20 m, 30 m, 40 m and 50 m, and T - R separation of 50 m. The plot shows the effect of varying dip angle of conductor on slingram response.

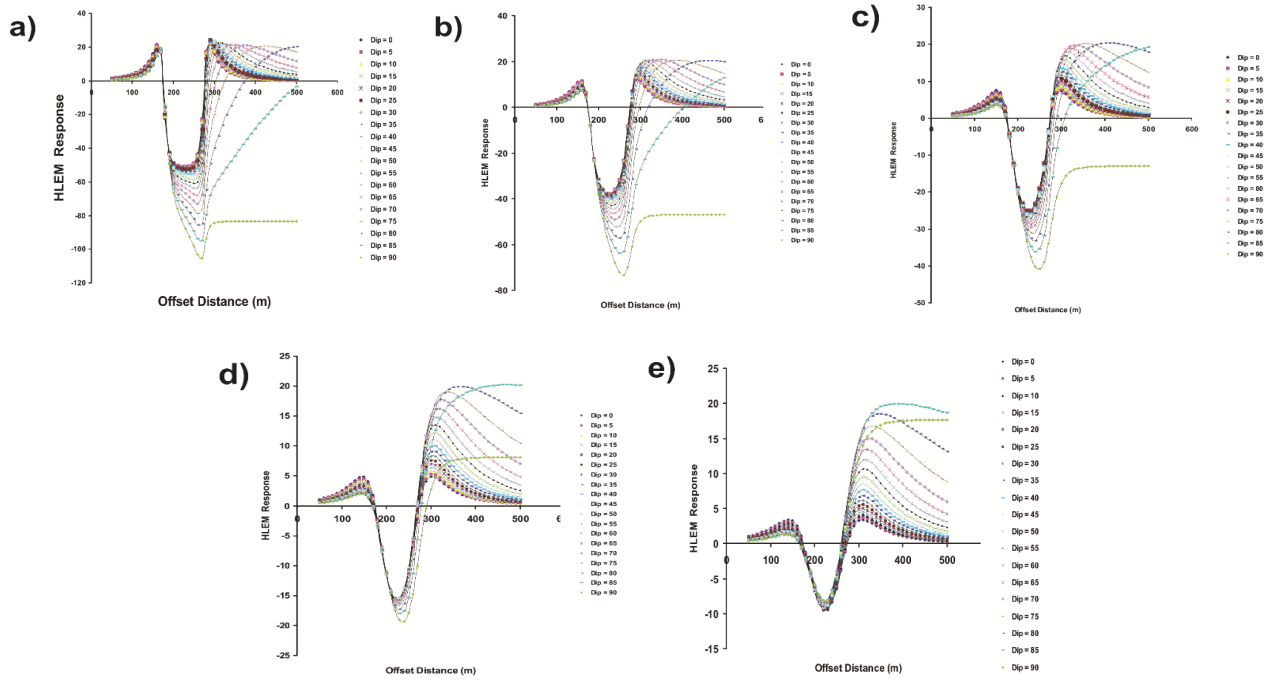

Figure 4. Superposition of HLEM anomaly responses for Model 2A (upper left panel), Model 2B (middle left panel), Model 2C (lower left panel), Model 2D (upper right panel) and Model 2E (middle right panel) with target dipping between 0 and 90 degrees, and depth of burial of 10 m, 20 m, 30 m, 40 m and 50 m, and T - R separatioon of 50 m. The plot shows the effect of varying dip angle of conductor on slingram response.

DOI: https://doi.org/10.30564/jgr.v3i3.3146

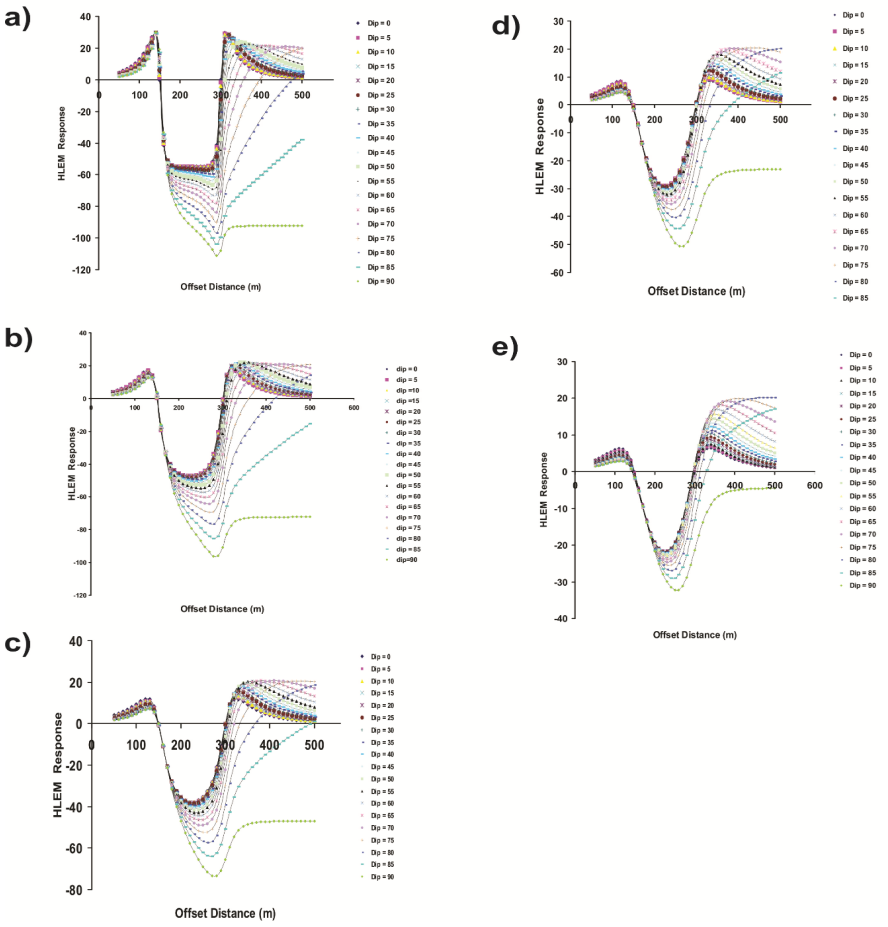

Figure 5. Superposition of HLEM anomaly responses for Model 3A (upper left panel), Model 3B (middle left panel), Model 3C (lower left panel), Model 3D (upper right panel) and Model 3E (middle right panel) with target dipping between 0 and 90 degrees, and depth of burial of 10 m, 20 m, 30 m, 40 m and 50 m, and T - R separation of 50 m. The plot shows the effect of varying dip angle of conductor on slingram response.

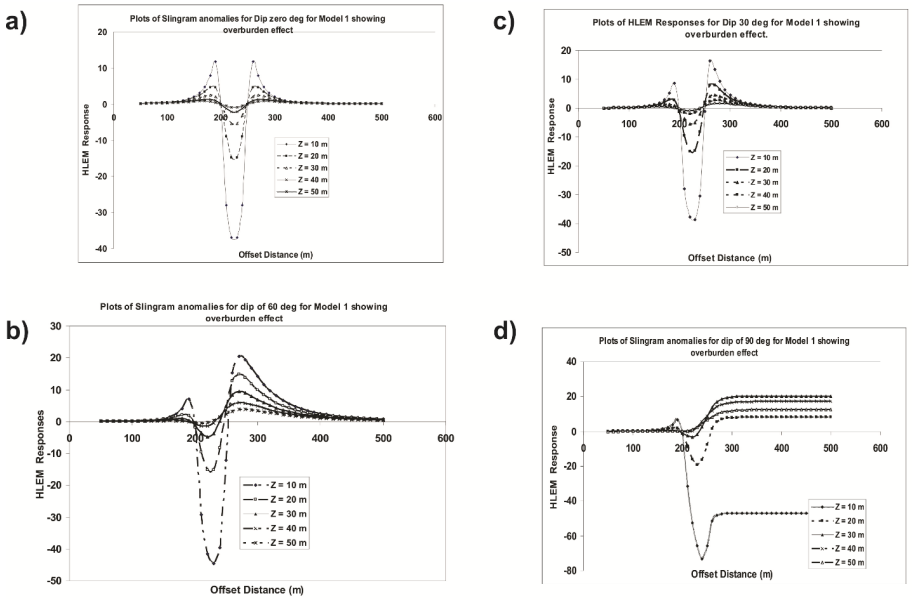

Figure 6. Slingram (HLEM) anomalies showing the overburden effect on the conductor. (0^o dip in upper left panel), (30^o dip in lower left panel), (60^o dip in upper right panel) and (90^o dip in lower left panel).

 DOI: https://doi.org/10.30564/jgr.v3i3.3146

enclosed by a conductive host rock is described by the dual of 'vortex' and 'galvanic' currents. The galvanic current dominates when the host rock is conductive while the vortex current dominates when the host rock is resistive. If the galvanic current dominates, only the location and depth of the buried conductor are determined. This is probably because buried conductor can generate natural telluric currents in the host and thus result in upsurge of ambient noise [37,38]. The conductor would then appear to be shallower and more resistive than it is actually. Comparing the responses of the broadside and in-line horizontal loop EM (slingram) configurations may help to resolve the ambiguities [39]. According to [40] the effects of the conductivity of a host rock on the horizontal loop response of a conductor with known conductivity for a homogenous half-space are in four parts. The first part describes an initial effect when the conductivity of the host increases from zero. There is a slight anticlockwise phase rotation of the anomaly as a result of the passage of quadrature currents from the host to the conductor. This means there is an enhancement of anomaly due to upsurge in scatter current density. The second part indicates that as the conductivity of the host continues to increase, there is a higher enhancement of the anomaly till it is about twice the response in free space. This is because there will be a clockwise phase rotation as a result of the phase shifts in the primary field. Further increase in the host conductivity leads to extra clockwise phase rotations and anomaly attenuation. These effects are as a result of losses experienced as the primary field travels to the conductor and as the secondary field travels from the conductor to the receiver. It should be noted that high frequency may not be enough to resolve significant target when using horizontal loop. This is because small lateral inhomogeneities in the conductivity of the host may create very profound effects. For this present study, the effect of the conductive host rock was not computed by us because that has been done by [30].

5.4 Effects of Coil Separation on the Buried Conductor

In other to examine the effects of coil separation (L) on the horizontal loop EM signature, for a vertical conductor buried at depth of 10 and 50 m, anomalies for coil separations (L) of 50, 100 and 150 m were computed and plotted together at dip angles of 0^o, 45^o and 90^o. The results obtained showed that the width of the main negative slingram anomaly clearly varies with the coil separation Figure 7 (a - f). The major effect of coil separation on slingram signature is the broadening of the anomaly and deeper penetration of depth of investigation. The implication of this is proper energization of the conductor in the subsurface as the coil separation is increased.

5.5 Effects of Dip on the Buried Conductor

Figure 8 (a - d) show the computed anomalies for a coil separation of L = 50 m with the target conductor at depths of z = 10, 20, 30, 40 and 50 m, dipping at d = 0^o, 30^o, 60^o and 90^o.

It can be observed that the anomalies are more symmetrical at lower angles and become increasingly asymmetrical as the angle increases (Figure 8a - d). Also, at smaller depth, the amplitude of the anomalies at the updip side is higher than that at the downdip side. However, as the depth increases (e.g. z = 30, 40, and 50, Figure 8d) the reverse is the case with respect to the amplitude. This confirms that horizontal loop EM anomalies lose their asymmetry and position of their peak amplitude at increasing depth for dipping conductor [41].

6. Conclusions

This study has attempted to characterize different geologic scenarios through model simulation of overburden occurrence, coil separation and dip in identifying mineralized zones using HLEM methods. The overburden thickness (z) of 10 m, 20 m, 30 m, 40 m, 50 m; having coil separation (L) of 50 m, 100 m, 150 m, and dip angle (α) that varies from 0^o to 90^o were used to constrain the models employed. This was done to investigate the effectiveness of horizontal loop electromagnetic method (HLEM) in mapping the mineralized Ifewara transcurrent fault/shear zone within the typical basement complex terrain of southwestern Nigeria.

We observed that the overburden layer is a major attenuator of the amplitude of HLEM anomalies. This result implies that in a typical HLEM survey, consideration must be given to the possibility of both conductive and inductive effect of the overburden on the conductor. Generally, different coil separations control the observed width of the anomalies and the depth of investigation; therefore, choosing appropriate coil separation is expedient when HLEM is used for mineral exploration. Doing this would assist in overcoming the high absorption of HLEM signals posed by the thick overburden overlying the conductor being investigated. On the other hand, as the dip angle increases, the HLEM responses become more asymmetrical as it deviates from vertical. High amplitude ratios of the HLEM anomaly indicate good conductivities. The relative amplitude of the responses is related to the depth of the conductor. Depth to the conductive source can be estimated from the amplitude of the responses obtained from the forward modeling. The depth of investigation is observed to be mainly dependent upon the frequency, coil separation, overburden thickness, and host conductivity. It is concluded that the methodology presented may provide a useful basis for the quantitative interpretation of HLEM data in similar terrain as considered in this study.

DOI: https://doi.org/10.30564/jgr.v3i3.3146

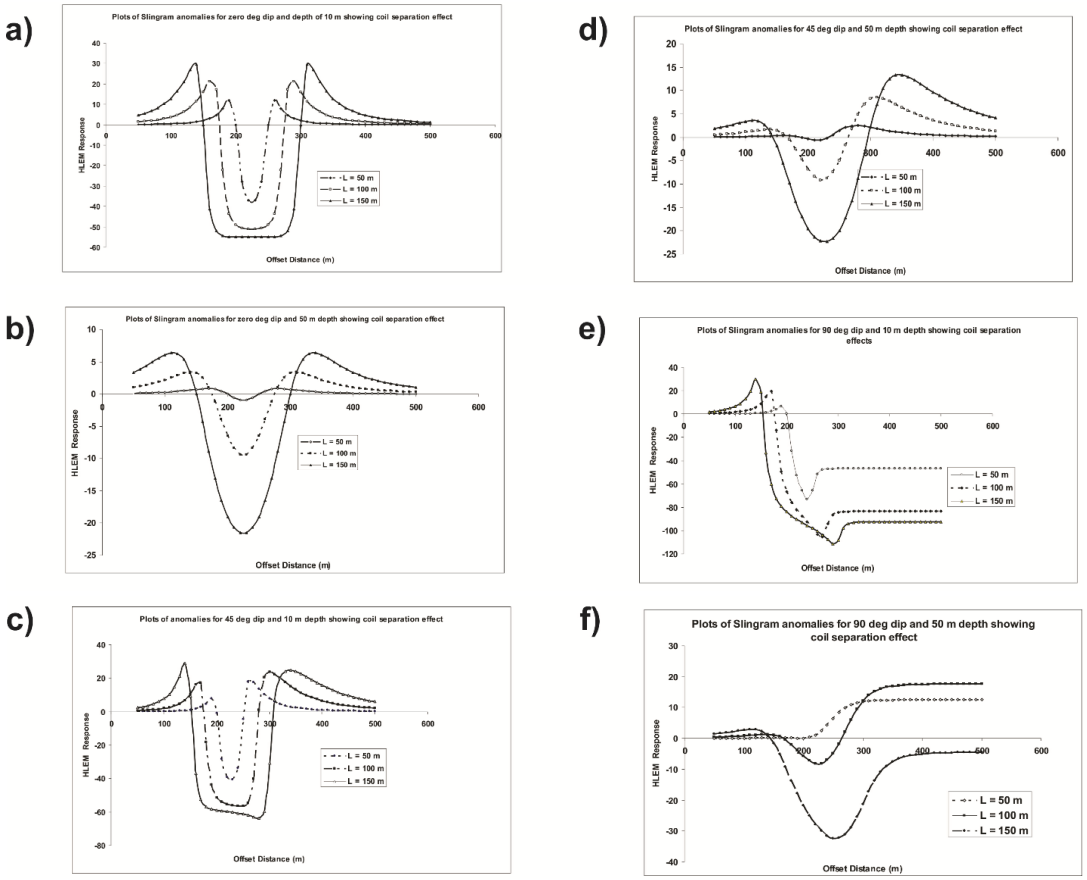

Figure 7. Slingram (HLEM) anomalies for vertically dipping conductor with varying coil separation L = 50, 100 and 150 m and conductor depth of 10 m depth (upper left panel); at 50 m depth (middle left panel). With the same coil separation, conductor dipping at 45^0 and overburden thickness of 10 m (lower left panel); at 50 m (upper right panel). Also with the same coil separation, horizontal conductor and overburden thickness of 10 m (middle right panel); and at 50 m (lower right panel).

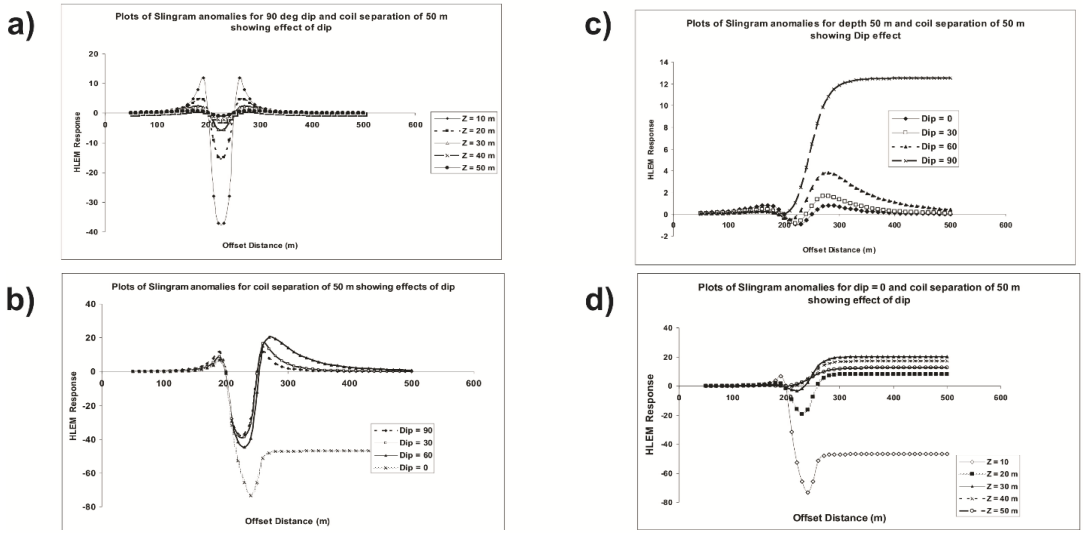

Figure 8. Slingram (HLEM) anomalies for vertically dipping conductor buried at 10, 20, 30, 40 and 50 m with coil separation of 50 m (upper left panel); vertical conductor buried at 10m depth with varying dip angle of 0^o, 30^o, 60^o and 90^o and coil separation of 50 m (lower left panel); vertical conductor buried at 50 m depth with coil separation of 50 m and varying dip angle of 0^o, 30^o, 60^o and 90^o (upper right panel); and horizontal conductor buried at 10, 20, 30, 40 and 50 m with coil separation of 50 m (lower right panel).

 DOI: https://doi.org/10.30564/jgr.v3i3.3146

References

[1] Ward, S. H., and Gledhill, T., (1957), Electromagnetic Surveying-ground methods, in Methods and case histories in mining geophysics: Bull. Can. Inst. Min. Metallurg., 63-70.

[2] Ward., S. H. and Hohmann., G. W. 1988. Electromagnetic Theory for Geophysical Applications, in Electromagnetic Methods in Applied Geophysics—Theory," Society of Exploration Geophysicists, Tulsa, Vol. 1, 1988, pp. 131- 311.

[3] Spies, B. R., and Frischknecht, F. C., 1991. Electromagnetic sounding. In: Nabighian MN (ed) Electromagnetic methods in applied geophysics, Volume 2, Applications. Society of Exploration Geophysics., Tulsa, 285-425.

[4] Wannamaker, P. E., Hohmann, G. W., and San-Filipo, W. A., 1984. Electromagnetic modeling of three-dimensional bodies in layered earths using integral equations. Geophysics, 49, 60-74.

[5] Newman, G. A., and Hohmann, G. W., 1988. Transient electromagnetic responses of high-contrast prisms in a layered earth. Geophysics, 53, 691-706.

[6] Lee, K. H., Liu, G., and Morrison, H. F., 1989. A new approach to modeling the electromagnetic response of conductive media. Geophysics, 54, 1180-1192.

[7] Xiong, Z., 1992. Electromagnetic modeling of three-dimensional structures by the method of system iteration using integral equations. Geophysics, 57, 1556-1561.

[8] Wang, T. and Hohmann, G. W., 1988. 'A finite-difference time-domain solution for three-dimensional electromagnetic modeling', Geophysics, 58, 797-809.

[9] Mackie, R. L., Madden, T. R., and Wannamaker, P. E., 1993. Three-dimensional magneto-telluric modeling using difference equations. Geophysics, 58, 215-226.

[10] Torres-Verdín, C., and Habashy, T. M., 1994. Rapid 2.5-dimensional forward modeling and inversion via a new nonlinear scattering approximation. Radio Science, 29, 1051-1079.

[11] Zhdanov, M. S., and Fang, S., 1996. 'Quasi-linear approximation in 3-D electromagnetic modeling', Geophysics, 61, 646-665.

[12] Liu, E. H., and Lamontage, Y., 1998. Geophysical application of a new surface integral equation method for EM modeling. Geophysics, 63, 411-423.

[13] Mitsuhata, Y., 2000. 2-D electromagnetic modeling by finite-element method with a dipole source and topography. Geophysics, 65, 465-475.

[14] Sasaki, K., 2001. Full 3-D inversion of electromagnetic data on PC. Journal of Applied Geophysics, 46:, 45-54.

[15] Hohmann, G. W., 1988. Numerical Modelling for Electromagnetic methods in geophysics in Nabighian, M. N., Ed., Electromagnetic methods in geophysics, Vol. 1, Soc. Explorations Geophysics. 313-363.

[16] Wesley, J. P., 1958. Response of a dike to an oscillating dipole. Geophysics, 23 (1), 128-133.

[17] Parasnis, D. S., (1971), Analysis of some multi-frequency, multiseparation electromagnetic surveys: Geophysical Prospecting, 19, 163-179.

[18] Telford, W. M., Geldart,L.P., Sheriff, R.E and Keys, D. A., 1976. Applied Geophysics, Cambridge University Press, 250 - 270.

[19] Palacky, G. J., Ritsema, I. L., and De Jong, S. J., 1981. Electromagnetic prospecting for groundwater in Precambrian terrains in the Republic of Upper Volta: Geophysical Prospecting, 29, p. 932-955.

[20] Adepelumi, A. A., Ako, B. D., Ajayi, T. R., Olorunfemi, A. O., Awoyemi, M. O and Falebita. D. E., 2008. Integrated geophysical mapping of the Ifewara transcurrent fault system, Nigeria. Journal of African Earth Sciences, 52 (4-5), 161-166.

[21] Akinde., A. S., Adepelumi, A .A and Dikedi., P. N., 2019. IFEWARA MYLONITE: Identifying the Neo-Tectonic Overprint Using Integrated Geophysical. Journal of Geology and Geophysics, 8 (2) 458, 1 -12.

[22] A Ako, B.D., Ajayi, T.R. and Alabi, A.O. (1978): A geochemical study of Ifewara area. Journal of Mining and Geology, Vol. 15(2), pp. 85 - 90.

[23] De Swardt, A.M.J. (1953): The geology of the country around Ilesha.Geological Survey of Nigeria, Bulletin. No. 23, pp 1-54.

[24] Elueze, A. A. (1982). Metallographic studies of ore minerals in the amphibolites of llesha Schist belts, southwestern Nigeria. Nigerian Journal Mining Geology, 19, 53-58.

[25] Turner, D.C. 1983. Recent advances in the study of the basement Complex of Nigeria. In: Oluyide P.O., et. al. (Eds). Precambrian Geology of Nigeria. Geology survey of Nigeria, 11 - 43.

[26] Rahaman, M.A. (1988): Recent Advances in the Study of the Basement Complex of Nigeria. In Precambrian Geology of Nigeria. Geological Survey of Nigeria, 11 - 41.

[27] Caby R., and Boesse J.M., (2001), Pan-African nappe system in southwest Nigeria: the Ife-llesha schist belt. Journal of African Earth Sciences, Vol 33, 2, 21 l-225.

[28] Frischknetch, F. C., Labson, V. F., Spies, B. R., and Anderson, W. L., 1991. Profiling Methods Using

DOI: https://doi.org/10.30564/jgr.v3i3.3146

Small Sources: Electromagnetic Methods in Applied Geophysics, Vol. 2, Application, Parts A and B, 105-270.

[29] Dondurur, D., and Sari, C., 2004. A Fortran 77 Computer Code for Damped Least-squares Inversion of Slingram Electromagnetic Anomalies over Thin Tabular Conductors: Computers and Geosciences, 30, 591-599.

[30] Duckworth, K., Krebes, E.S., 1995. A Quickbasic program for the computation of the response of a thin tabular perfect conductor to a two coil horizontal coplanar electromagnetic prospecting system. Computers & Geosciences 21 (2), 333-343.

[31] Duckworth, K., and O'Neil, D. A., 1989. Turam responses in a scale model conductive environment for single and paired conductors. Canada Journal of Exploration Geophysicists, 25. 115-137.

[32] Duckworth, K., Calvert, H.T., Juigalli, J., 1991. A method for obtaining depth estimates from the geometry of Slingram profiles. Geophysics, 56 (10), 1543-1552.

[33] Joshi, M. S., Gupta, O. P and Negi, J. G., 1988. On the effects of thickness of the half-plane model in HLEM induction prospecting over sulphide dykes in a highly resistive medium. Geophysical Prospecting, 36, 551-558.

[34] Lowrie, W., and West, G. F., (1965), The effect of a conductive overburden on electromagnetic prospecting measurements. Geophysics, 30 (4), 624-632.

[35] Poddar, M., 1982. Interpretation of pulse EM anomalies over Gani conductors: Geophysical Prospecting. 30, 86-100.

[36] McNeill, J. D., Edwards, R. N., and Levy, G. M., 1984. Approximate calculations of the transient electromagnetic response from buried conductors in a conductive half-space: Geophysics, 49, 918-924.

[37] Lilley, F. E. M., and Woods, D. V., 1978. The channeling of natural electrics by orebodies: Bulletin of Australian Society of Exploration Geophysics., 9, 62-63.

[38] Negi, J. G., Gupta, O. P., and Joshi, M. S., 1987. Corrections for conductivity estimates in induction prospecting of sulphide-dykes in a layered environment: Geophysical Prospecting, 35, 718-734.

[39] Gupta, 0. P., Joshi, M. S., and Negi, J. G., 1980. Scale model electromagnetic response to inline and broadside systems at skew traverses of a dipping half-plane embedded in a conductive host rock: Geophysical Prospecting, pp.119-134.

[40] Hanneson, J.E., West, G.F., 1984. The horizontal loop electromagnetic response of a thin plate in a conductive earth: Part II—computational results and examples. Geophysics 49 (4), 421-432.

[41] Dondurur., D (2005), Depth Estimates for Slingram Electromagnetic Anomalies from Dipping Sheet-like Bodies by the Normalized Full Gradient Method: Pure and applied geophysics, 162, 2179-2195.

 DOI: https://doi.org/10.30564/jgr.v3i3.3146

BILINGUAL PUBLISHING CO.
Pioneer of Global Academics Since 1984

Journal of Geological Research
http://ojs.bilpublishing.com/index.php/jgr-a

ARTICLE

Integrated Geophysical and Hydrogeochemical Characterization and Assessment of Groundwater Studies in Adum West Area of Benue State, Nigeria

Moses Oghenenyoreme Eyankware[1,2*] Christopher Ogwah[1] Umayah Otitie Star[3]

1. Department of Geology, Faculty of Science Ebonyi State University, Abakaliki, Nigeria
2. Geomoses Consultancy Limited Warri, Delta State, Nigeria
3. Department of Physics, Faculty of Science Delta State, University, Abakaliki, Nigeria

ARTICLE INFO

Article history
Received: 04 May 2021
Accepted: 08 June 2021
Published Online: 20 June 2021

Keywords:
Groundwater
Resistivity
Contamination
Aquifer protective capacity
Nigeria

ABSTRACT

Integration of geophysical and hydrogeochemical methods has been scientifically proven to be useful in vulnerability study and groundwater characterization. Subsurface geoelectric parameters such as resistivity and thickness obtained from geophysical method (Vertical Electrical Sounding VES) was used to determine aquifers vulnerability, longitudinal resistance (ρL) and transverse unit resistance (Rt). Thirty four water samples were collected from groundwater sources for physicochemical analysis. Estimated results from longitudinal conductance (S), (Rt) and (ρL) showed that the values ranges from 0.03 to 2.5mhos, 103.64 to 1964417.8 Ω/m^2 and 215.41 to 65731.68 Ω-m respectively. Result from S suggested that 50 % of groundwater is considered to be vulnerable to contamination from the earth surface, while the remaining 50 % is considered to be slightly vulnerable to surface contamination. Further findings obtained from hydrogeochemical analysis such as Gibb's and Chadba plots revealed that groundwater is highly influenced by rock water interaction, groundwater is classified to be $Na^+ + HCO_3^-$, $Ca^{2+} + Mg^{2+} + HCO_3^-$, $Na^+ + Cl^-$ and $Ca^{2+} + Mg^{2+} + Cl^-$ water type. Deduction from Soltan classification suggested that groundwater is classified to be of $Na^+ - HCO_3^-$ and $Na^+ - SO_4^{2-}$ water type. Results obtained from Ec and pH suggested that the values were below WHO permissible limit, while result obtained from TDS showed that at some sampling points TDS values were above WHO limit. Based on pH value obtained groundwater within the study area fell within slightly basic to acidic.

**Corresponding Author:*
Moses Oghenenyoreme Eyankware,
Department of Geology, Faculty of Science Ebonyi State University, Abakaliki, Nigeria & Geomoses Consultancy Limited Warri, Delta State, Nigeria;
Email: geomoses203@gmail.com

DOI: https://doi.org/10.30564/jgr.v3i3.3197

1. Introduction

Report from various scholars suggested that groundwater account for over 95 percent of global storage of fresh water [1-3]. Based on this there is high demand for groundwater across the world, although human activities have negatively influence on groundwater quality. There are varieties of human activities that Parameters such as threat to groundwater quality within the study area. There are varieties of human activities that poses as threat to groundwater quality within the study area. These activities include leakage from sewage systems, solid waste dumpsites, household waste pits, peri-urban agriculture, underground storage tanks, surface water infiltration spots and petrol service stations. On a global scale, several methods have been used to determine groundwater potential and asses groundwater vulnerability. Several scientific methods have been developed to constantly monitor groundwater quality to further advert several health related disease associated with drinking water. [4] reported that groundwater vulnerability assessment is considered paramount in evaluating anthropogenic activities with respect to the advancement of population liability insurance and the evaluation of economic impacts of disposal cost in highly vulnerable areas. Preliminary information and criteria for decision-making in such areas as designation of land use controls, delineation of monitoring networks and management of water resources in the context of regional planning are related to protection of groundwater quality [5]. Several reports by various scholars have proven that the combination of VES and hydrogeochemical studies is to considered successful in assessment of groundwater vulnerable to surface contamination in sedimentary and hard rock terrain [6-9]. [10,11] were of the opinion, that the VES is one of the geoelectrical method mostly used in measuring the vertical alterations of electrical resistivity of rock unit. This method has been recognized to be more suitable for a hydrogeological survey of sedimentary basins than the other resistivity methods. [12] further reported that the successful use of VES in determination of aquifer protective capacity and groundwater water potential. Findings from [13]; [14] suggested that the selection of geophysical methods in groundwater studies rely on the contrast between the physical properties of the target and the surrounding medium. Report from previous authors revealed that the delineation and characterization of groundwater potential within the Benue Trough becomes necessary as water samples from some existing wells and boreholes in the study area were below acceptable limits, especially during the dry season when most of the well and boreholes most have drop to a minimum yield and sometimes get dried up. Due to lack of hydrogeological information of the Benue Trough and improper delineation of the water bearing unit to facilitate the precise identification of desired water bearing unit before drilling and well completion for sustainable supply of potable water to the inhabitant of the study area [15,16]. [12] were of the opinion that basic resistivity parameters such as thickness, depth and resistivity of rock unit are vital in the determination of secondary aquifer which in turn help in the assessment of aquifer vulnerability. Findings according to [17] showed the successful use of VES in assessment of groundwater vulnerability in southern eastern part of Nigeria. [18] used surface geophysical method to decipher the groundwater potential in Mian Channu area of Pakistan. [19] further reported the successful use of hydrogeophysical method in determination of transmissivity, storativity of Njaba River Basin, Nigeria. An integration of VES data and hydraulic properties was also used in delineation of aquifer potential zones in central Uganda [20]. [21] also use the VES method to estimate hydraulic conductivity in alluvial aquifers of Pakistan. [22] reported the successful use of VES method in the determination of Quaternary aquifer of semi arid region of Khanasser of Syria. [23] used near-surface geophysical methods in estimating hydraulic conductivity and porosity of Ruhrtal aquifer in Germany. [24] were of the opinion that groundwater vulnerability is the risk of contaminates dispose near groundwater surface to influence groundwater quality. According to [25] parameters such as permeability, porosity, local geology and thickness of aquifer are considered to major factors in determining aquifer vulnerability. Reconnaissance survey within the study area, was is line with report by [24] which stated that pit toilets and dumpsites are in most case sited indiscriminately without taking into consideration the hydrogeological settings of the area, in so doing rendering the future of groundwater at risk. [26] suggested that groundwater flow also enhances the spread of contaminant in aquifer, the flow of these contaminations is highly controlled by inter-granular pores, fissures and interconnected fractures. Water bearing unit (aquifer) vulnerability is usually high when the earth material provide protection to groundwater repositories from surface contaminants, while aquifer vulnerability will be on the low side when natural factor that provide protection from surface contaminants. If groundwater protection studies are considered mandatory, it is therefore necessary to take into consideration factor that may trigger vulnerability of groundwater in order to ensure sustainable groundwater management strategy. For effective groundwater management it is therefore mandatory to have preliminary knowledge of the properties of water baring rocks. This is based on the fact that such

 DOI: https://doi.org/10.30564/jgr.v3i3.3197

properties have great influence on aquifer repositories. [27-31] stated that the heterogeneous nature of the subsurface rocks varies widely depending on the local geology of the area. With all the aforementioned factors that play a role in groundwater pollution and aquifer vulnerability it is therefore necessary to constantly monitor groundwater within the study area.

Geology/Hydrogeology

The study area lies within Eze Aku Formation of the Southern Benue Trough, is known to be one of major stratigraphic unit in the Southern Benue Trough erected by the shell D'' Arcy geologists, in the 1950. The term Eze Aku shale group appears to have been introduced by [32]. The Eze Aku Group includes all the stratigraphic units that was deposited from the late Cenomanian to Turonian in the Southern Benue Trough. And from the western to southeastern flank of the some aniticlinorial core, [33] and [34] indentified lithofacies broadly similar to those of the western flank. It is noteworthy that a condensed arm of the Eze Aku facies extends far southeastwards and partially overlies the Odukpani area between the Oban massif and the elements of the Nkporo group in that extremity. Because of folding and facies changes the thickness of the main mass of the group which is the shale facies, is not clear [16]. According to [35]; [16] Eze Aku unit is subdivided into several lithofacies; the sandstone, siltstone, shale and limestone. The thickness of the Eze Aku group is estimated to between the ranges of 600 to 1,200 m [16]. The hydrogeological characteristics of the Southern Benue Trough are directly dependent on their structure, climate and geology of the area. This makes it be extremely poor in groundwater prospect [16]. Report according to Nwajide, [16] aquiferous unit of the Eze Aku Group are formed in the sandstone and occasionally an fractured limestone.

2. Materials and Methods

A total of 26 VES was carried out within the study area as shown in Figure 2 using ABEM Terrameter SAS 1000, Schlumberger array configuration was employed for each VES profile with a maximum half current (AB/2) electrode separation of 150 m and half potential (MN/2) electrode of 10 m. The observed field data were converted to apparent resistivity (ρa) values using the following equation (1):

$$\rho a = \pi \left(\frac{\left(\frac{AB}{2}\right) - \left(\frac{MN}{2}\right)}{MN} \right) \Delta V / I \quad (1)$$

Apparent resistivity data was plotted against the current electrode spacing (AB/2) to generate geoelectrical

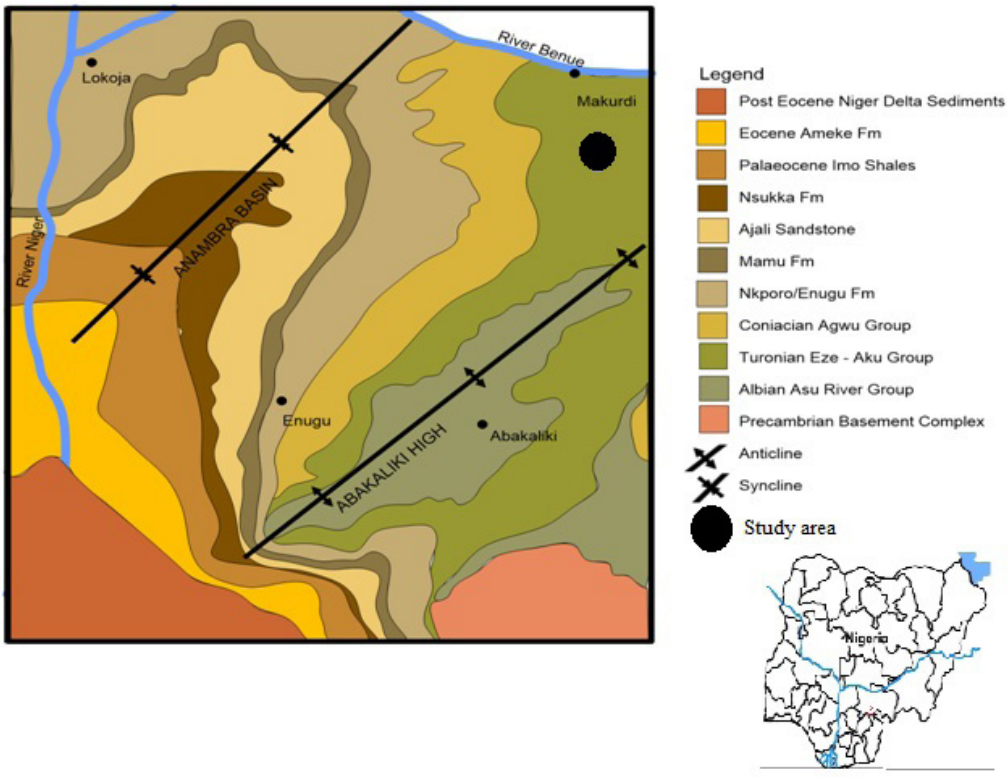

Figure 1. Modified after [16]

DOI: https://doi.org/10.30564/jgr.v3i3.3197

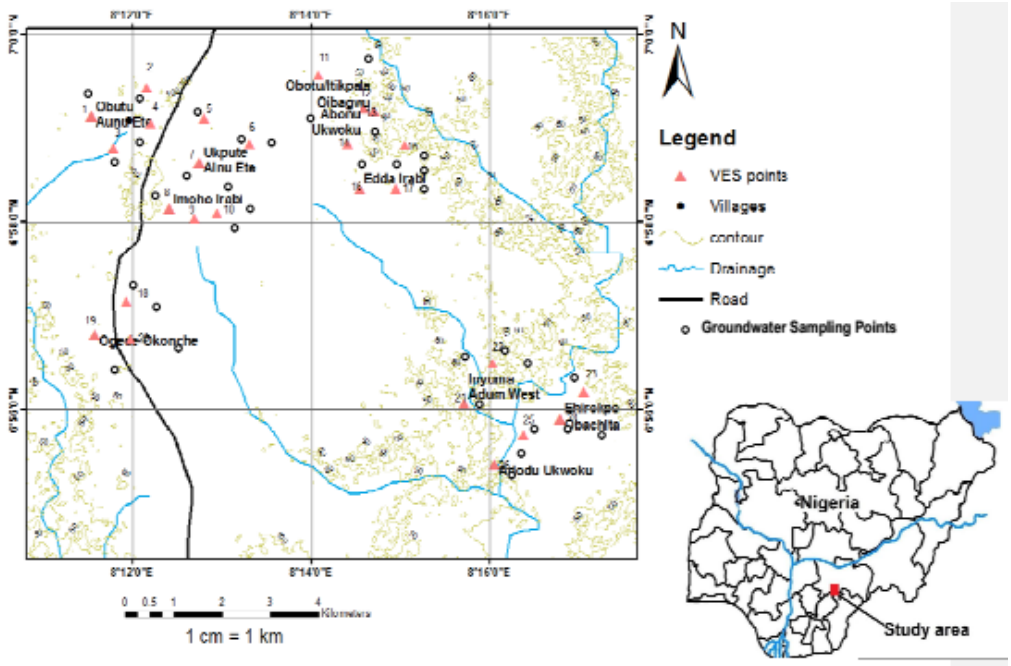

Figure 2. Topography Map of the study area showing VES points.

curves. The IX1D software was used to enhance VES data obtained from the field, with this we were able to generate sounding curve. Information from sounding curve was used to produce geoelectric section. According to report by [36] some parameters related to the different combinations of thickness and resistivity of the geoelectric layer are important for the analysis was used in understanding of the geologic model. The parameters are Dar Zarrouk Longitudinal conductance (*S*), Longitudinal Resistance (ρL), and Transverse Unit Resistance (*Rt*), respectively, as shown in equations 2 to 6 respectively.

$$S = \frac{h}{p} \tag{2}$$

$$T = hp \tag{3}$$

Longitudinal unit conductance (S) was calculated from the formula given below. For 'n' layers, the total longitudinal conductance is

$$S = \sum_{i=1}^{n} \frac{h_i}{\rho_i} = \frac{h_i}{\rho_i} + \frac{h_2}{\rho_2} + \ldots + \frac{h_n}{\rho_n} \tag{4}$$

as proposed by [22,17]

Transverse unit resistance (T) was calculated for the equation given below.

The total transverse unit resistance is

$$Rt = \sum_{i=1}^{n} h_i\rho_i = h_i\rho_i + h_2\rho_2 + \ldots + h_n\rho_n \tag{5}$$

as proposed by [17,37]

Longitudinal resistance was computed for shown below. The longitudinal resistivity is

$$\rho_L = \frac{H}{S} = \frac{\sum_{i=1}^{n} h_i}{\sum_{i=1}^{n} \frac{h_i}{\rho_i}} \tag{6}$$

as proposed by [12]

Groundwater Sampling

Physicochemical parameters were determined using appropriate titrimetric methods described by America Public Health Association [38] standard method see Table 2. A total of 34 groundwater was randomly sampled for physicochemical properties within the study area as shown in Figure 2 and Table 5.

Table 1. Hydrogeochemical Indices

Parameters	Equation Parameters were calculated in (meq/L)	Equation Number	References
Soltan Classification	$r1 = (Na^+ - Cl^-)/SO_4^{2-}$	7a	[39]
	$r2 = [(K^+ + Na^+) - Cl^-)]/SO_4^{2-}$	7b	
Gibbs Plots	Cations $Na^+/(Na^+ + Ca^{2+})$	8a	[40]
	Anions $Cl^-/(Cl^- + HCO_3^-)$	8b	
Chadba Plots	$HCO_3^- - (Cl^- + SO4^{2-} + NO_3^-)$	9a	[41]
	$Ca^{2+} + Mg^{2+}/(Na^+ + K^+)$	9b	

Table 2. Method used to analyze physicochemical parameters.

S/No	Parameters	Analytical Method
1	pH	pH meter HachsensION + PH1 portable pH meter and Hachsens ION + 5050 T Portable Combination pH Electrode
2	Electrical Conductivity (EC)	HACH conductivity
3	Total dissolved solids (TDS)	TDS meters (model HQ14D53000000, USA).
4	Magnesium (Mg^{2+})	EDTA titrimetric method
5	Calcium (Ca^{2+})	Titrimetric method
6	Chloride (Cl^{-})	Titrimetric method
7	Nitrate (NO_3^{-})	Ion-selective electrode (Orion 4 star)
8	Sulphate (SO_4^{2-})	Turbidimetric method using a UV-Vis spectrometer
9	Potassium (K^{+})	Jenway clinical flame photometer (PFP7 model)
10	Sodium (Na^{+})	Jenway clinical flame photometer (PFP7 model)
11	Bicarbonate (HCO_3^{-})	Titrimetric method

Table 3. Representative results of interpreted layer parameters from the study area

VES	Layer resistivity (ohm-m)						Depth (m)						Curve Type	No of layers
	ρ1	ρ2	ρ3	ρ4	ρ5	ρ6	d1	d2	d3	d4	d5	d6		
VES-01	399.9	169.5	1.21	183.9	9.3	∞	1.6	9.7	10.2	53.3	∞		H	5
VES -02	164.2	149.1	18.6	1566.9	8.5	∞	0.5	5.3	13.6	19.1	∞		QH	5
VES -03	333.6	147.5	8.2	1213.3	∞		1.4	17.0	27.1	∞			KH	4
VES-04	533.2	175.4	12.4	1229.0	690.1	∞	2.2	8.6	9.0	28.8	∞		H	5
VES-05	1488.9	540.1	125.3	319.7	2.3	∞	0.6	3.0	9.6	24.5			HK	5
VES -06	1335.4	47.7	966.9	8.4	1010.7	8.9	0.6	1.7	2.3	2.9	15.7	∞	HK	6
VES-07	3111.7	125.2	442.1	272.0	55.8	9188.6	0.6	0.9	3.8	16.2	50.1	∞	QQA	6
VES-08	313.5	24.2	1008.5	6.8	∞		2.4	6.6	15.0	∞			HK	4
VES -09	3195.5	338.6	1255.6	105.4	∞		0.8	7.1	23.23	∞			HK	4
VES -10	333.7	63.8	13.5	1850.7	∞		4.3	14.5	46.1	∞			HK	4
VES-11	1644.5	135.6	2143.9	48.0	∞		2.1	5.7	20.0	∞			HK	4
VES-12	629.0	154.2	2059.3	209.8	760.2	65.2	0.8	2.3	2.5	11.1	23.3	∞	HK	6
VES -13	1073.1	447.6	186.0	7304.9	48.8	∞	0.5	3.9	10.8	27.5	∞		HK	5
VES -14	275.5	710.2	4.8	484.9	72.6	7196.5	0.8	3.3	3.6	24.6	89.1	∞	QQ	6
VES -15	973.8	173.2	1585.0	6.8	∞		3.9	11.2	32.0	∞			HK	4
VES -16	369.9	139.6	15.3	545.6	5.7	∞	0.5	3.3	14.7	19.4	∞		H	4
VES -17	789.2	768.5	82.2	805.9	56.9	∞	1.7	5.1	8.4	26.7	∞		HK	4
VES -18	533.2	175.4	12.4	1229.0	690.1	∞	2.2	8.6	9.0	28.8	∞		H	5
VES -19	970.6	336.3	133.5	79.6	0.9	∞	1.6	2.0	11.8	56.9	∞		Q	5
VES -20	551.2	1.7	456.1	6.1	420.7	27.6	0.5	0.6	2.6	3.9	16.8	∞	HKQ	6
VES -21	1488.9	540.1	125.3	319.7	2.3	∞	0.6	3.0	9.6	24.5	∞		HK	5
VES -22	164.9	33.3	187.1	5.3	∞		0.9	19.4	43.2	∞			HK	4
VES -24	804.2	129.2	76.0	7458.1	∞		0.6	8.5	63.3	∞			QH	4
VES -25	132.8	30.1	102.6	1.0	171.9	∞	1.6	5.5	15.6	16.8	∞		HKA	5
VES -26	859.8	456.4	89.5	16183	550.6	∞	0.9	3.8	9.1	21.1	∞		H	5

DOI: https://doi.org/10.30564/jgr.v3i3.3197

3. Results

Resistivity, Thickness and Depth

Table 4. Results of Dar-Zarrouks Parameter

Sampling Code	Longitudinal conductance (S)	Transverse resistance(T)	longitudinal resistivity (ρL)
VES-01	0.16	8603.26	611.77
VES -02	0.48	103.64	3428.3
VES -03	1.33	2798.3	478.4
VES-04	0.09	26594.12	15565.67
VES-05	0.78	5677.90	215.41
VES -06	0.10	13801.	3367.05
VES-07	0.77	3352.2	1080.06
VES-08	0.18	9391.45	1398.7
VES -09	0.03	25121.55	5915.3
VES -10	2.50	2532.4	438.75
VES-11	0.03	7014.88	4058.3
VES-12	0.06	12309.7	65731.68
VES -13	0.04	125475.7	2578.36
VES -14	0.98	16892.46	2063
VES -15	0.72	22020.7	593.34
VES -16	0.05	37914.4	1148.97
VES -17	0.77	3352.2	1080.06
VES -18	0.069	18724.4	2470.81
VES -19	0.07	26594.07	15564.7
VES -20	0.05	18470.9	14789.7
VES -21	0.65	18440.5	1239.37
VES -22	0.46	6743.77	1435.01
VES -24	0.65	5234.62	407.36
VES -25	1.31	3275.07	268.07
VES -26	0.05	196417.8	17437.75

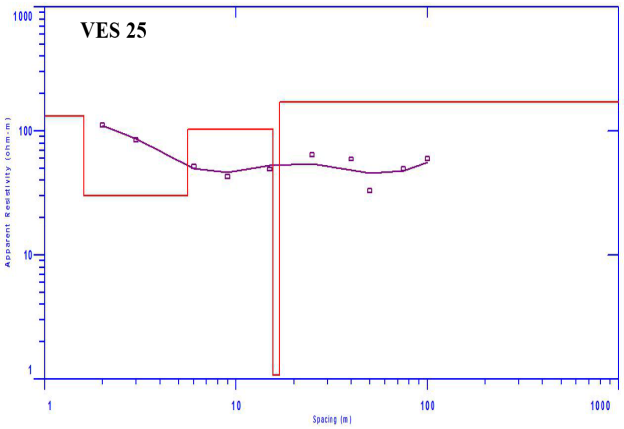

Figure 3. VES points at Ehirekpe Obachite

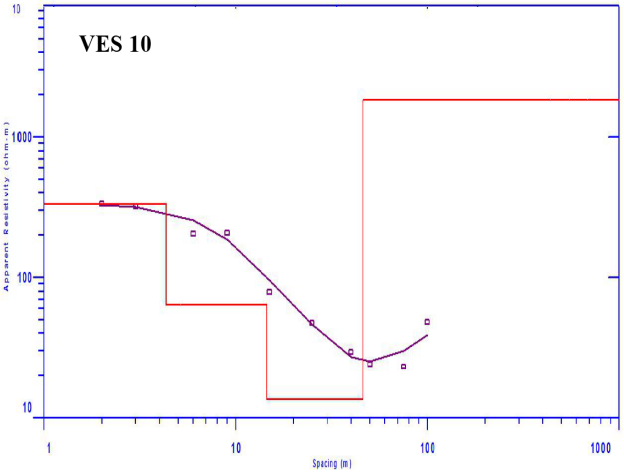

Figure 4a. VES points at Adum West

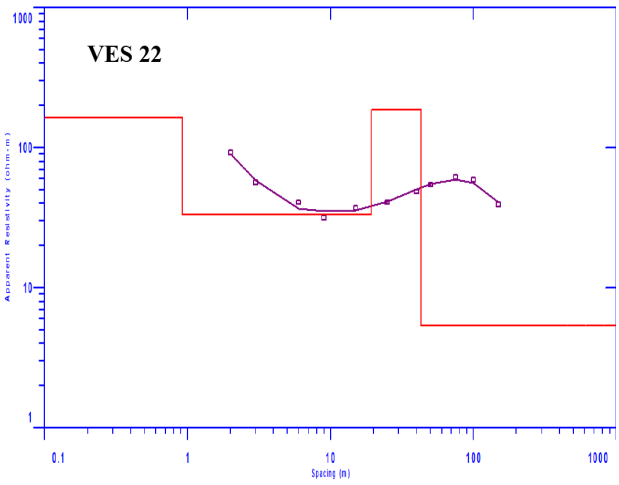

Figure 4b. VES points at Obutu Aunu Ete

 DOI: https://doi.org/10.30564/jgr.v3i3.3197

Table 5. Results of physicochemical Parameters.

Sampling points	Ec (µS/cm)	pH	TDS (mg/L)	Na^+ (meq/L)	K^+ (meq/L)	Mg^{2+} (meq/L)	Cl^- (meq/L)	HCO_3^- (meq/L)	SO_4^{2-} (meq/L)	NO_3^- (meq/L)	Ca^{2+} (meq/L)
GT-1	849	6.3	264	2.11	0.09	0.68	0.01	0.02	0.00	0.01	0.30
GT-2	495	6.9	163	1.94	0.40	0.57	0.00	0.07	0.02	0.01	0.10
GT-3	693	6.5	375	0.84	0.81	0.89	0.00	0.11	0.01	0.02	0.05
GT-4	930	7.2	616	0.39	0.74	1.87	0.09	0.09	0.22	0.04	0.01
GT-5	1034	7.3	270	1.42	0.25	2.68	0.02	0.21	0.30	0.01	0.02
GT-6	442	6.2	104	2.70	0.14	1.98	0.06	0.04	0.12	0.03	0.04
GT-7	630	6.6	759	0.87	0.10	1.89	0.03	0.06	0.11	0.02	0.07
GT-8	393	7.1	1055	1.37	0.05	0.96	0.11	0.03	0.07	0.01	0.01
GT-9	701	7.3	386	1.47	0.03	0.55	0.07	0.09	0.10	0.03	0.02
GT-10	1003	7.5	200	1.58	0.07	0.71	0.21	0.23	0.04	0.04	0.08
GT-11	920	6.9	145	1.21	0.50	0.68	0.03	0.01	0.02	0.05	0.01
GT-12	829	6.5	707	1.41	0.06	0.96	0.00	0.08	0.01	0.02	0.02
GT-13	611	6.3	79	1.02	0.02	1.84	0.21	0.05	0.03	0.06	0.03
GT-14	502	6.9	546	1.07	0.08	1.65	0.20	0.14	0.06	0.04	0.04
GT-15	417	7.3	239	0.91	0.04	0.08	0.10	0.10	0.01	0.03	0.06
GT-16	696	7.0	132	1.31	0.07	0.64	0.00	0.42	0.05	0.02	0.01
GT-17	1211	6.7	435	2.17	0.02	0.78	0.05	0.41	0.08	0.03	0.03
GT-18	920	6.8	233	1.82	0.10	0.13	0.11	0.21	0.01	0.01	0.05
GT-19	834	6.9	637	0.91	0.05	0.68	0.06	0.07	0.04	0.03	0.04
GT-20	794	6.4	108	1.23	0.03	0.02	0.07	0.15	0.01	0.02	0.02
GT-21	401	6.5	113	1.47	0.06	1.96	0.04	0.06	0.06	0.13	0.01
GT-21	923	6.6	806	0.43	0.04	0.57	1.00	0.08	0.13	0.02	0.02
GT-22	581	6.8	459	1.82	0.16	0.12	0.63	0.10	0.21	0.02	0.06
GT-23	702	6.9	186	1.45	0.02	0.85	1.06	0.03	0.23	0.03	0.07
GT-24	1008	6.6	865	1.20	0.01	0.42	0.05	0.18	0.01	0.02	0.01
GT-25	933	6.9	380	0.82	0.11	1.86	0.08	0.22	0.02	0.01	0.03
GT-26	789	6.7	93	0.31	0.14	2.01	0.05	0.03	0.11	0.04	0.05
GT-27	1092	6.6	860	0.49	0.03	0.79	1.00	0.19	0.02	0.03	0.04
GT-28	1001	7.0	115	1.60	0.08	1.98	0.96	0.04	0.13	0.01	0.06
GT-29	729	7.1	329	1.82	0.10	0.64	0.06	0.02	0.02	0.03	0.02
GT-30	482	6.9	84	0.74	0.06	0.22	0.00	0.12	0.03	0.01	0.01
GT-31	509	6.5	101	1.65	0.04	1.07	0.07	0.10	0.01	0.02	0.05
GT-32	802	6.8	174	0.58	0.06	0.64	0.06	0.07	0.10	0.02	0.07
GT-33	915	6.7	108	1.04	0.14	0.12	0.64	0.18	0.11	0.01	0.01
GT-34	804	6.6	579	0.84	0.05	1.07	0.03	0.21	0.03	0.10	0.03
Min	393	6.2	79	0.31	0.01	0.02	0	0.01	0	0.01	0.01
Max	1211	7.5	1055	2.7	0.81	2.68	1.06	0.42	0.3	0.13	0.3
Stan Dev.											
WHO, 2010	1400	6.5-8.5	500	200	2.0	150	600	**	400	50	

DOI: https://doi.org/10.30564/jgr.v3i3.3197

Table 6. Computed Values of Hydrogeochemical Parameters

Sampling points	Soltan Classification		Gibbs		Chadba Plot	
	r1	r2	Cations	Anions	Cations	Anions
GT-1	0	0	0.87	0.33	-1.22	0
GT-2	1.92	117	0.95	0	-1.67	0.04
GT-3	84	165	0.94	0	-0.71	0.08
GT-4	1.36	4.94	0.97	0.5	0.75	-0.26
GT-5	1.1	5.5	0.98	0.08	1.03	-0.12
GT-6	7.63	23.1	0.98	0.6	-0.82	-0.17
GT-7	7.6	8.54	0.92	0.33	0.99	-0.1
GT-8	18	18.7	0.99	0.78	-0.54	-0.16
GT-9	14	14.3	0.98	0.43	-0.93	-0.11
GT-10	34.25	36	0.95	0.47	-0.86	-0.06
GT-11	59	84.5	0.99	0.75	-1.02	-0.09
GT-12	141	1.46	0.98	0	-0.49	0.05
GT-13	27	27.66	0.97	0.8	0.83	-0.25
GT-14	14.5	15.83	0.96	0.58	0.54	-0.16
GT-15	13.5	85	0.93	1	-0.81	-0.04
GT-16	26.2	27.6	0.99	0	-0.73	0.35
GT-17	26.5	26.75	0.98	0.1	-1.38	0.25
GT-18	1.7	181	0.97	0.34	-1.74	0.08
GT-19	0.81	22.5	0.95	0.46	-0.26	-0.06
GT-20	1.15	119	0.98	0.31	-1.22	0.05
GT-21	1.37	24.83	0.99	0.66	0.44	-0.17
GT-21	-0.7	-0.04	0.95	0.92	0.12	-1.07
GT-22	0.98	6.42	0.96	0.86	-1.8	-0.76
GT-23	0.16	1.78	0.95	0.97	-0.55	-1.29
GT-24	1.14	116	0.99	0.21	-0.78	0.1
GT-25	37	42.5	0.96	0.26	0.96	0.11
GT-26	0.15	3.63	0.86	0.62	1.61	-0.17
GT-27	-0.53	-24	0.92	0.84	0.31	-0.86
GT-28	4.92	5.53	0.96	0.96	0.36	-1.06
GT-29	88	93	0.99	0.75	-0.26	-0.09
GT-30	24.66	26.67	0.98	0	-0.57	0.08
GT-31	158	162	0.97	0.41	-0.57	0
GT-32	52	5.8	0.89	0.46	0.07	-0.11
GT-33	3.63	4.9	0.99	0.78	-1.07	-0.58
GT-34	27	28.67	0.96	0.14	0.21	0.05

4. Discussion

Previous scholars have successfully used the integration of application VES and hydrogeochemical studies in identification of aquifer's geometry, lithology and groundwater quality [42,43].

Dar-Zarrouk Parameters of the Study Area

Equations 2-6 was used to derive aquifer protective capacity and area of with high groundwater potential, estimated results obtained from aforementioned equations is presented in Table 4.

Longitudinal Conductance (*S*)

S is one of the Dar Zarrouk parameters used to determine aquifer vulnerability. According to [44] *S* evaluates the attribute of a conducting layer in contrast with the transverse resistance in determining the characteristics of resisting layer. [12] were of the view that an area with low S value signifies poor and weak aquifer protective zone and considered to be susceptible to contamination, while an area with high *S* value signifies high protective area. The highest value of *S* was observed at VES location 10 with value of 2.5 mhos and the least *S* was observed at VES location 9 with value of 0.03 mhos as shown in Figure 5. From Table 7, it was observed that 42 % of VES points fell within moderate category, 38 % fell within poor category and lastly, 20 % fell within weak category. A similar conducted by [12] at sub-urban area of Abakaliki revealed that aquifer vulnerability ranges from moderate, weak and poor. [45] were of the view that aquifer if given protection by sufficient thickness and local geology layers which is referred to protective layer.

Table 7. Aquifer protective capacity of the study area against [45]

Rating	Remarks	Remarks
> 10	Excellent	
5-10	Very good	
0.2-4.9	Moderate	VES-02, 03, 05, 07, 10, 13, 14, 15, 17, 21, 22, 23, 24, 28
0.1-0.19	Weak	VES-01, 08, 12, 19, 26, 27
<0.1	Poor	VES-04, 09, 06, 11, 12, 13, 16, 18, 20, 25

DOI: https://doi.org/10.30564/jgr.v3i3.3197

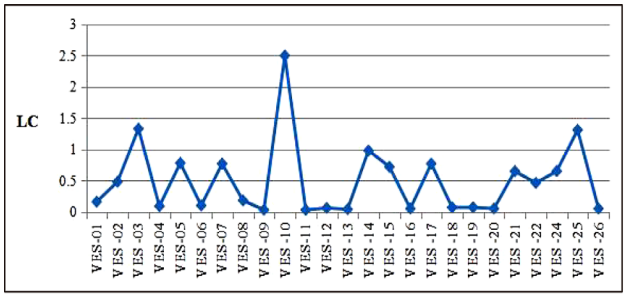

Figure 5. Barchart of LC against VES points.

Transverse Unit Resistance (*Rt*)

Rt value for this study ranges from 103.64 at VES-2 to 196417.8 Ω/m^2 at VES-25 see Table 6. It has been observed that the transmissivity of water bearing unit is directly proportional to its transverse resistance. Hence, high Rt values correspond to high transmissivity values and vice versa. The high transmissivity values however, suggest that the water bearing units of the formation are highly permeable, porous and freely allow fluid movement within the aquifer, which possibly may enhance the migration and circulation of contaminants in the groundwater aquifer system while low transmissivity is suggestive of high percentage of impervious clay which retards fluid movement within the aquifer.

Longitudinal Resistance (ρL).

The estimated value of ρL ranges from 215.41 at VES location 5 to 65731.68 Ω-m at VES location 12. ρL [17] were of the view that variation in ρL value can be use to demarcates the saline, brackish and fresh water aquifers into three different regions based on their attained magnitudes.

Hydrogeochemical Assessment of Groundwater Quality

Hydrogeochemical model such as Gibbs, Chadba and Soltan derive from equation 7 to 9 was used to characterize groundwater within the study area. According to [46] groundwater experiences series of chemical reactions and impact processes as it moves from one region to another below the subsurface, Therefore hydrogeochemical assessment of groundwater is essentially mandatory to characterize groundwater in order to know the what it can be used for.

Gibbs Plot

Gibb's plot is used to be establish the relationship and the chemical constituent of groundwater and their respective aquifer such as rock chemistry, precipitation and evaporation rate. Gibb's plot is usually a plot of cations and anions against total dissolved solid. The plot is a ratio of [$(Na^+)/ (Na^+ + Ca^{2+})$] and other ratio for [$Cl^-/(Cl^- + HCO_3^-)$]. From Figure 6 it was observed that the major factor that influences groundwater chemistry is rock water interaction. This is in line with previous study conducted by [47] which stated rock water interaction is a major player in groundwater chemistry.

Chadba Plot

[2] acknowledge that groundwater can be characterized using different kinds of hydrogeochemical model

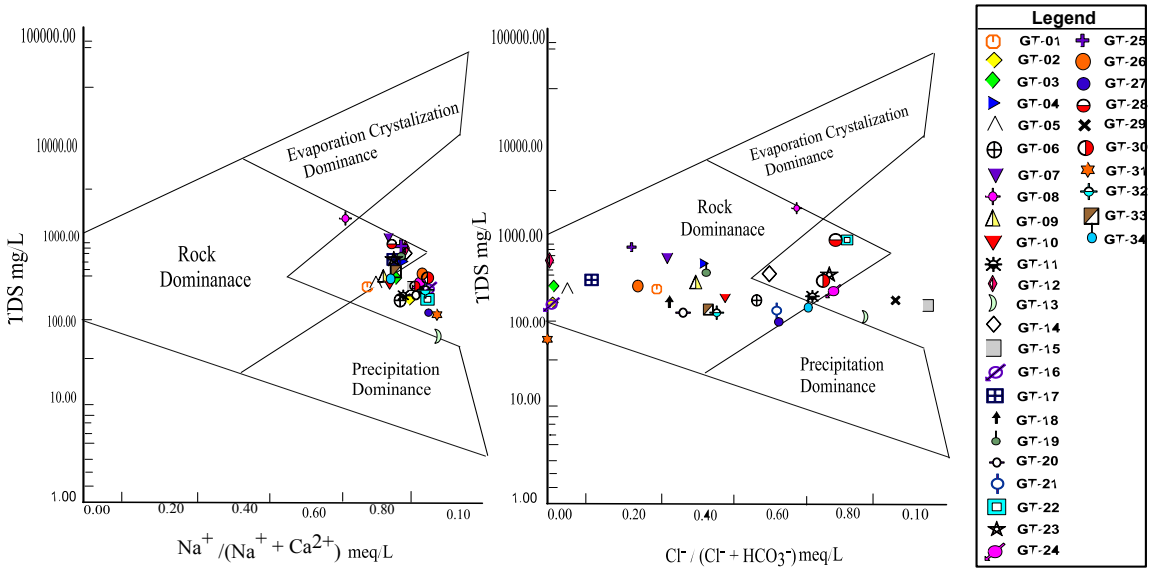

Figure 6. Gibb's Plot of Groundwater geochemistry.

DOI: https://doi.org/10.30564/jgr.v3i3.3197

an example "the Chadba plot can be used to characterize groundwater." This plot is used in interpreting groundwater evolution trends and also aid in understanding groundwater geochemistry. It is a cross-plot such as $Ca^{2+} + Mg^{2+}$ ($SO_4^{2-} + HCO_3^-$) versus $Na^+ + Cl^-$, $Na^+ + K^+$ versus total cation and Na^+ versus Cl^-. According to [48] the plot is used to characterize water into two major category temporary and permanent hardness. For this study groundwater fell within four categories namely; $Na^+ + HCO_3^-$, $Ca^{2+} + Mg^{2+} + HCO_3^-$, $Na^+ + Cl^-$ and $Ca^{2+} + Mg^{2+} + Cl^-$ water type as shown in Figure 7. From Figure 7 it was observed that sample locations GT- 04, 05,07, 13, 14, 17, 18, 21, 26, 27, 28 and 32 is groundwater with alkali metals exceed alkaline earth and weak acidic exceed string acidic anion. While sample locations GT-25 and 34 were classified as groundwater that showed alkaline earhs and weak acidic exceed both alkali metals and strong acidic anions'. It' is dominantly represented as $Ca^{2+} + Mg^{2+} + HCO_3^-$. Sample location GT- 06, 08, 09, 10, 11, 15, 19, 22, 23, 24 and 29 was categorize to be dominated by $Na^+ + Cl^-$. Lastly, sample locations GT-01, 02, 03, 12, 16, 20, 24, 30 and 31 is dominantly said to be of $Ca^{2+} + Mg^{2+} + Cl^-$ water type.

Soltan Classification

[39] classified groundwater based on Cl^-, $SO42^-$ and $HCO3^-$ concentrations. From Table 6. It was observed that sample locations GT-1, 19, 21, 22, 23, 26 and 27 were classified to be $Na^+SO4_2^-$ water type, while ample locations GT-2, 3, 4, 5, 6, 7, 8, 9, 10, 11, 12, 13, 14, 15, 16, 17, 18, 20, 21, 25, 28, 29, 30, 31, 32, 33and 34 were classified to Na^+. HCO_3^- water type. Findings from Table 6 revealed that sample locations GT-1 and 21 is classified to be of deep meteoric water percolation type that implies that the groundwater is influenced by precipitation [47]. While sample locations GT-2, 3, 4, 5, 6, 7, 8, 9, 10, 11, 12, 13, 14, 15, 16, 17, 18, 19, 20, 22, 23, 24, 25, 26, 27, 28, 29, 30, 31, 32, 33 and 34 fell within shallow meteoric water.

Comparison of Groundwater Quality to WHO, (2010) Set Limit Standard

The value of Ec for this study ranges from 393 to 1211µS/cm, the highest concentrations of Ec was observed at sample location GT-17 with Ec value of 1211 µS/cm with least value of 393 µS/cm at sample location GT-8 as shown in Figure 8. The high concentration of Ec in groundwater around GT-17 can be attributed to the fact that groundwater is in contact with more dissolved inorganic constituents [48]. [49] reported that high concentration of Ec depends on temperature and type of ions present in groundwater.

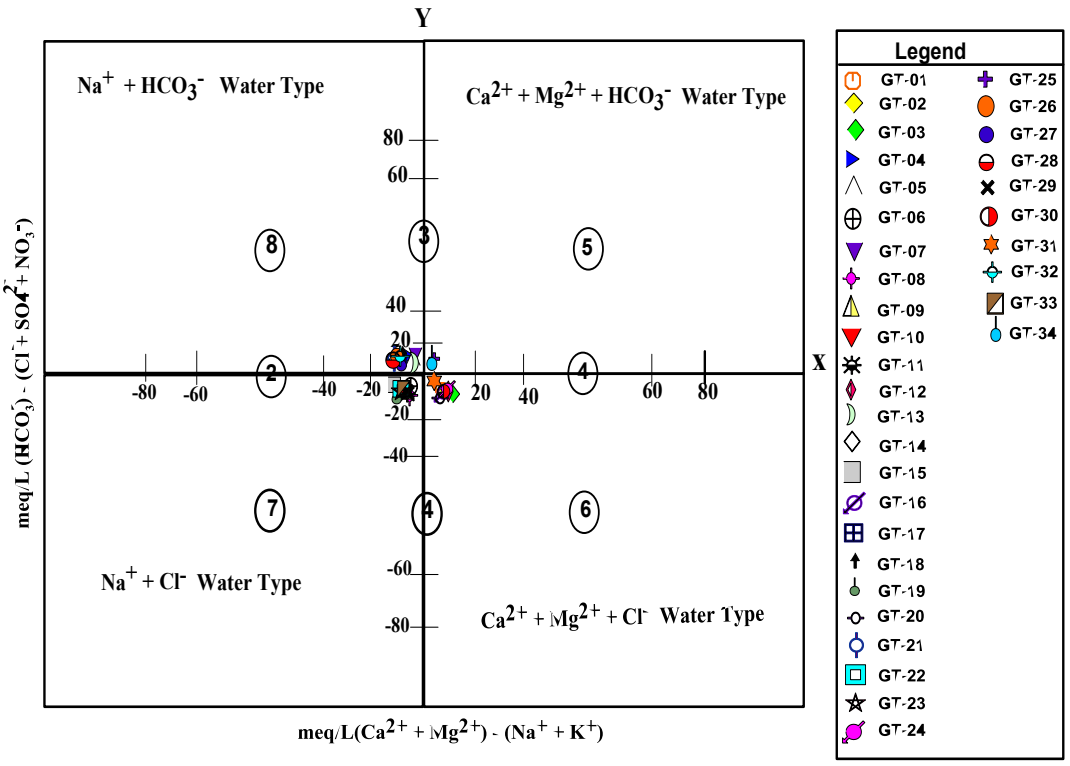

Figure 7. Chadba's diagram showing groundwater type of the study area.

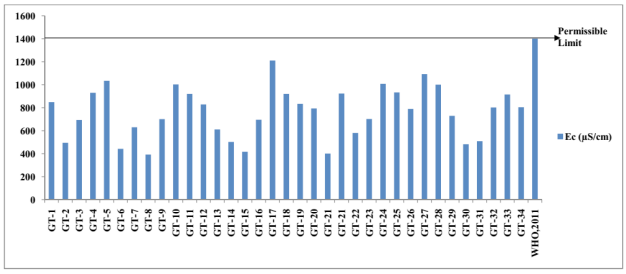

Figure 8. Plots of Ec against WHO, (2011)

pH of water is one of the major factors that provide needed information on groundwater geochemical equilibrium [50]. pH value for this study ranges from 6.2 to 7.5 with the lowest concentration of pH at sample location GT-6 with a value of 6.2.While the highest pH value was observed at sample location GT-10 with value of 7.5 as shown in Figure 9. High concentration of pH in groundwater could be attributed to aquifer configuration and other geological or anthropogenic factors [51]. pH values obtained from the study revealed that groundwater ranges from acidic to basic.

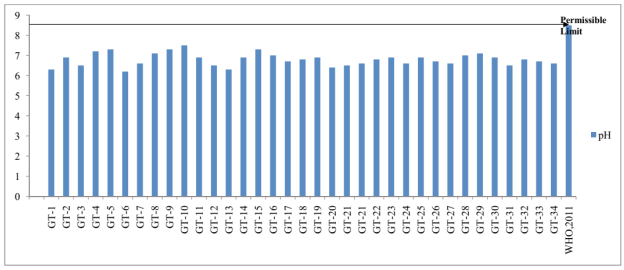

Figure 9. Plots of pH against WHO, (2011)

Total Dissolved Solid (TDS)

TDS measure the overall concentration of all mineral makeup dissolved in water. [52] reported that TDS is linked to water hardness. From Figure 10. It was observed that sample locations GT- 4, 7, 8, 12, 14, 19, 21, 24, 27 and 34 were above the [53] permissible limit. According to [54] the presence of high concentration of TDS in groundwater can be attributed to water waste discharge. Similarly, [55] further reported that high concentration of TDS in groundwater can also be attributed to geological activities, agricultural, human and industrial waste respectively.

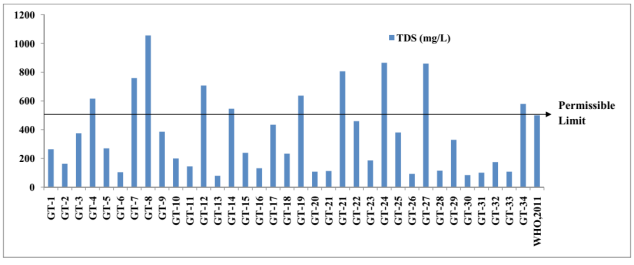

Figure 10. Plots of TDS against WHO, (2011)

5. Conclusions

Since there is a steady increase in demand for groundwater and decline on groundwater quality due to contamination that infiltrate from the surface into subsurface water (groundwater). It is of upmost importance to constantly monitor groundwater from time to time. Hence to an integrated approach was used to assess groundwater vulnerability and a major factor that influence its geochemistry. The use of VES was to determine aquifer vulnerability and groundwater potential, while hydrogeochemical studies were used to evaluate the major factors that influences groundwater chemistry and also characterize groundwater within the study area. Deduction from VES showed that the study area is underlain by four (4) to six (6) lithology. Result obtained from longitudinal conductance suggested that aquifer protective capacity fell within poor to moderate category". That implies that aquifer is considered vulnerable to contamination from the surface. Further findings suggested that VES location 2 showed more prospect of high groundwater potential when compared to other part of the study area." Findings from hydrogeochemical analysis revealed that groundwater is influenced mainly by rock water interaction. It was also observed that groundwater is characterized to be temporary to permanent hard. Findings from pH results showed that groundwater fell within slightly acidic to basic category.

References

[1] Shiklomanov, I. A. (1998). Global renewable water resources. In: Zebedi H (ed) Water: a looming crises? Proceeding of the international Conference on World water Resources at the beginning of the 21st century. Unesco/IHP, Paris, pp 1-25.

[2] Eyankware, M. O.,Aleke, C. G., Selemo, A. O. I., Nnabo, P. N. (2020a). Hydrogeochemical studies and suitability assessment of groundwater quality for irrigation at Warri and environs., Niger delta basin, Nigeria. Groundwater for Sustainable Development. DOI: https://doi.org/10.1016/j.gsd.2019.100293.

[3] Healy, R. W., Winter, T. C., LaBaugh, J. W., Franke, O. L. (2007). Water budgets: foundations for effective water-resources and environmental management. USGS Report, Circular 1308.

[4] Krishnaraj S., Vijayaraghavan, K., Murugesan V., Rajivgandhi, R., Sarma, V. S. (2011). Integrated techniques to identify groundwater vulnerability to pollution in a highly industrialize terrain, Tamilnadu, India.Environ Monit Assess 182:47-60. DOI: 10.1007/s10661-010-1857-x.

[5] De Ketelaere D, Hotzl H, Neukum C, Civita M,

DOI: https://doi.org/10.30564/jgr.v3i3.3197

Sappa G (2004). Hazard analysis and mapping. In F. Zwahlen (Ed.), Vulnerability and risk mapping for the protection of carbonate (karst) aquifers. Final report COST Action 620. European Commission, Directorate-General for Research, EUR 20912:86-105.

[6] Olayinka, A. I, Olorunfemi, M. O. (1992). Determination of geoelectric characteristics of Okene area and implication for boreholes siting. J Min Geol 28:403-412.

[7] Oladapo, M. I., Akintorinwa, O. J. (2007). Hydrogeophysical study of Ogbese Southwestern, Nigeria. Global J Pure and Applied Sci 13(1):55-61.

[8] Kai, S., Guangxu, Y., Fei W., Jian, L., Dan, L. (2020). Application of Geophysical and Hydrogeochemical Methods to the Protection of Drinking Groundwaterin Karst Regions. International Journal of EnvironmentalResearch and Public Health. 17, 3627. DOI: 10.3390/ijerph17103627.

[9] Olorunfemi, M. O., Fasuyi, S. A. (1993). Aquifer types, geoelectric and hydrogeologic characteristics of part of the Central Basement Terrain of Niger State Nigeria. J Afr Earth Sci 16(1):309-317.

[10] Chambers JF, Wilkinson PB, Penn S,Meldrum PI, Kuras O, Loke MH, Gunn DA.(2013).River terrace sand and gravel depositreserve estimation using three-dimensionalelectrical resistivity tomography forbedrock surface detection. J. Appl.Geophy. 2013;93:25-32.

[11] Orlando L.(2013). Some considerations onelectrical resistivity imaging forcharacterization of waterbed sediments. J.Appl. Geophy. 2013;95:77-89.

[12] Eyankware, M.O.,Ogwah, C., Selemo, A. O. I. (2020b). Geoelectrical parameters for the estimation of groundwater potential in fracture aquifer at sub-urban area of Abakaliki, SE Nigeria. International Journal of Earth Science and Geophysics. 6:031, https: // doi: 10.35840/2631-5033/1831.

[13] Ebong, D. E., Anthony, E. A., Anthony, A. O. (2014). Estimation of geohydraulic parameters from fractured shales and sandstone aquifers of Abi (Nigeria) using electrical resistivity and hydrogeologic measurements. Journal of African EarthSciences 96: 99-109.

[14] Eduvie, M. O. (2002). Hydro-geological geophysicalevaluation of groundwater resources of the gundumiformation and around Daura, North Western Nigeria, Water Resources. Journal of Nigeria Associationof Hydro-geologist (NAH) 13: 46-49.

[15] Eyankware, M. O., Selemo, A. O. I., Obasi, P. N., Nweke, O.M. (2020c). Evaluation of groundwater vulnerability in fractured aquifer using geoelectric layer susceptibility index at Oju, Southern Benue Trough Nigeria. Geological Behavior, 4(2): 63-67.

[16] Nwajide, C. S. (2013). Geology of Nigeria‟s Sedimentary Basin. CSS Bookshops Ltd Lagos, pp. 56- 98.

[17] Oli, I. C., Ahairakwem, C. A., Opara, A. I., Ekwe, A. C., Osi-Okeke, I., Urom, O. O., Udeh, H. M., Ezennubia, V. C. (2020) Hydrogeophysical assessment and protective capacity of groundwater resources in parts of Ezza and Ikwo areas, southeastern Nigeria. International Journal of Energy and Water Resources. https://doi.org/10.1007/s42108-020-00084-3.

[18] Hasan, M., Shang, Y., Akhter, G., and Jin, W. (2017). Geophysical assessment of groundwater potential: a case study from Mian Channu Area, Pakistan. Groundwater, 56, 783-796.

[19] Uma, K.O. (1989). An appraisal of the ground waterResources of the Imo River Basin. Nigerian Jour. Mining and Geol., 25:305-315.

[20] Batte, A. G., Barifaijo, E., Kiberu, J. M., Kawule, W., Muwanga, A., Owor, M., Kisekulo, J. (2010). Correlation of Geoelectric Data with Aquifer Parameters to Delineate the GroundwaterPotential of Hard rock Terrain in Central Uganda. Pure Appl. Geophys. 167, 1549-1559.DOI 10.1007/s00024-010-0109-x.

[21] Sikandar, P. and Christen, E.W. (2012). Geoelectrical sounding for the estimation of hydraulic conductivity of alluvial aquifers. Water Resources Management, 26, 1201-1215.

[22] Asfahani, J. (2013). Groundwater potential estimation using vertical electrical sounding measurements in the semi-arid Khanasser Valley region, Syria. Hydrological Sci. J. 58 (2), 468-482.

[23] Niwas, S. and Celik, M. (2012). Equation estimation of porosity and hydraulic conductivity of Ruhrtal aquifer in Germany using near surface geophysics. Journal of Applied Geophysics, 84, 77-85.

[24] Villumsen, A., Sonderskov, C. (1982). Vulnerability maps: a promising tool in groundwater protection. Aqua 5:466-468.

[25] Harter T Walker LG (2001) Assessing vulnerability of groundwater,3. Retrieved 30/8/2018 from https:// www.dhs.ca.gov/ps/ddwem/dwsap/DWSAPindex. html.

[26] Eyankware, M. O., Ephraim, B. E. (2021). A comprehensive review of water quality monitoring and assessment in Delta State, Southern Part of Nigeria. Journal of Environmental & Earth Sciences. 3(1); 16-28.

[27] EugeneOkorie, J. O, Obiora DN, Ibuot, JC, Desmond O. Ugbor, D. O. (2020). Geoelectrical investigation of groundwater potential and vulnerability of Oraifte, Anambra State, Nigeria. Applied Water Science,

10:223 https://doi.org/10.1007/s13201-020-01304-1.

[28] Ibuot. J. C., Okeke, F. N., George, N. J., Obiora, D. N. (2017). Geophysical and physicochemical characterization of organic waste contamination of hydrolithofacies in the coastal dumpsite of Akwa Ibom State, southern Nigeria. Water Sci Technol Water supply 17(6):1626-1637.

[29] Obiora, D. N., Ibuot, J. C., George, N. J. (2016). Evaluation of aquifer potential, geoelectric and hydraulic parameters in Ezza North, Southeastern Nigeria, using geoelectric sounding. Int J Environ Sci Technol. 13:435-444.

[30] Alhassan, D. U., Obiora, D. N., Okeke, F. N. (2015). The assessment of aquifer potentials and aquifer vulnerability of southern Paiko, northcentral Nigeria, using geoelectric method. Global J Pure Appl Sci 21:51-70.

[31] Eyankware, M.O.,Nnajieze, V.S., Aleke, C.G. (2018). Geochemical assessment of water quality for irrigation purpose, in abandoned limestone quarry pit at Nkalagu area, Southern Benue TroughNigeria. Environ Earth Science, https://doi.org/10.1007/s12665-018-7232-x.

[32] Murat, R. C. (1972). Stratigraphy and Paleogeography of the Cretaceous and lower Tertiary in Southern Nigeria. In Proc. of the Conf. on African Geology held at Ibadan, Nigeria. Pp. 251-266.

[33] Banejree L (1980). A Sub-tidal Bar Model for the Eze-Aku Sandstone, Sediment. Geology, 25:291-309.

[34] Amajor, L. C. (1987). The Eze-Aku Sandstone Ridges Turonian of Southeastern Nigeria: A Reinterpretation of their Depositional Origin. Nig. J. of Mining and Geo, 23(1):17-26.

[35] Reyment, R. A. (1965). Aspects of the Geology of Nigeria: The Stratigraphy of the Cretaceous and Cenozoic Deposits. Ibadan University Press.

[36] Zohdy, A. A. R., Eaton, G. P., Mabey, D. R. (1974). Application of surface geophysics to groundwater investigations. Washington: United State Geophysical Survey.

[37] Nwachukwu, S. R., Bello, R., Ayomide, O., Balogun, A. O., 2019.Evaluation of groundwater potentials of Orogun, South-South part of Nigeria using electrical resistivity method.Applied Water Sci. 9:184 https://doi.org/10.1007/s13201-019-1072-z.

[38] APHA (American Public Health Association), (2003), Standard methods for examination of water and wastewater specifications, Washington DC, 6, 19th edition.

[39] Soltan, M. E. (1999). Evaluation of groundwater quality in Dakhla Oasis (Egyptian Western Desert). Eviron Monit Assess 57:157-168.

[40] Gibbs, R. J (1970) Mechanisms controlling world water chemistry. Science, v.170, pp.1088-1090.

[41] Chadha, D. K. (1999). A proposed new diagram for geochemical classification of natural waters and interpretation of chemical data. Hydrogeol J 7:431-439.

[42] Aweto, K. E. (2012).Resistivity methods in hydro-geophysical investigation for groundwater in Aghalokpe, Western Niger Delta.Global Journal of Geological Science.11; 47-55.

[43] Ryan, Michael P., Pierce, Herbert A., Johnson, Carole D., Sutphin, David M., Daniels, David L., Smoot, Joseph P., Costain, John K., Çoruh, Cahit, and Harlow, George E. (2007). Reconnaissance borehole geophysical, geological and hydrological data from the proposed hydrodynamic compartments of the Culpeper Basin in Loudoun, Prince William, Culpeper, Orange and Fairfax Counties, Virginia. [Version 1.0]: U.S. Geological Survey Open File Report 2006-1203,3-42.

[44] Yungul, S. H., (1996). Electrical methods in geophysical explorationof sedimentary basin. Chapman and Hill, U.

[45] Olusegun OA, Adeolu OO, Dolapo FA (2016) Geophysical investigation for groundwater potential and aquifer protective capacity around Osun State University (UNIOSUN) College of Health Sciences. Am. J. Water Resour. 4(6):137-143. https://doi.org/10.12691/ajwr-4-6-3.

[46] Ojo, A. O., Oyelami, C. A., Adereti, A.O. (2014). Hydro-geochemical and geophysical Study of Groundwater in the Suburb of Osogbo, South Western Nigeria. J Earth Sci Clim Change 5: 205.
DOI: 10.4172/2157-7617.1000205.

[47] Eyankware, M.O., Nnabo, P.N., Ogwah, C. (2020d). Impact of past mining activity on water resources around active and abandoned mines in Ebonyi State, South-Eastern Nigeria- A mini review. Hydro Science and Marine Engineering, 2(2): 29-35.

[48] Eyankware, M.O., Selemo, A.O.I., Ogwah, C. (2019a). Use of modelling approach in evaluation of fractured shale aquifers for irrigation purpose; a case study of Oju, Lower Benue Trough Nigeria. Pakistan Journal of Geology. 3(1): 1-12.

[49] Adimalla N., Venkatayogi, S. (2018). Geochemical characterization and evaluation of groundwater suitability for domestic and agricultural utility in semi-arid region of Basara, Telangna State,South India. Appl Water Sci 8:44. https://doi.org/10.1007/s13201-018-0682-1.

[50] Hem, J. D. (1985). Study and interpretation of the chemical characteristics of natural water, 2nd edn. US Geol Surv Water Supply Paper, 2254:363.

DOI: https://doi.org/10.30564/jgr.v3i3.3197

[51] Prashant K., Prarabdh T., ArkoprovoB., Tapas, A. (2020). Geophysical and hydrogeological investigationfor the saline water invasion in the coastal aquifers of WestBengal, India: a critical insight in the coastal salineclay-sand sediment system. Environ Monit Assess, 192:562 https://doi.org/10.1007/s10661-020-08520-x.

[52] Eyankware, M. O., Omo-Irabor, O. O. (2019b). An Integrated Approach To Groundwater Quality Assessment In Determining Factors That Influence TheGeochemistry And Origin Of Sandstone Aquifers Southern Niger Delta Region Of Nigeria. Malaysian Journal of Geosciences, 3(2): 23-32.

[53] WHO (World Health Organization). (2011). Guideline for drinking water quality Recommendations, 4th Edition. Vol 1. Pp219-230.

[54] FEPA (1991). Federal Environmental Protection Agency Guideline and Standard for Environmental Pollution Control in Nigeria. pp. 25 -26.

[55] Appelo, C.A.J., Postma, D. (2005). Geochemistry, groundwater and pollution (Amsterdam: CRC Oress, Taylor & Francis Group).

 DOI: https://doi.org/10.30564/jgr.v3i3.3197

BILINGUAL PUBLISHING CO.
Pioneer of Global Academics Since 1984

Journal of Geological Research
http://ojs.bilpublishing.com/index.php/jgr-a

ARTICLE

Geochemistry of Volcanic Rocks of Beka, North East of Ngaoundéré (Adamawa Plateau, Cameroon): Petrogenesis and Geodynamic Context

Pauline Wokwenmendam Nguet[1*] Benjamin Ntieche[2] Joseph Legrand Tchop[1,3] Bouba Christian Mana[4] Eddy Ferdinand Mbossi[1,3]

1. Research Center for Geophysics and Volcanology, Institute of Geological and Mining Research, PO Box 370 Buea, Cameroon
2. Geology laboratory, Higher Teacher Training College, University of Yaoundé I, PO Box 47 Yaoundé, Cameroon
3. Department of Earth Sciences, Faculty of Sciences, University of Yaoundé I, PO Box 812 Yaoundé, Cameroon
4. Research Center for Geology and Mining, PO Box 333 Garoua, Cameroon

ARTICLE INFO

Article history
Received: 3 June 2021
Accepted: 28 June 2021
Published Online: 5 July 2021

Keywords:
Alkali lavas
Fractional crystallization
Partial melting
Spinel lherzolite
Volcanic zone within plate

ABSTRACT

Beka area is situated in the Adamaoua Plateau of Cameroon in central Arica. Lavas in this area has not been studied before the present work. The volcanism of Beka is characterized by basalt, trachyte and phonolite domes and flows. The petrographic study shows that basaltic lavas have porphyritic microlitic textures. The felsic lavas indicate trachytic textures. The rocks are composed of olivine, clinopyroxene, plagioclase and iron-titanium oxide minerals for the basalts; clinopyroxene, alkali feldspar (including foids), sphene and titanomagnetite for the felsic lavas. Chemical analyses show that basaltic lavas are basanites. Felsic lavas contain modal feldspathoid (nepheline in phonolites). All these lavas belong to the same series, because the felsic lavas are derived from the differentiation of basaltic lavas by fractional crystallization. They show an alkaline nature according to their geochemistry. Trace elements including Rare Earth Elements characteristics show that rocks emplaced in the Winthin Plate volcanic zone. They derived from an evolved parent magma showing a low degree of partial melting and characteristics closer to a modified and evolved primitive spinel lherzolite.

1. Introduction and Geological Setting

The Beka area is a unit of the Adamawa plateau in Cameroon (Figure 1). It is delineated at its western and northern parts by many mountains namely Tchabal Nganha (1923 m with an average altitude of 1100 m), Tchabal Ngaoundaba (1960 metres), Tchabal Mbabo (2450 metres) and Mount Mambila (2428 metres). Several petrographic, geochemical [1,2], geochronological [3], geophysical [4] and structural [5] studies have been done for the characterization of the Adamaoua plateau. In the structural aspect, the Adamaoua Plateau is made up of a Pan-African metamorphic and plutonic basement bounded to the north by the Adamawa fault and to the south by the << Djérèm and Mbéré >> faults [6]. It is intensely crosscut by a major N70°E fault cluster locally masked by Cenozoic basaltic flows. Studies

**Corresponding Author:*
Pauline Wokwenmendam Nguet,
Research Center for Geophysics and Volcanology, Institute of Geological and Mining Research, PO Box 370 Buea, Cameroon;
Email: nguetpauline@yahoo.fr

DOI: https://doi.org/10.30564/jgr.v3i3.3325

on brittle deformations have been carried out on the northern (Ngaoundéré cliff area) and southern (South-Adamawa trench) edges of the Adamaoua Plateau [6] confirming the Pan-African heritage for the basement.

The southern edge of the Adamawa plateau is affected by the WSW-ENE mylonitic bands extending up to the Foumban area. That structural direction also corresponds in the south (of the plateau) to Pan-African mylonitic faults showing W-E shortening and marked by strike-slip shears and folding. The structure of the plateau corresponds to a horst on the southern edge, whereas the northern part is made up of an escarpment developed during the compressional phase of the Late Cretaceous. The South-Adamawa trench contains important sedimentary evidence of Mesozoic history. However, there are no known Tertiary sediments, as the tectonic reactivation of the trench at this time was accompanied by a general uplift. Other works show that the bedrock of the Adamawa area belongs to the Central African Fold belt and is cut by a N70°E strike-slip fault system [7,8]. It is mainly composed of metamorphic rocks cut by Neoproterozoic granitoids.

The Adamawa Plateau was formed during the Tertiary period and then uplifted up to 1 km from the surrounding areas [9,10]. It is largely covered by huge basaltic and basalto - andesitic volcanic outpourings of mainly Tertiary age, which spill over into the middle part of the southern trough [11]. The plateau is then also presented as a volcanic horst of about 200 km wide, bounded to the north and south, as mentioned above, by Pan-African faults, generally oriented N70 degre.

Depending on several author's work, the volcanism of the Adamawa plateau remains a matter of debate. It either belongs to the Cameroon Volcanic Line (CVL) or rather related to the replay of Pan-African faults, resulting from the reactivation of the N70° E sinistral trans - tensional shear zone, at the onset of the opening of the Central Atlantic Ocean in the Aptian - Albian age [7] and the separation of Africa and South America [12-14]. Indeed, the CVL has a "Y"-shaped distribution of volcanoes, where Adamawa represents the NE branch of the "Y". The dolerite dyke swarms near Biden, 5 km south-east of "Ngaoundéré" [15], Likok, 70 km south-east of "Ngaoundéré" [16] and Mbaoussi, 40 km north-east of "Ngaoundéré", are linked to one or more tectonic events that affected the continental crust of central Africa.

The relationship between the Cameroon Volcanic Line and the Adamawa plateau remains complex. Several hypotheses have been put forward on this subject: the reactivation of the pan-African crust [17], and the orientation of the dyke swarms resulting from the reworked Pan-African fault network of the Adamawa Plateau [7] during Ordovician (450 Ma) and Jurassic episodes; (ii) [18] the opening of the South Atlantic Ocean during the late Jurassic to Cretaceous; (iii) [19] mentioned the development of the Cretaceous Djerem and Mbere basins of northern Cameroon and (iv) [18] the development of the West and Central African rift systems. (v) [20] mentioned that a rapid rotation (20 Ma ago between 8° and 9°) of the African plate would have induced an inflection of the Cameroon Volcanic Line which extends from the Gulf of Guinea and progressively curves from N30°E to N70°E on the Adamawa plateau. (vi) [21] suggests a 7° rotation of the African plate (from a pole in Sudan 80 Ma ago (Santonian)), which would have cut the lithosphere from the Benue trench asthenosphere and moved it to the present geographical location of the Cameroon Volcanic Line. The hypothesis of a gradual shift from N30°E to N70°E is also mentioned [22,23].

Geochemical data on the Adamaoua plateau, consisting essentially of various granitoids, syn- to late tectonic, punctuated by volcanic massifs, have been acquired. Granitoids display negative Nb-Ta and Ti anomalies. They are a calc-alkaline suite with a type I signature, defined by [24]. All the studied granitoids are enriched in Large Ion Lithophile Elements (LILE) compared to High Field Strength Elements (HFSE) [25]. They are believed to be derived from the differentiation of enriched mafic magmas from the subcontinental lithospheric mantle with possible crustal assimilation. The Adamawa plateau basement is intensely dissected by the Pan-African faults (N70° E) [7], which were remobilised during the Albian-Aptian period, exposing numerous types of volcanic rocks: basanite, basalt, hawaiite, mugearite, benmoreite, trachyte, rhyolite, phonolite. The differentiated lavas show peralkaline affinities [16,25,26]. Studies on the dyke swarms of the Adamawa plateau suggest for one of the identified dolerite dykes, a continental tholeiite composition [15] associated with post-PanAfrican extensional magmatism [16]. The chemical characteristics of these rocks have been interpreted as fingerprints of a source with sub-continental lithospheric mantle characteristics as well as E - MORB components that would have been contaminated during an ancient subduction event.

The geochronological information consists of Th-U-Pb monazite, Pb/Pb or U/Pb zircon dates are acquired on the Pan-African granitoids. The latter is composed of Neoproterozoic granites of 615 to 575 ± 27 Ma [5,24,27,28], cutting a late Archean bedrock, remobilized and composed of meta-sedimentary and meta-igneous rocks that have undergone medium to high grade Pan-African metamorphism. The Neoproterozoic ages are either those of the recrystallized domains, or those of the deposition of sediments, or are characteristic of the metamorphism of the Tcholliré region [28]. Available volcano dating assigns ages

 DOI: https://doi.org/10.30564/jgr.v3i3.3325

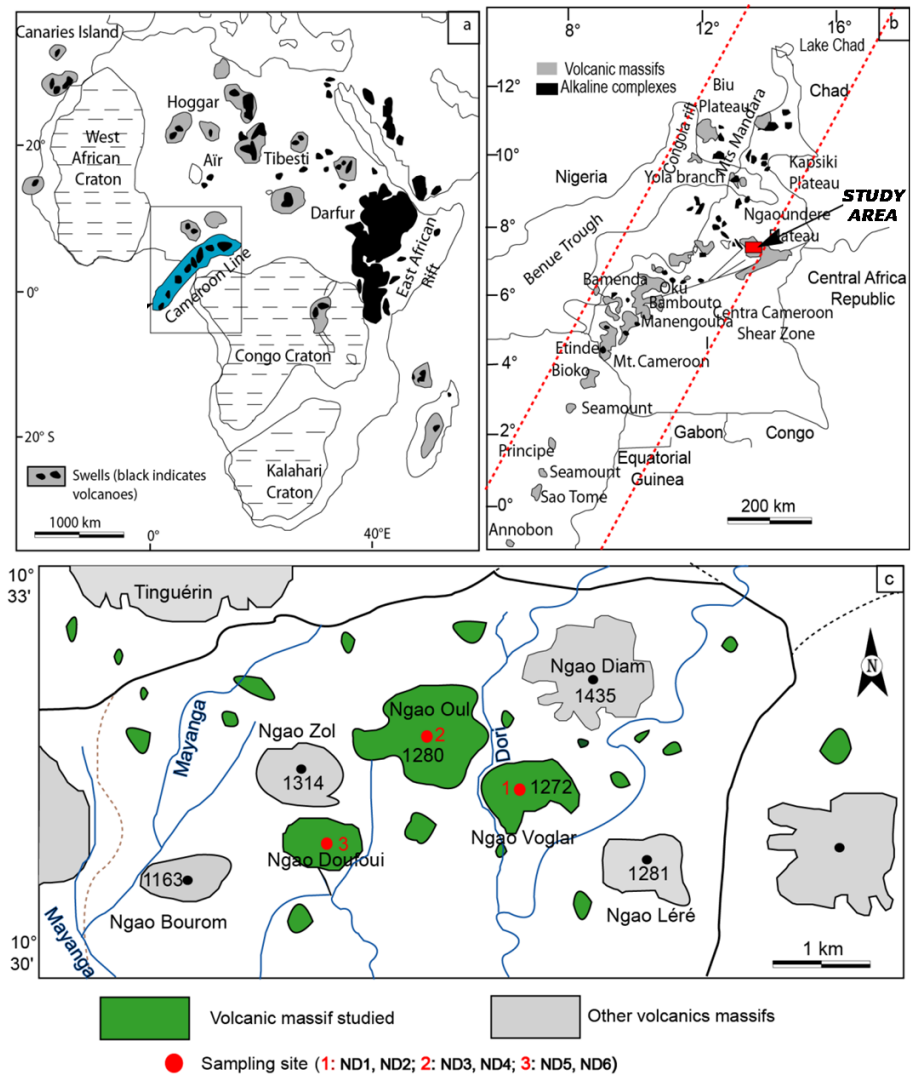

Figure 1: a) Location map of the CVL and the main geological features of Africa. b) Main volcanic centers and alkaline complexes of the CVL from [8] c) Simplified geological map of the study area showing the studied massifs.

of 7-11 Ma (K/Ar method) for the Adamawa lavas [2,25,26,29], and gave probable Mio-Pliocene ages for the Adamawa volcanism.

Geophysical investigations indicate various information on the crust and lithospheric mantle beneath the Adamawa Plateau. According to the gravity data (negative Bouguer anomalies) of [4], and the seismic data of [30], the thickness of the lithosphere beneath the Adamawa plateau is about 80 km. Gravity data suggest a Moho between 18 and 30 km. [22] estimated the depth of the Moho to be 33 km using seismic refraction. According to [31], the Moho discontinuity lies between 33 and 36 km beneath the Adamawa plateau, specifically 33 km beneath the "Ngaoundéré" area. [32] highlighted the isotropic nature of the upper mantle beneath the CVL. The lithosphere - asthenosphere boundary (LAB) is 100 km beneath the CVL, compared to 250 km beneath the Congo craton. The Low Velocity Zone (LVZ) is 200 km below the CVL.

As mentioned above, several research studies have been carried out on the volcanic formations of the Adamawa plateau. In the town of "Ngaoundéré" and its surroundings, effusive flows of alkaline basalts have contributed to the formation of the relief on the plateau [33]. According to the work of [34], the volcanic rocks are derived from the source characterized mainly by spinel lherzolites. The volcanic formations in the vicinity of "Ngaoundéré" have been grouped into three emission series [35,36], and in accordance with the observations of [36] in western Cameroon: (1) the old basaltic series of terminal Cretaceous age [36], (2) the trachytic and phonolitic-dominated intermediate series; (3) the recent basaltic series (south of "Ngaoundéré").

The trachytic and phonolitic dominated series is rep-

DOI: https://doi.org/10.30564/jgr.v3i3.3325

resented by 35 necks, domes and sloped-dome (dome flowed) of differentiated lavas associated with basaltic flows of Mio-Pliocene basalt age (10.0 to 7.0 ± 0.2 Ma), [2,25,33] and differentiated lavas (11.39 ± 0.03 to 9.28 ± 0.03, [7]. Two large strato-volcanoes; Tchabal Nganha [1,3] and Djinga-Tadorgal [37] consist of basaltic, trachytic, phonolitic flows and volcanic breccias, crossed by numerous trachytic and phonolitic necks. One basalt and two trachytes have been dated K - Ar at 7.2 - 7.9 and 7.9 - 9.8 (± 0.2) Ma, respectively [12]. To the west of the Adamawa plateau, the Tchabal Mbabbo massif consists of large basaltic flows accompanied by trachyte necks, phonolite and rhyolitic breccias [26,3]. In the south of "Ngaoundéré", there are numerous recent strombolian cones (0.4 Ma ± 0.2, [2]. The Dibi projections contain plagioclase peridotite nodules [38]. Nodules of garnet peridotites were discovered in the pyroclastic projections of Youkou [39]. The basaltic flows and domes of trachytic and phonolitic composition that outcrop in the Beka region (Figure 3) will be the subject of the present study.

In this study, we present, for the first time, petrographic and geochemical data (major, trace and rare earth elements) of the Beka lavas, located to the North-East of "Ngaoundéré". We acquired these data in order to characterize the petrogenesis and geotectonic setting of the Beka rocks in particular and compare them to that of other lavas from the Cameroon Volcanic Line in general.

2. Analytical Method

Six thin slides were made at the GEOPS Laboratory (Geosciences-Environment Laboratory of the University of Paris Saclay) in France; the whole rock chemical analyses of the representative lavas (major, trace including Rare Earth Elements) were carried out by ICP - AES (Inductively Coupled Plasma - Atomic Emission Spectrometry) and ICP - MS (Inductively Coupled Plasma - Mass Spectrometry) at the ACMEL laboratory in Vancouver, Canada. All the samples were carefully selected and then ground. After each sample, the grinder was systematically cleaned with compressed air. These analyses were carried out on 0.2 g of rock powder and the analytical accuracies varied between 0.04 and 0.1 % for major elements and 0.1 to 0.5 ppm for trace and rare earth elements. The loss on ignition was determined by the weight difference after ignition at 1000 °C.

3. Results

3.1 Outcrops and Field Relationships

Basaltic, trachytic and phonolite outcrops are present in the Beka area (Figure 2). The basaltic lava of Beka occurs in the form of sub-rounded ball of approximately 270 cm diameter at an altitude of 1272 m. At about 30 m from the base of the hill, the basaltic lava consists of centimetre (30 - 80 cm) to metric (0.90 cm - 1.3 m) blocks (Figure 2a). The blocks have rough surfaces with many ten centimetre crystals of pyroxene comparable to coal platelets. The balls display a smooth surface with little crystals of olivine and pyroxene. The last 30 m to the upper part consists entirely of prismatic lavas. In place, slabs of basaltic lava flow have covered the granitic bed rocks.

The trachytic massif of Beka (Figure 2b) is one of the most voluminous trachytic plutons in the study area. It is a sloped-dome (dome flowed) with a length of 300 m and a width of about 150 m. It is located at an altitude of 1280 m at about 110 m above the bedrock. The lava is dark green to dark grey and presents a grayish color when altered. It is covered by a centimeter (1.5 to 5 cm) whitish to light yellow weathering patina. The fresh matrix has a pisolitic-like struc-

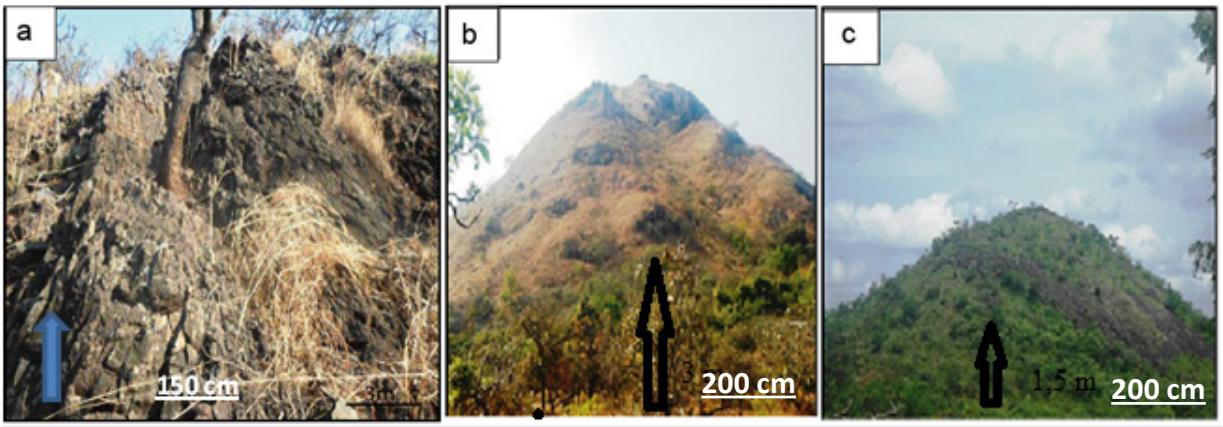

Figure 2. Panoramic view of the Beka lava outcrops, a) prismatic volcanic massif in its upper part; b) trachytic flow dome; c) phonolitic massif.

 DOI: https://doi.org/10.30564/jgr.v3i3.3325

ture characterized by dark concretions consisting of mineral aggregates of variable diameter (0.5 to 1.5 cm).

The Beka phonolite massif is a roughly conical dome with an almost circular base. It rises to an altitude of 1314 m, with a 12 m high above the bedrock and about 300 m diameter. The massif is prismatic, especially on its southern flank. The massif presents steep slopes hosting mechanically degraded prisms showing intense fracturations. The prismatic rock has an anastomosing appearance. The lava has a dark green color and is characterized by the presence of spherical balls of dark grey color, 0.5 to 2 cm in diameter. The phonolite balls present fine grained texture packed by a grey matrix (Figure 2c).

3.2 Petrography

3.2.1 Basalts

The basalts of Beka have in general a microlitic texture. In place it displays porphyritic texture and consist of olivine, clinopyroxene, feldspars and ferro - titanium oxides. Olivine, clinopyroxene and iron - titanium oxides occur as phenocrysts (Figure 3a) and are distributed in a groundmass consisting of microlites of the same minerals. The olivine phenocrysts (0.5 x 0.3 mm, 20% of the volume of the rock) are automorphic to subautomorphic. They are corroded in the rims and sometimes in the cores (Figure 3a). Inclusions of iron-titanium oxides are sometimes observed on phenocrysts. Some olivine crystals show some corrosion gulfs in the cores while others show cracks filled with serpentine alteration product (Figure 3b). Clinopyroxene phenocrysts (1 x 0.4 mm, 25 % by volume of the rock) are automorphic and occur in various shapes (elongated, stocky and sometimes rectangular) (Figure 3a). Some clinopyroxene crystals are strongly cracked and show in the cores and sometimes at their edges some corrosion gulfs in which microcrystals of titanium iron oxides are observed (Figure 3b).

The iron-titanium oxide phenocrysts (0.4 x 0.3 mm) are not abundant in the rock (10 % of volume of the rock). They are associated with olivine and clinopyroxene phenocrysts or occur as inclusion in olivine and clinopyroxene phenocrysts (Figure 3a).The matrix of the studied basalts consists of plagioclase and clinopyroxene microlites and microcrystals of olivine and iron-titanium oxides. No preferential orientation of the microlites is observed.

The iron-titanium oxide microcrystals are relatively abundant (15% by volume of the rock) in the matrix. They are in the form of dotted lines and small dark squares (Figure 3b). Olivine microcrystals are the least represented in the matrix (5% by volume of the rock). They are mostly observed around phenocrysts of the same phase. Plagioclase microlites are the most abundant (20%). They are elongated in the form of small needles for the smallest and small rods of less than 1 mm for the most developed laths. Clinopyroxene microlites (less than 0.5 mm and 5% by volume of the rock) are stocky or in the form of small elongated rods.

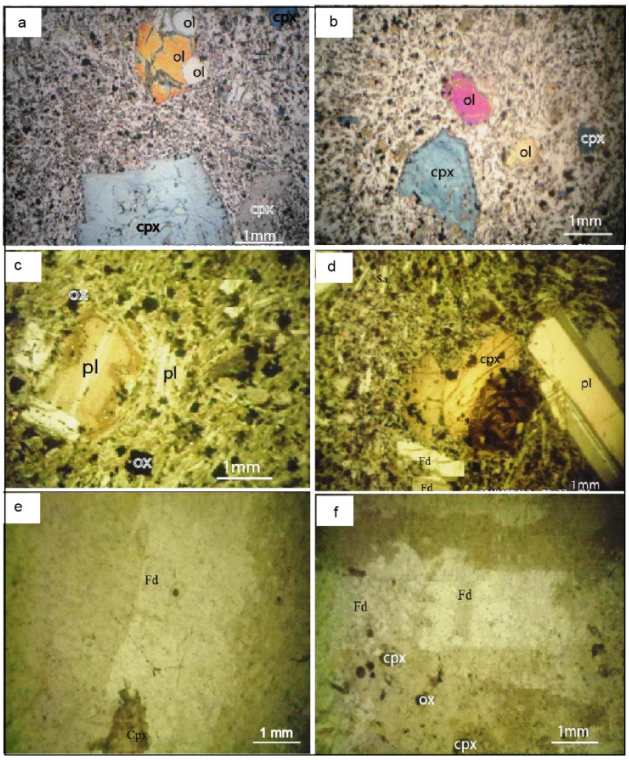

Figure 3. Thin sections microphotographs of representative samples of the Beka study area a) destabilized phenocrysts of olivine in the basalts, b) microlitic porphyitic texture of the basalts, c) destabilized sanidine crystals in its core, d) trachytic texture of the trachytic lavas, e, f) porhyritic texture of the phonolitic lavas. Cpx: clinopyroxene, Pl: plagioclase, Ol: olivine, Ox: oxide.

3.2.2 Trachytes

The trachyte samples have a classical trachytic texture (Figure 3d).They are generally composed of phenocrysts of clinopyroxene, alkali feldspar, plagioclase and iron-titanium oxides. These phenocrysts are distributed in a microlitic matrix composed mainly of plagioclase, clinopyroxene and iron-titanium oxide microcrysts. Alkali feldspar phenocrysts (1.5 x 1 mm,) occur as elongated, automorphic laths. They constitute about 30% of the volume of the rock. They are in place cracked, or resorbed by the matrix. Plagioclase phenocrysts (1.5 x 1 mm, 30% of volume of the rock) are mostly automorphic and others have a xenomorphic appearance. The latter is sometimes corroded in their edg-

DOI: https://doi.org/10.30564/jgr.v3i3.3325

es by mesostasis and contain numerous microcrystals of iron-titanium oxides in these edges (Figure 3b). Clinopyroxene phenocrysts (1.2 x 0.8 mm) occupy about 15 % of volume of the rock. They are automorphic to subautomorphic, cracked and sometimes corroded at the edges by mesostasis. They contain inclusions of iron-titanium oxide crystals and are sometimes completely altered to a brownish product (Figure 3d).

The matrix of the trachytic lavas consists mainly of plagioclase, clinopyroxene and iron-titanium oxide microcrystals. The iron-titanium oxide microcrystals are less than 0.1 mm in size, and occupy about 10% of volume of the rock. They are present in the matrix and or as inclusions in plagioclase phenocrysts (Figure 3c). Alkali feldspar microlites (10%) are the most abundant in the matrix. They occur as small elongated needles or acicular rods. They are in place preferentially oriented (Figure 3d). Clinopyroxene microlites are automorphic and less abundant (5% of volume of the rock).

3.2.3 Phonolites

The phonolite lavas have a classic, porphyritic and microlitic texture (Figure 3f) with more or less hyalloclastic varieties. Alkali feldspar phenocrysts (1.5 x 0.8 mm in size and 25% of volume of the rock) are abundant in phonolites. They are automorphic with a tabular shape and display a cloudy, hazy appearance (Figure 3e). Clinopyroxene phenocrysts (1.3 x 0.8 mm, about 20% of volume of the rock) are automorphic. They are green and are regularly corroded in the cores and sometimes in the rims by matrix. The iron-titanium oxide phenocrysts (1.2 x 0.9 mm, 10% of volume of the rock) are sub-automorphic and often corroded in the cores and rims.

The groundmass of the Beka phonolite consists mainly of alkali feldspar microlites, clinopyroxene and iron-titanium oxide microcrystals. The iron-titanium oxide microcrystals (less than 0.1 mm, about 10% of volume of the rock) are scattered in the matrix and sometimes included in clinopyroxene phenocrysts or placed at the edges of alkali feldspar phenocrysts. Alkali feldspar microlites (less than 0.1 mm) are the most abundant in the matrix (30% of volume of the rock). They are small acicular rods showing a preferential orientation in some places. Clinopyroxene microlites are rare (5% of volume of the rock) and occur as sub-tabular or xenomorphic crystals.

3.3 Geochemistry

3.3.1. Major Elements

The geochemistry of major and trace elements including Rare Earth Elements was carried out on selected samples based on their freshness and representativeness. According to the TAS (Total Alkali vs. Silica) diagram from [40,41], the volcanic rocks of the Beka area are basalts, trachytes and tephri-phonolites (Figure 4, Table 1). These lavas are compared to other alkaline lavas of the LVC (Figure 4), namely those of the Kapsiki Plateau (tephrite basanite and trachyte) [42], Mt Cameroon (tephrite basanite) [43] and the Bamoun Plateau (basalts) [44]. On the SiO_2 - K_2O after [45], all the sample from the Beka area plot within the shoshonitic fields (Figure 4).

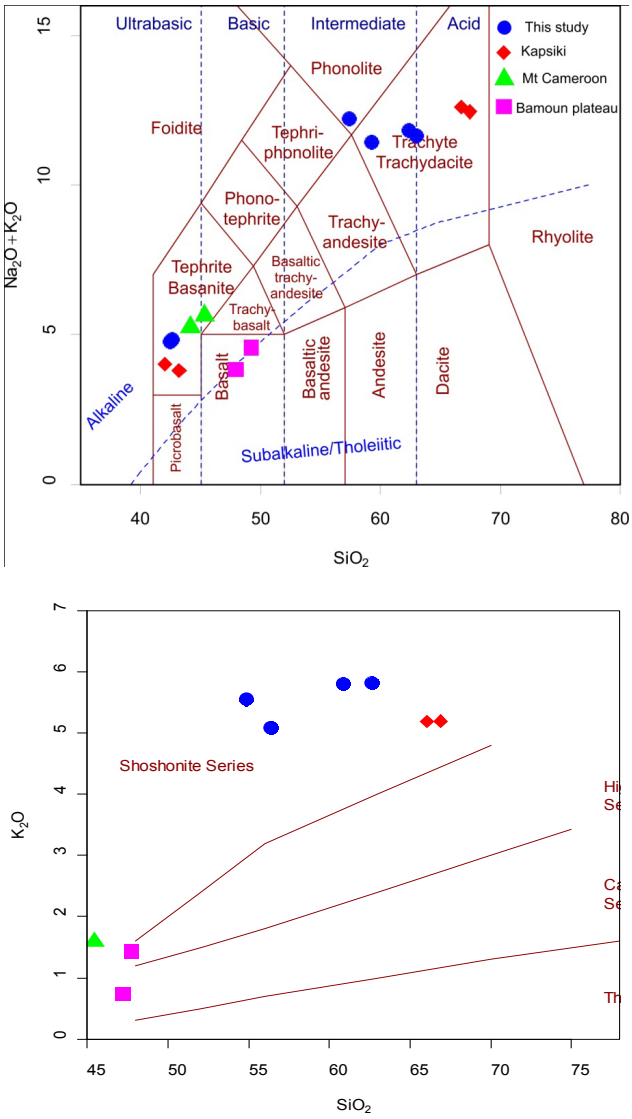

Figure 4. a)Total alkali-silica diagram of the Beka lavas after [40]; the line separating the alkaline - subalkaline domain is from [41]. Datas from the Kapsiki Plateau [42], Mt Cameroon [43] and the Bamoun Plateau [44] are taken for comparison; b) SiO_2 - K_2O diagram after [45]

On the binary diagrams of major elements versus silica, (Figure 5a-c) the Beka samples show positive correlations

DOI: https://doi.org/10.30564/jgr.v3i3.3325

between SiO_2 and K_2O, Na_2O and Al_2O_3 indicating feldspar accumulation. While in (Figure 5d-h), the elements MgO, Fe_2O_3, CaO, TiO_2 and P_2O_5 show negative correlations with SiO_2, thus indicating the fractionation of minerals, such as olivine, clinopyroxene and iron-titanium oxides.

3.3.2. Trace Elements

The trace elements of the Beka lavas are represented in Table 1. The Ni, Co and Cr contents vary respectively from 22.51 to 23.42 ppm; 43.15 to 42.12 ppm and 24.42 to 25.2 ppm in the basalt. Trace element contents are low and are sometimes near the detection limit in the differentiated lavas. In Figure 6d - h, the binary diagrams of Ba, Nd, La, Rb and Zr elements as a function of silica show positive correlations, indicating globally incompatible behaviour throughout the series. The elements Co, Sc, V, Cu, although not represented in this diagram, show positive correlations in the evolved terms, contrary to the basaltic lavas where negative correlations are observed. Their concentration decreases according to the evolution of the silica content (Table 1). These same variations are observed on the Beka lavas as well as on the Kapsiki Plateau, Mont Cameroon and Bamoun Plateau lavas.

The Rare earth spectra normalized to the primitive mantle of [46], are presented in Figure 7. They are characterized by the enrichment in Light Rare Earth Elements contents that reach 90 to 300 times the mantle values (Figure 7). The lowest values of light rare earths are found in basalts. The multi-element spectras of the Beka lavas are normalized to the primitive mantle of [47] (Figure 8). Basalts are characterized by very strong negative anomalies in Sc and slightly in Th and Ta. Slight positive anomalies are observed in Nb, Ba, Sr and Ce in the basalts.

4. Discussion

4.1 Crustal Contamination

In the absence of isotopic analyses, arguments presented for crustal contamination are speculatives. The contamination of the Beka felsic and basaltic lavas is discussed here on the basis of their geochemical characteristics. The interaction

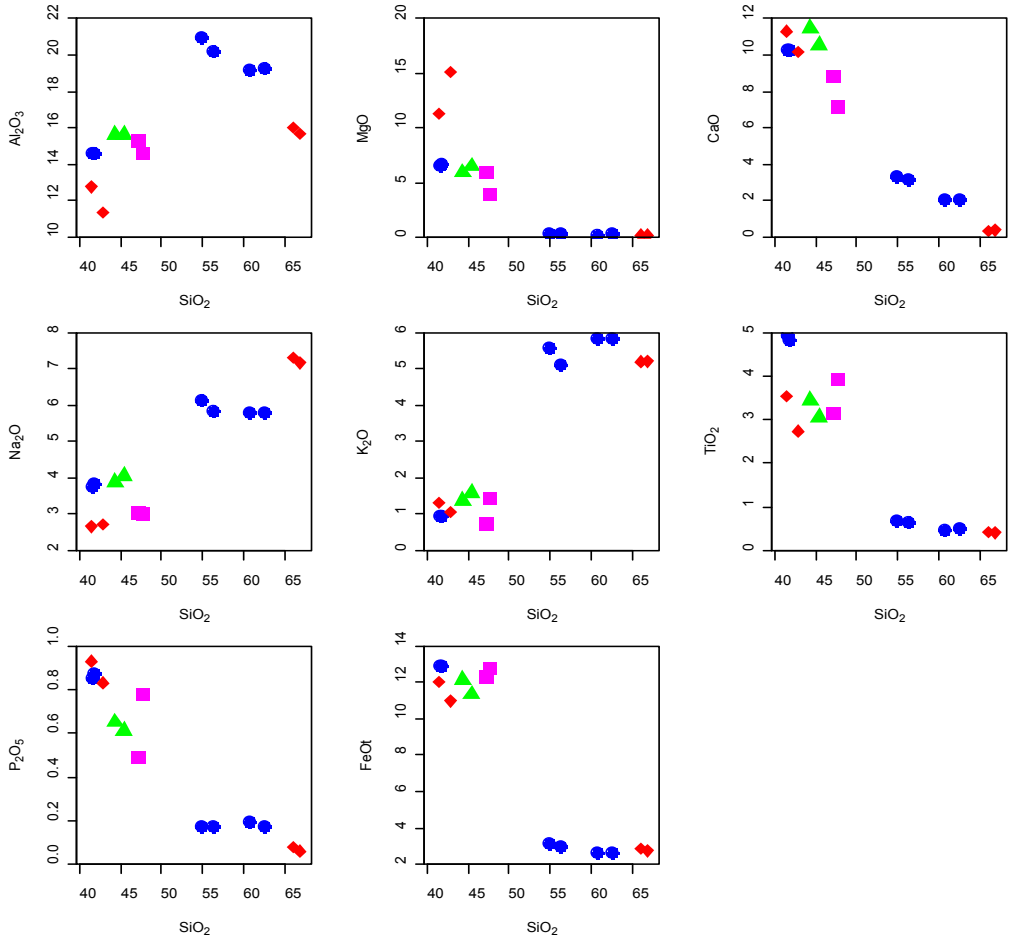

Figure 5. Variation in major element composition as a function of silica (SiO_2).

DOI: https://doi.org/10.30564/jgr.v3i3.3325

Table 1. Geochemical data for representative lavas of the Beka area

Lavas	Basalt		Trachyte		Phonolite	
Samples	**ND1**	**ND2**	**ND3**	**ND4**	**ND5**	**ND6**
Majors elements (%)						
SiO_2	41.57	41.91	62.66	60.87	54.89	56.37
TiO_2	4.9	4.8	0.48	0.47	0.68	0.65
Al_2O_3	14.58	14.59	19.21	19.19	20.9	20.16
Fe_2O_3	14.31	14.33	2.92	2.93	3.49	3.24
MnO	0.2	0.2	0.2	0.19	0.24	0.23
MgO	6.55	6.57	0.21	0.2	0.24	0.25
CaO	10.3	10.25	2.02	2.03	3.28	3.14
Na_2O	3.73	3.81	5.78	5.77	6.13	5.8
K_2O	0.94	0.93	5.82	5.8	5.55	5.09
P_2O_5	0.85	0.87	0.17	0.19	0.17	0.17
LOI	1.79	1.88	1.97	1.98	3.07	4.05
Total	99.72	100.14	101.44	97.64	98.64	99.15
Traces elements (ppm)						
Be	1.89	1.9	94	93	4.9	4.8
Rb	45.2	45.19	203	204	137	138
Sr	967.14	967.1	377	375	1820	1923
Sc	0.44	0.44	1.55	1.6	1.3	1.2
Ba	563.52	563.5	1150	1152	840	841
V	320	319	25	23	27	29
Cr	24.42	26.2	5.3	4.7	0	0
Co	43.15	42.12	2.4	1.8	1.8	1.2
Ni	22.51	23.42	2.5	2	0	0
Cu	31.4	31.39	178	180	10	11
Zn	159.1	158.9	245	244	158	156
Y	32.08	32.07	74.2	74.4	40.1	32.3
Zr	434	435	956	955	820	812
Nb	86.9	86.91	227.2	228	193	196.8
Hf	9.29	9.29	18	19	19.5	18
Ta	5.86	5.86	14.2	15	13.1	12.3
Th	6.12	6.12	22.7	23	22.56	23.9
U	1.776	1.774	3.96	3.88	5.9	4.41
REE (ppm)						
La	53.1	53.06	131.7	131.9	157.5	159
Ce	114.9	114.08	186	187	231	223
Pr	12.83	12.82	40	39.5	23	23
Nd	55.85	55.83	131	132	72	73
Sm	11.36	11.37	8.2	8.3	9.84	8.3
Eu	3.56	3.56	2.88	2.89	2.86	2.73
Gd	9.66	9.67	14.18	14.25	8.07	8.08
Tb	1.31	1.31	0.96	0.98	1.12	1.03
Dy	6.88	6.88	12.6	12.5	6.95	6.96
Ho	1.15	1.16	2.43	2.42	1.5	1.4
Er	2.91	2.91	7	7.01	3.78	3.77
Tm	0.37	0.368	1.07	1.06	0.59	0.58
Yb	2.3	2.29	4.03	4.05	4.8	4.6
Lu	0.34	0.34	1.11	1.09	0.66	0.65

 DOI: https://doi.org/10.30564/jgr.v3i3.3325

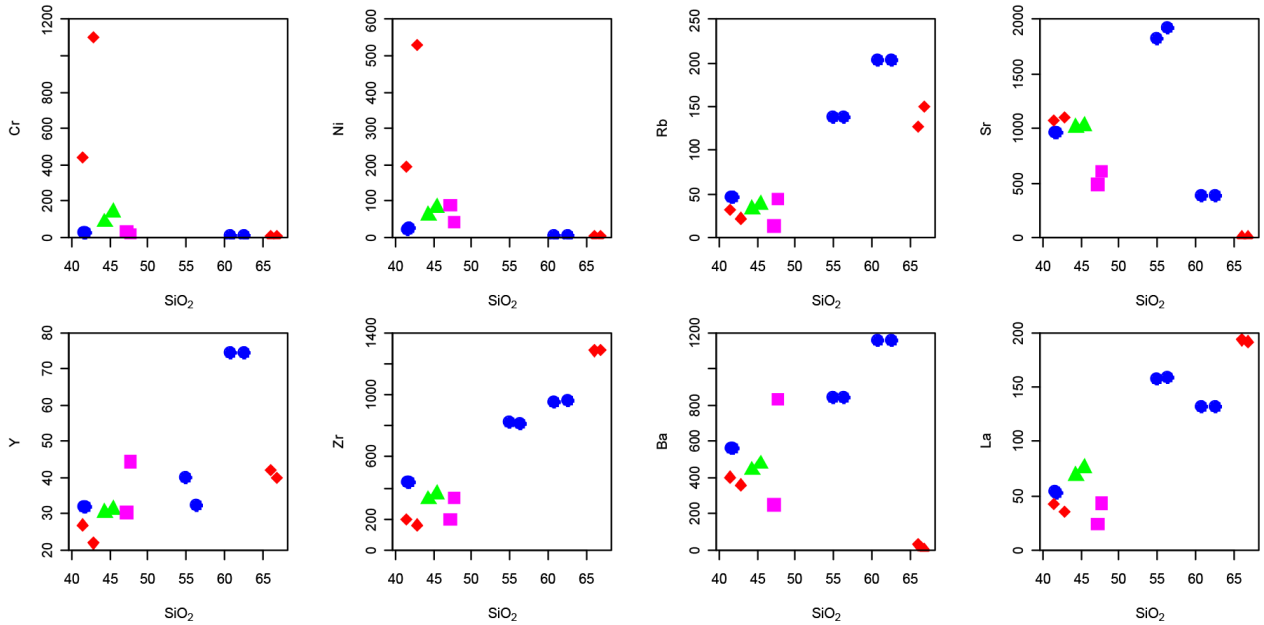

Figure 6. Variation of some trace elements (ppm) as a function of silica (SiO_2) (wt%), and comparison with datas from the Kapsiki Plateau, Mt. Cameroon and Bamoun

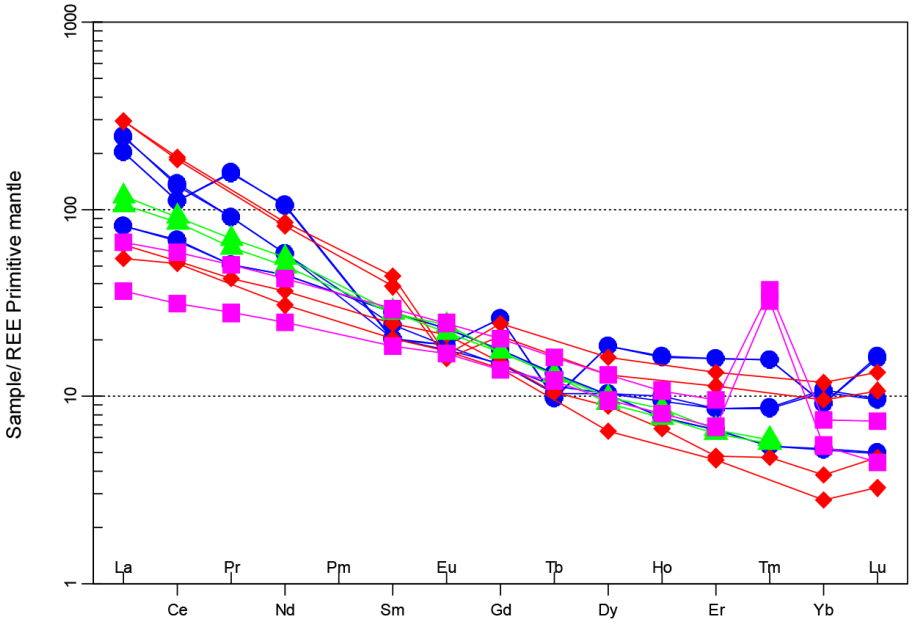

Figure 7. Rare earth spectra of lavas normalized to the primitive mantle [46], and compared to some lavas from Mt. Cameroon, Bamoun Plateau and Kapsiki Plateau.

of the magma with the rocks can modify its composition. The influence of the crustal contamination can be analyzed through major and trace element contents and ratios.

Contamination is sometimes suggested by the presence of basement enclaves and/or other rocks. This was not observed in the Beka formations. The contents of major elements such as SiO_2 and TiO_2 can be used to detect a magma contamination. The high TiO_2 (4.8 - 4.9 %) and the low SiO_2 (41.57 - 41.91 %) contents of the basalts reflect their non-contamination or very negligible degree of contamination. Their TiO_2 contents are close to those of other uncontaminated lavas of the Cameroon Volcanic Line with a mantle origin similar to that of the OIBs [46,47,48,49].

In general, the behaviour of certain trace elements,

DOI: https://doi.org/10.30564/jgr.v3i3.3325

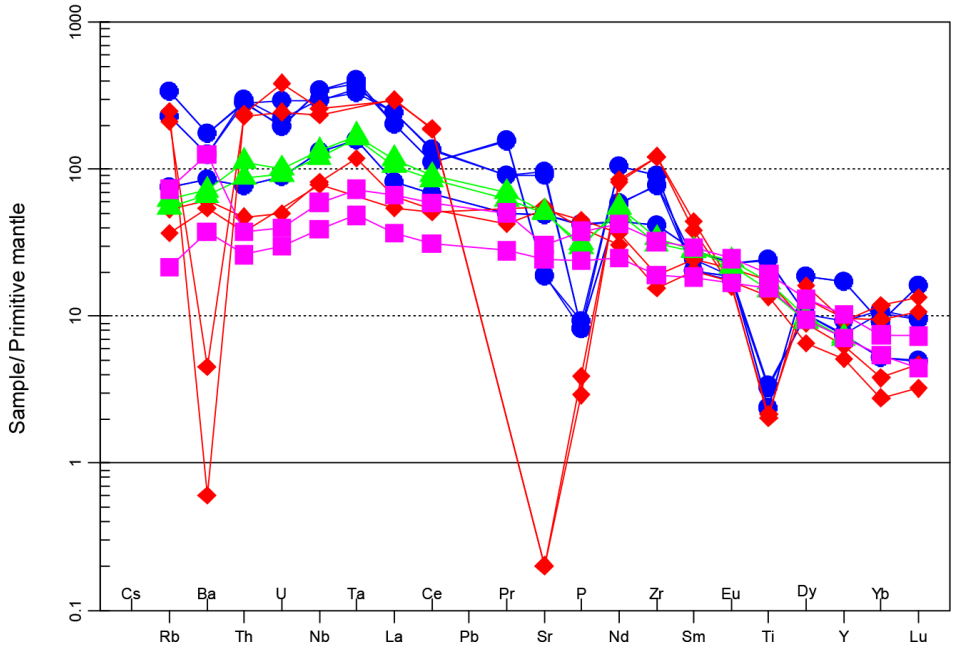

Figure 8. Multi-element spectra of Beka lavas normalized to the primitive mantle [46].

such as Sr, Zr, Ta and Nb are used to test the implication of crustal contamination, [50]. Very often crustally contaminated mafic rocks show significant negative Nb and Zr and positive Sr anomalies on the multi-element diagram [51]. Also high LREE values with flat HREE spectra indicate contamination of the mafic rocks by the crust. The Rare Earth Elements and multi-element spectras show respectively a steep slope and the absence of systematic negative anomalies in Nb and Ta. This leads us to believe that the Beka rocks have not been contaminated, or are contaminated in a negligible way. Basaltic alkaline magmas are often enriched in Nb and then have relatively low Rb/Nb ratio. Crustal rocks and melts derived therefrom on contrary generally have higher Rb/Nb ratios [52]. The Rb/Nb ratio of the Beka rocks is comprised between 0.41 and 1.22, with only one sample showing a ratio >1. This is consistent with the fact that the majority of the Beka rocks are not contaminated by the crust.

On the Nb/Y vs Rb/Y diagram [53,54,55] (Figure 9), several samples of the Beka rocks as well as those of Mount Cameroon, and of the Kapsiki plateau formations are plotted within the field of uncontaminated alkaline basaltic and felsic rocks. The Nb/Y vs Rb/Y diagram of [54,55], shows that melts could be separated into contaminated and uncontaminated groups. The first ones have higher Rb/Y ratios and low Nb/Y values, and the second ones are positively and steeper slope.

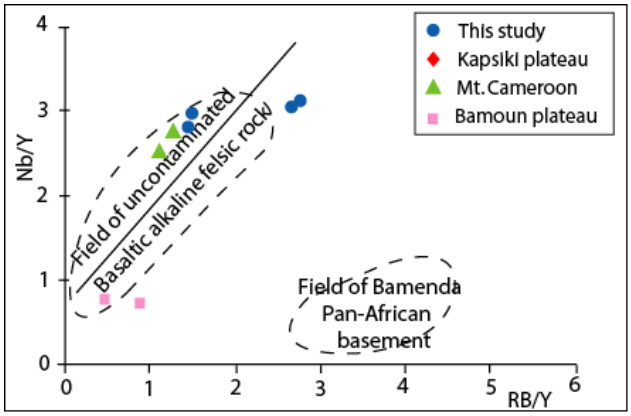

Figure 9. Nb/Y vs Rb/Y plot according to [54,55] used for the studied lavas

4.2 Beka Rocks Emplacement and Magmatic Evolution

The study of the different processes and mechanisms that led to the magmatic differentiation and petrographic diversity gives an idea about the different petrogenetic processes involved in the formation of the rocks. These processes and mechanisms are amount others the fractional crystallization, partial melting, magma mixing or crustal contamination.

4.2.1 Fractional Crystallization

The geochemical analyses of major, trace and rare earth elements in Table 1 show that SiO_2, Al_2O_3, Na_2O and K_2O contents are low in the basalts compared to those of

 DOI: https://doi.org/10.30564/jgr.v3i3.3325

the same oxides in the trachytes and phonolites. On the other hand, TiO_2, Fe_2O_3, MgO, CaO and to a lesser extent P_2O_5 contents are high in basalts compared to felsic lavas. The decrease in TiO_2, MgO, CaO and P_2O_5 reflects the crystallization of iron-titanium oxide minerals, olivine and plagioclase in basalts. The high contents of SiO_2, Al_2O_3, Na_2O and K_2O in the differentiated lavas suggest the accumulation of alkali feldspar crystals in these rocks.

Such a consideration is supported by the high percentages of alkali feldspar crystals in the differentiated lavas. The positive Hf and Zr anomalies could reflect the accumulation of feldspars in the Beka lavas. The trace element data show that the transition element contents of the first series (Co, Ni, Cu and Zn) are low compared to those of the primitive lavas deriving directly from the partial melting of a mantle source [53].

The Beka Basalts may have evolved through the crystallization of olivine crystals, clinopyroxene, plagioclase and iron-titanium oxide crystals from an already evolved parent magma. Such variations underlining an evolution of the parent magma by the process of fractional crystallization are indicated in some other volcanic rocks of the Cameroon Volcanic Line (the lavas of the Kapsiki Plateau, Mount Cameroon and the Bamoun Plateau).

4.2.2 Geotectonic Setting

In Figure 10, two models through the combination of four presumed immobile trace elements (Th, Ta, Y and Hf) are used to determine the geotectonic setting of the Beka rocks. The Th/Ta vs. Y discrimination diagrams of [54,55] and the Th/Hf vs Ta/Hf diagrams of [56] show that the rocks plot in the Within Plate Volcanic Zone fields. This geotectonic framework is consistent with the evolution of the alkaline rocks of the Cameroon Volcanic Line which are intraplate in character. In Figure 10a, all lavas from the Kapsiki, Bamoun and Mount Cameroon plateaus are in the same geotectonic field as the Beka lavas, with the exception of two samples from the Kapsiki Plateau, which are plotted in the Active Continental Margin (ACM) field. This would indicate contamination of the Kapsiki Plateau lavas by the basement rocks. Using the Zr - Ti diagram after [57] and on the Zr - Zr/Y diagram after [58], all the samples (Beka area, Bamoun plateau, Mount Cameroon and Kapsiki) plot in and outside the within plate basalts fields. (Figure 11).

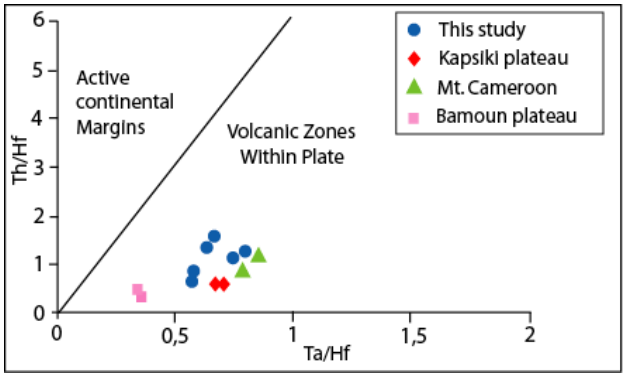

Figure 10. Geotectonic context of the Beka lavas according to Th/Hf vs Ta/Hf diagram of [56].

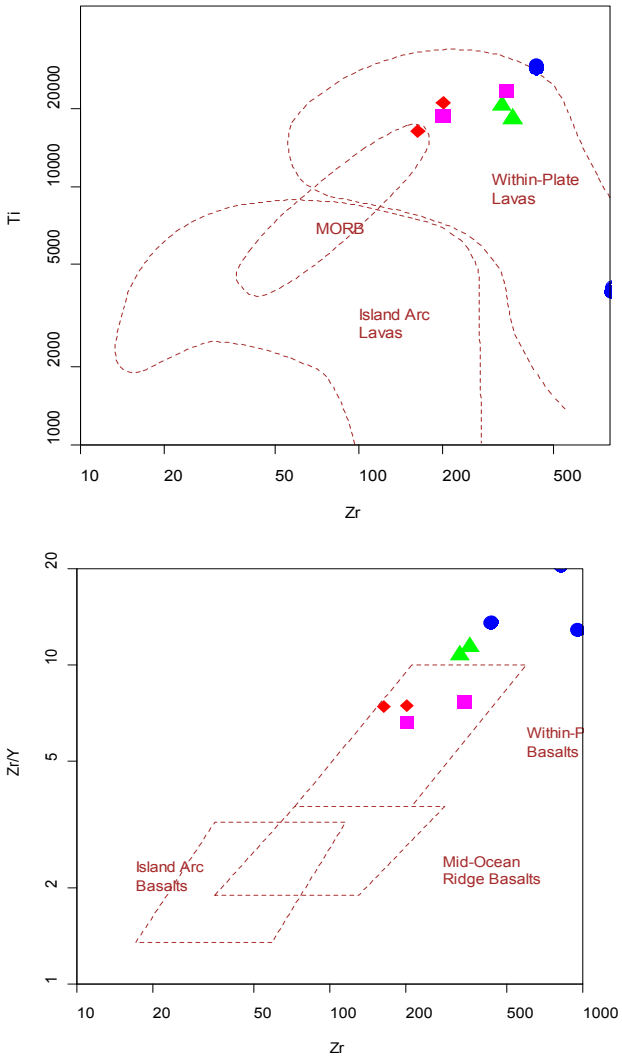

Figure 11. a) Geotectonic context of the Beka lavas according to Ti vs Zr after [57] and **b)** Zr/Y vs Zr diagrams after [58].

4.2.3 Petrogenesis and Origin of Magmas

It is generally known that Large Ion Lithophile Ele-

DOI: https://doi.org/10.30564/jgr.v3i3.3325

ments (LILE) such as Rb, Ba and Cs can be mobile during crustal contamination. They show extreme fractionation between the earth's crust and mantle during magma rising, [58,59]. Zr, Hf, Nb, Ta, Th, Y, P and Ti High Field strength elements (HFSE) are immobile during magmatic processes [59,60]. In addition transition metals (Sc, V, Cr and Ni), HFSE are relatively stables during crustal contamination [61,62]. So, they are usually used to study the petrogenesis of rocks, magma sources and even the tectonic contexts of rocks.

The Major elements of the studied lavas show that they are alkaline to hyperalkaline in nature (Figure 4).

Understanding melting conditions can be obtained through the gradient of REE patterns of rocks [63]. The fusion of a mantle source at low percentage shows a slightly inclined (fractionated) REE patterns, and denote an origin from an enriched mantle source. A higher degree of mantle fusion [64] is compatible with flat REE patterns, showing a depleted mantle source.

In the Beka studied lavas, the Rare Earth Elements are normalized to the primitive mantle [46] and are steeply sloping and characterized by enrichment in Light Rare Earth contents that reach 90 to 300 times the mantle values (Figure 7, Table 1). These values show that the lavas studied resulted from much evolved mantle parental magma [65,66]. The low values for Heavy Rare Earth Element may suggest the presence of garnet residue in the source of the lavas. The REE profiles of the Beka samples are inclined (Figure 10) and may indicate their derivation from a relatively low degree of partial melting from a mantle source. The negative Eu anomalies attest a fractionation of the feldspar (Figure 7).

There is an increase in incompatible elements from Rb to Ta. These high incompatible element contents compared to the compatible one are an argument for a low partial melt rate of the source. The trace element spectra, normalized to the primitive mantle of [46] of the Beka lavas in Figure 10, show correlations with each other. There is a parallelism with the trace element spectra of the Bamoun, Kapsiki and Mount Cameroon lavas. This would indicate a similarity in some of their geochemical characteristics. Contents of compatible elements decrease progressively, indicating that the magma has evolved with the fractionation of minerals rich in Cr and Ni as olivine and clinopyroxene. The low Ni (22-23 ppm) and MgO (6.55-6.57 wt%) contents of the basalts are worthy and reveal the evolved character of their parent magma.

Magmas with intermediate or felsic composition can be formed through several process such as assimilation, fractional crystallization, interaction of felsic and coeval mafic magmas [64]; partial melting of crustal material [67,68]; or partial melting of the metasomatized mantle wedge. The absence of mafic enclaves or mafic-felsic mingling in the study area excludes the hypothesis of interaction of felsic and coeval mafic magmas. Also the geochemical variations of majors and traces (geochemistry section) suggested an evolution of lavas by fractional crystallization from a basaltic magma to trachytic and hyper alkaline phonolitic lavas. [15,24,25] have already shown this kind of differentiation from basalt towards rocks with peralkaline affinities.

The plot of Ta/Yb vs. Th/Yb according to [69] in Figure 12a, shows that the studied samples are placed in the mantle array, in the vicinity of the E-MORB pole for trachytes and basalts, and the sub-continental lithospheric mantle (SCLM) one for the phonolites, suggesting the mantle as their magma source. The source of the Beka phonolitic lavas located around the SCLM, would then be closer to the crust-mantle boundary, which is between 20 and 30 km in the Adamaoua plateau according to [4]. Such results have been evoked in the neighboring area of Beka, by [15,16]. Indeed, these authors interpreted chemical characteristics of their studied rocks as fingerprints of a source with SCLM characteristics as well as E - MORB components that would have been contaminated during an ancient subduction event. The Ce/Y vs Zr/Nb diagram after [70] (Figure 12b) of the partial melting and mantle source melting rates of this work show that the composition of studied lavas is close to mantle spinel lherzolites. But the low Ni and MgO contents of the Basalts lead us to conclude that this "mantle spinel lherzotite" source has undergone a notable modification and evolution. [33] has already evoked mantle spinel lherzotite source for the volcanism of some area in the Ngaoundéré district.

The geochronological data of volcanic products (basalt, trachyte and phonolite) of the present study are not yet available. But it is important to mention the Miocene - Pliocene ages of the neighboring lavas in the NE part of "Ngaoundéré", dated by different authors [2,3,25,26].

5. Conclusions

Beka area is a North East of Ngaoundéré's locality situated in the Adamaoua Plateau of Cameroon in central Africa. Lavas in this area have not been studied before the present work. The volcanism of Beka is characterized by basalt domes, trachyte and phonolite domes and flows. The basaltic lava are blocks which show rough surfaces with visible crystals of olivine and pyroxene. The upper basalt dome is entirely of prismatic lavas. The trachytic massif with an altitude of 1280 m is one of the most voluminous trachytic plutons in the study area. The fresh matrix has a pisolitic - like structure characterized by dark

 DOI: https://doi.org/10.30564/jgr.v3i3.3325

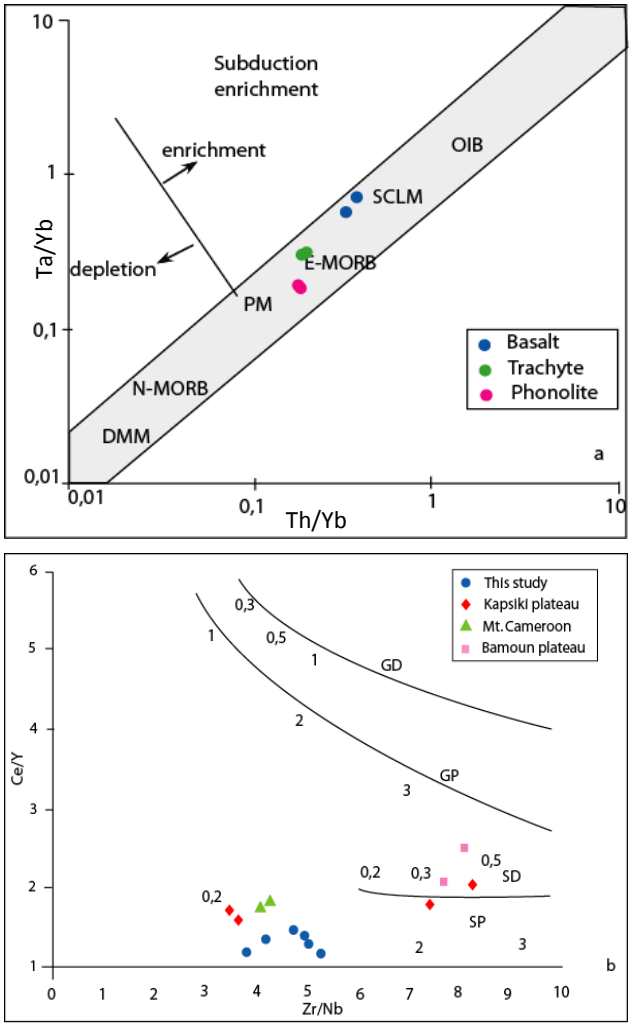

Figure 12. (a) Ta/Yb vs. Th/Yb log-log diagram of [69] for the Beka lavas. Note the placement of samples in mantle array; (b) Ce/Y vs Zr/Nb diagram by [70] of the partial melting and mantle source melting rates applied to studied lavas. GD = depleted garnet lherzolite; GP = Primitive Garnet Lherzolite; SD = depleted spinel lherzolite; SP = primitive spinel lherzolite

concretions consisting of mineral aggregates of variable diameter up to 1.5 cm. The phonolite massif is a roughly conical dome with an almost circular base which rises to an altitude of 1314 m. The massif is prismatic, especially on its southern flank.

Basalts rocks have in general a microlitic texture. In place they display porphyritic texture and consist of olivine, clinopyroxene, feldspars and ferro-titanium oxides minerals. The phenocrysts are distributed in a groundmass consisting of microlites of the same minerals. The trachyte samples have a classical trachytic texture. They are composed of phenocrysts of clinopyroxene, alkali feldspar, plagioclase and iron-titanium oxides. These phenocrysts are distributed in a microlitic matrix composed mainly of plagioclase, clinopyroxene and iron-titanium oxide microcrysts. The phonolite lavas have a classic, porphyritic and microlitic texture with more or less hyalloclastic varieties. Minerals are a mixture of phenocrysts and microcrysts: Phenocrysts are alkali feldspar, clinopyroxene, iron-titanium oxide, the groundmass consists mainly of alkali feldspar microlites, clinopyroxene and iron-titanium oxide microcrystals.

The lavas belong to the same magmatic series, and show an alkaline and probably uncontaminated nature. They have evolved through fractional crystallization from basaltic magma to felsic lavas. Their geotectonic characteristics indicate a "Within Plate Volcanic Zone". The geochemical features show that the studied lavas may derive from evolved parent magma showing a low degree of partial melting of an evolved primitive spinel lherzolite source.

Conflicts of Interest

There is no conflict of interest.

Acknowledgement

The authors would like to thank Professor Jacques Marie Bardintzeff of the Laboratory of Petrography - Volcanology, University of Paris 11, for making the thin sections.

References

[1] Nono, A., Déruelle, B., Demaiffe, D., Kambou, R. Tchabal Nganha volcano in Adamawa (Cameroon): petrology of a continental alkaline lava series. J. Volcano. Geotherm. Res, 1994, 60, 147-178.

[2] Temdjim, R., Njilah, I.K., Kamgang, P., Nkoumbou, C. Données nouvelles sur les laves felsiques de Ngaoundéré (Adamaoua, Ligne du Cameroun): chronologie K─Ar et pétrologie. African Journal of Science and Technology (AJST), Science and Engineering, 2004, 5(2), 113-123.

[3] Fagny, A. M., Nkouandou, O. F., Déruelle, B., Ngounouno, I. Revised petrology and new chronological data on the peralkaline felsic lavas of Ngaoundéré volcanism (Adamawa plateau, Cameroon, Central Africa): evidence of open - system magmatic processes. Analele Stiintificeale Universitatii "Al. I. Cuza" din Iasi Seria Geologie, 2012, 58 (2), 5-22.

[4] Poudjom Djomani Y.H., Diament M., Albouy Y. Mechanical behaviour of the lithosphere beneath the Adamawa Uplift (Cameroon, West Africa) based on gravity data. Journal of African Earth Sciences, 1992, 15 (1), 81-90.

DOI: https://doi.org/10.30564/jgr.v3i3.3325

[5] Ganwa, A.A., Frisch, W., Siebel, W., Ekodeck, G.E., Cosmas, S.K., Ngako, V. Archean inheritances in the pyroxene-amphibole bearing gneiss of the Méiganga area (Central North Cameroon): Geochemical and $^{207}Pb/^{206}Pb$ age imprints. C.R. Géoscience, 2008, 340, 211-222.

[6] Dumont, J.F. Etude structurale des bordures Nord et Sud du plateau de l'Adamaoua: Influence du contexte atlantique. Géodynamique, 1987, 2 (1), 55-68.

[7] Moreau, C., Regnoult, J.M., Déruelle, B., Robineau, B. A new tectonic model for the Cameroon Line, central Africa. Tectonophysics, 1987, 139, 317-334.

[8] Ngako, V., Njonfang, E., Aka, F.T., Affaton, P., Nnange, J.M. The North-South Paleozoic to Quaternary trend of alkaline magmatism from Niger-Nigeria to Cameroon: Complex interaction between hotspots and Precambrian faults. Journal of African Earth Sciences, 2006, 45 (3), 241-256.

[9] Okereke, C.S. Contrasting modes of rifting: the Benue trough and the Cameroon Volcanic Line, West Africa. Tectonophysics, 1987, 775-784.

[10] Nnange, J., Poudjom Djomani, Y. Fairhead, J. and Ebinger C. Determination of the isostatic compensation mechanism of the region of the Adamawa Dome, west central Africa using the admittance technique of gravity data, Afr. J. Sci. Technol., Sci. Eng. Ser., 2001, 1(4), 29-35.

[11] Le Maréchal, A. & Vincent, P.M. Le fossé crétacé du sud Adamaoua (Cameroun). Cahier ORSTOM, Sér. Géol, 1971, 1, 67-83.

[12] Gouhier, J.,Nougier, J., Nougier, D. Contribution to the volcanology study of Cameroon (Cameroon Line-Adamawa). Ann. Fac. Sci. Univ. Yaoundé, Cameroon, 1974, 17, 3-49.

[13] Fitton, J.G., The Benue trough and Cameroon line - A migrating rift system in West Africa. Earth Planet. 537 Sci. Lett., 1980, 51, 132-138. DOI:10.1016/0012-821X(80)90261-7.

[14] Aka, F.T, Nagao, K., Kusakabe, M., Ntepe, N. Cosmogenic helium and neon in mantle xenoliths from the Cameroon Volcanic Line (West Africa): Preliminary observations, Journal of African Earth Sciences, 2009, 55, 175-184.

[15] Vicat J.P, Ngounouno, I., Pouclet, A. Existence de dykes doléritiques anciens à composition de tholéiites continentales au sein de la province alcaline de la ligne du Cameroun. Implication sur le contexte géodynamique. Comptes Rendus de l'Académie des Sciences, Paris. IIA, 2001, 332 (4), 243-249.

[16] Nkouandou O.F., Fagny A.M., Iancu G.O., Bardintzeff J.M. Petrology and geochemistry of doleritic dyke of Likok (Cameroon, Central Africa). Carpathian Journal of Earth and Environmental Sciences, 2015, 10(1), 121-132.

[17] Ashwal, L.D., Burke, K. African lithospheric structure, volcanism, and topography. Earth and Planetary Science Letters, 1989, 96, 8-14.

[18] Fairhead, D., Okereke, C.S. Depth and major density contrast beneath the West-African rift system in Nigeria and Cameroon based on the spectral analysis of gravity data. J. Afr. Earth Sci, 1988, 7(56), 769-777.

[19] Ngangom, E., Etude tectonique du fossé Crétacé de la Mbéré et du Djérem, Sud- Adamawa, Cameroun. Bull. Centr. Rech. Explor. Prod. Elf-Aquitaine, 1983, 7, 339 -347.

[20] Freeth, S.J. Deformation of the African plate as a consequence of membrane stress domains generated by post - Jurassic rift. Earth Planet. Sci. Let., 1979, 45, 93-104.

[21] Fitton, J.G. Active versus passive continental rifting evidence from the West Africa rift system. Tectonophysics, 1983, 94, 473-481.

[22] Stuart, G.W., Fairhead, J.D., Dorbath, L. and Borbath, C. A seismic refraction study of the crustal structure association with the Adamaoua plateau and Garoua rift, Cameroun, West Africa. Geophys. J. R. Astron. Socc., 1985, 81, 1-12.

[23] Browne, S.E., Fairhead, J.D. Gravity study of the Central African Rift System: a model of continental disruption. The Ngaoundéré and Abu Gabra rifts. In: Morgan, P., Baker, B.H. (editors). Processes of planetary rifting. Tectonophysics, 1983, 94, 187 -203.

[24] White, A.J.R, Chappell, B.W., Ultrametamorphism and granitoid genesis. Tectonophysics, 1977, 43:7-22.

[25] Nkouandou, O. F., Ngounouno, I., Déruelle, B., Onhenstetter, D., Montigny, R., Demaiffe, D. Petrology of the Mio-Pliocene Volcanism to the North and East of Ngaoundéré (Adamawa-Cameroon). Comptes Rendus Geoscience, 2008, 340, 28-37. http://dx.doi.org/10.1016/j.crte.2007.10.012.

[26] Fagny, M. A., Nkouandou, O. F., Temdjim, R., Bardintzeff, J. M., Guillou, H., Stumbea, D., Boutaleb, A. New K-Ar ages of Tchabal Mbabo alcaline volcano massif, Cameroun Volcanic Line and Adamawa plateau (Central Africa). International journal of advanced Geosciences, 2016, 4 (2), 62-71. DOI: 10. 14419/ijag.v4i2.6516.

[27] Tchameni, R., Pouclet, A., Penaye, J., Ganwa, A.A., Toteu, S.F. Petrography and geochemistry of the Ngaoundere Pan-African granitoids in Central North Cameroon: implications for their sources and geological setting. J Afr Earth Sci., 2006, 44, 543-560.

[28] Bouyo, H.M., Toteu, S.F., Deloule, E., Penaye, J.,

Van Schmus, W.R. U-Pb and Sm-Nd dating of high - pressure granulites from Tcholliré and Banyo regions: Evidence for a Pan-African granulite facies metamorphism in north - central Cameroon. J. Afr. Earth Sci., 2009, 54, 144-154.

[29] Itiga, Z., Bardintzef, J.M., Wotchoko, P., Wandji, P., Bellon, H. Tchabal Gangdaba massif in the Cameroon Volcanic Line: a bimodal association. Arab. J. Geosci., 2014,7 (11), 4641-4664.

[30] Dorbath, C., Dorbath, L., Fairhead, J.D., Stuart, G.W. A teleseismic delay time study across the Central African Shear Zone in the Adamawa region of Cameroon, West Africa. Geophysical Journal of the Royal Astronomical Society, 1986, 86, 751-766. 23.

[31] Tokam, A.P.K., Tabod, C.T., Nyblade, A.A., Juli, A.J.,Wiens, D.A.,Pasyanos, M.E. Structure of the crust beneath Cameroon, West Africa, from the joint inversion of Rayleigh wave group velocities and receiver functions. Geophys. J. Int., 2010, 183, 1061-1076.

[32] De Plaen, R. S. M., Bastow, I. D., Chambers, E. L., Keir, D., Gallacher, R. J., and Keane, J. The development of magmatism along the Cameroon Volcanic Line: evidence from seismicity and seismic anisotropy. J. Geophys. Res. Solid Earth, 2014, 119. DOI: 10.1002/2013JB010583.

[33] Nkouandou, O.F., Ngounouno,I., Déruelle, B.Géochimie des laves basaltiques récentes des zones Nord et Est de Ngaoundéré (Cameroun, plateau de l'Adamaoua, Afrique centrale) : pétrogenèse et nature de la source. Int. J. Biol. Chem. Sci., 2010, 4, 984-1003.

[34] Nkouandou, O.F., Temjim, R. Petrology of spinell herzolite xenoliths and host basaltic lava from Nga-Voglar volcano, Adamawa Massif (Cameroon Volcanic Line, West Africa): equilibrium conditions and mantle characteristics. Journal of Geosciences, 2011, 56, 375-387.

[35] Guiraudie, C., Carte géologique de reconnaissance à l'échelle de 1/50000, territoire du Cameroun Ngaoundéré Ouest. Sers. Mine Cam., Paris, 1955, 1 carte et notice 23p.

[36] Lasserre, M. Contribution à l'étude géologique de l'Afrique. Etude de la partie orientale de l'Adamaoua (Cameroun Central). Bull. Dir. Mines Geol., 196l, 4, 1-131.

[37] Mbowou, G.I.B., Ngounouno, I., Déruelle, B. Pétrologie du volcanisme bimodal du Djinga Tadorgal (Adamaoua, Cameroun). Rev. Cames -série A, 2010, vol. 11, 36-42.

[38] Girod, M. Le massif volcanique de l'Atakor (Hoggar, Sahara algérien). Etude pétrologique, structurale et volcanologique, 1968, Thèse Doct. d'Etat, Paris, 401p.

[39] Temdjim, R., Contribution à la connaissance du manteau supérieur du Cameroun au travers de l'étude des enclaves ultrabasiques et basiques remontées par les volcans de Youkou (Adamaoua) et de Nyos (Ligne du Cameroun). Thèse de Doctorat d'Etat, Université de Yaoundé1, 2005, 339 p.

[40] LeBas, M.J., LeMaitre, R.W., Streckeisen, A., and Zanettin, B. A chemical classification of volcanic rocks based on the total alkali-silica diagram: Journal of Petrology, 1986, 27, 745-750.

[41] Irvine, T.N., and Baragar, W.R.A. A Guide to the Chemical Classification of the Common Volcanic Rocks. Canadian Journal of Earth Science, 1971, 8, 523-548.

[42] Ngounouno, I., Déruelle, B., Demaiffe, D. Petrology of the bimodal Cenozoic volcanism of the Kapsiki plateau (far northern Cameroon, Central Africa). J. Volcanol. Geothermal Res., 2000, 102, 21-44.

[43] Déruelle, B., Bardintzeff, J.M., Cheminée, J.L., Ngounouno, I., Lissom, J., Nkoumbou, C., Etamé, J., Hell, J.V., Tanyileke, G., N'ni, J., Ateba, B., Ntepe, N., Nono, A., Wandji, P., Fosso, J., Nkouathio, D.G. Eruptions simultanées de basalte alcalin et de hawaiite au Mont Cameroun (28 mars - 17 avril 1999). C R Acad. Sci. Paris, Sciences de la Terre et des planètes / Earth and planetary Sciences, 2000, 33, 525-531.

[44] Atouba, L.C. O., Gilles, C., Moundi, A., Agranier, A., Bellon, H., Nonnotte, P., Nzenti, J. P., Kankeu, B., Mantle sources beneath the Cameroon Volcanic Line: geochemistry and geochronology of the Bamoun plateau mafic rocks. Arab J Geosci., 2016, 9, 270.

[45] Peccerillo, A., and Taylor, S.R. Geochemistry of Eocene Calc - Alkaline Volcanic Rocks from the Kastamonu Area, Northern Turkey. Contributions to Mineralogy and Petrology, 1976, 58, 63-81.

[46] McDonough, W.F., Sun, S.S. The composition of the earth.ChemGeol, 1995, 120, 223-253.

[47] Ngounouno, I., Déruelle, B., Montigny, R., Demaiffe, D. Les camptonites du Mont Cameroun, Afrique. C R Geosciences, 2006, 338, 537-544.

[48] Wandji, P., TsafacK, J.P.F., Bardintzeff, J-M., Nkouathio, D.G., Kagou Dongmo, A., Bellon, h., Guillou, h. Xenoliths of dunites, wehrlites and clinopyroxenite in the basanites from Batoke volcanic cone (Mount Cameroon, Central Africa) : petrogenetic implications. Mineral Petrol., 2009, 96, 81-98.

[49] Kamgang, P., Njonfang, E., Nono, A., Gountie, D.M., Tchoua, F. Petrogenesis of a silicic magma system: geochemical evidence from Bamenda Mountains, NW Cameroon, Cameroon Volcanic Line. Journal of

DOI: https://doi.org/10.30564/jgr.v3i3.3325

African Earth Sciences, 2010, 58, 285-304.

[50] Arndt, T., Czamanske, G.K., Wooden, J.L., Fedorenko, V.A. Mantle and crustal contributions to continental flood volcanism. Tectonophysics, 1993, 223, 39-52.

[51] Zhao, J.X., Mc.Culloch, M.T., Korsch, R.J. Characterisation of a plume-related ≈ 800 a magmatic event and its implications for basin formation in central-southern Australia. Earth and Planetary Science Letters, 1994, 121, 349-367.

[52] Ewart, A., Milner, S.C., Armstrong, R.A., Duncan, A.R. Etendeka volcanism of the Goboboseb Mountains and Messum Igneous Complex, Namibia. Part I: geochemical evidence of Early Cretaceous Tristan plume melts and the role of crustal contamination in the Paraná-Etendeka CFB. Journal of Petrology, 1998, 39, 191-225.

[53] Cain, K., Sun, M., Yuan, C., Zhao, G., Xiao, W., Long, X., Wu, F. Geochronological and geochemical study of mafic dykes from the northwest Chinese Altai: implications for petrogenesis and tectonic evolution. Gondwana Res., 2010, 18:638-652.

[54] Weaver, B.L., Tarney, J. Empirical approach to estimating the composition of the continental crust. Nature, 1984, 310, 575-577.

[55] Cox, K.G., Hawkesworth, C.J. Geochemical stratigraphy of the Deccan Traps at Mahabaleshwar, Western Ghats, India, with implications for open system magmatic processes. Journal of Petrology, 1985, 26, 355-377.

[56] Leeman, W.P., Hawkesworth, C.J. Open magma systems: trace element and isotopic constraints. Journal of Geophysical Research, 1986, 91, 5901-5912.

[57] Pearce, J.A. Trace element characteristics of lavas from destructive plate boundaries. In: Thorpe, R.S. (Ed.), Andesites: Orogenic Andesites and Related Rocks. John Wiley, Chichester, 1982, pp. 525-548.

[58] Pearce, J.A., Norry, M.J. Petrogenetic implications of Ti, Zr, Y, and Nb variations in volcanic rocks. Contr. Mineral. and Petrol., 1979, 69, 33-47.

[59] Green, T.H., Edgar, A.D., Beasley, P., Kiss, E., Ware, N.G. Upper mantle source for some hawaiites, mugearites and benmoreites. Contrib. Mineral., 1974, 48, 33-43.

[60] Gorton, M.P., Schandl, E.S. From continents to island arcs: a geochemical index of tectonic setting for arc-related and within-plate felsic to intermediate volcanic rocks. Canadian Mineralogist, 2000, 38, 1065-1073.

[61] Sun, S.S., McDonough, W.F. Chemical and isotopic systematics of oceanic basalts: implications for mantle composition and processes. In: Saunders AD, Norry MJ (eds) Magmatism in the Ocean Basins, vol 42. Geological Society of Special Publication, London, 1989, pp 313-345.

[62] Staudigel, H., Plank, T., White, B., Schmincke, H.U. Geochemical luxes during sealoor alteration of the basaltic upper oceanic crust: DSDP sites 417 and 418. In: Bebout GE, Scholl SW, Kirby SH, Platt JP (eds) Subduction top to bottom. American Geophysical Union, Washington, DC, 1996, pp 19-38.

[63] Cullers, R.L., Graf, J.L. Rare earth elements in igneous rocks of the continental crust: predominantly basic and ultrabasic rocks. In: Henderson P (ed) Rare earth element geochemistry. Elsevier, Amsterdam, 1984, pp 237-274.

[64] Pearce, J.A. Basalt geochemistry used to investigate past tectonic environments on Cyprus. Tectonophysics, 1975, 25:41-67.

[65] Manikyamba, C., Kerrich, R., Khanna, T.C., Satyanarayanan, M., Krishna, A.K. Depleted arc basalts, with Mg andesites and adakites: a potential paired arc- back-arc oh the GaHutti greenstone terrane, India. Geochim Cosmochim Acta, 2009, 73, 1711-1736.

[66] Pearce, J.A., Cann, J.R. Tectonic setting of basic volcanic rocks determined using trace element analyses. Earth Planet SciLett., 1973, 19, 290-300.

[67] Winchester, J.A, Floyd, P.A. Geochemical magma type discrimination; application to altered and metamorphosed basic igneous rock. Earth Planet Sci. Lett., 1976, 28, 459 -469.

[68] Hirschmann, M.M., Ghiorso, M.S., Wasylenki, L.E., Asimow, P.D., Stolper,E.M. Calculation of peridotite partial melting from thermodynamic models of minerals and melts. I. Method and composition to experiments. J. Petrol., 1998, 39, 1091-1115.

[69] Pearce, J.A. The role of the Sub-continental Lithosphere in Magma Genesis at Active continental Margins. In: Hawkesworth, C.J., Norry, M.J. (Eds.), Continental basalts and mantle xenoliths. Shiva Publications, Nantwich, Cheshire, 1982, pp. 230-249.

[70] Hardarson, B.S., Fitton, J.G. Increased mantle melting beneath snaefellsjokull volcano during Late Pleistocene deglaciation. Nature, 1991, 353, 62-64.

 DOI: https://doi.org/10.30564/jgr.v3i3.3325

BILINGUAL PUBLISHING CO.
Pioneer of Global Academics Since 1984

Journal of Geological Research
http://ojs.bilpublishing.com/index.php/jgr-a

ARTICLE

Structural Exploration of Aeromagnetic Data over Part of Gwagwalada, Abuja for Potential Mineral Targets Using Derivatives Filters

Priscillia Egbelehulu[1*] Abu Mallam[1] Abel U. Osagie[1] Adewumi taiwo[2]

1. Department of Physics, University of Abuja, Abuja, Nigeria
2. Department of Physics, Federal University lafia, Nasarawa, Nigeria

ARTICLE INFO

Article history
Received: 10 August 2021
Accepted: 23 August 2021
Published Online: 25 August 2021

Keywords:
Aeromagnetic
Derivative filters
Faults
Mineralization

ABSTRACT

Aeromagnetic data are consistently used for economic interest targeting and geological mapping. Besides solving problems that are concerned with the basement, the method has become a useful tool in exploring minerals, hydrocarbons occurrence, groundwater investigations, and geothermal potentials. This study analyses aeromagnetic data from the Nigerian Geological Survey Agency acquired at 100 m terrain clearance over a section of Gwagwalada in Abuja. The study area spans longitudes 7.0875° E to 7.1458° E and latitude 8.9625° N to 9.0° N (about 27 km^2). After a reduction to the equator (RTE) transformation, the data is downward continued by 50 m. Different filters are applied to outline area of alteration associated to mineral deposit. Regional geologic structures trend NE - SW. The application of vertical derivatives (FVD and SVD) to the RTE grid enhanced shallow structures which trend NE - SW. Horizontal gradients along the X- and Y- directions enhance geological contacts attributable to blind faults. The Tilt derivative (TD) accentuated fault lines which trend NE - SW.

1. Introduction

Aeromagnetic exploration is often times carried out to investigate the distributions of bedrock lithologies and structures. Magnetic method is one of the oldest of all geophysical exploration techniques. With several innovation and improvements in the designs of field equipment's, it has become feasible to map the crustal sections at different scales. From a high magnetic basement to a weak sedimentary contact either at regional or at local scale [1]. Magnetic method plays an important role in mineral investigation which ranges from structure delineations to detect possible areas of ore deposits, since minerals are structurally controlled. Thus, delineating them plays a key role in the localization of mineralization [6].

Magnetic method responds to ferromagnetic materials and detects metallic objects composed of iron and steel [15]. It is concerned with the estimation of the earth's magnetic field intensity. Despite varieties of rock types available on the Earth crust, majority of them exhibit magnetic properties, either as a result of the present geomagnetic field, or as a result of remnant magnetization obtained in geological past, or combination of them [2]. Aeromagnetic data are consistently used for economic interest targeting and geological mapping [9]. Besides solving problems that are concerned with the basement, the method has become a useful tool in exploring minerals, hydrocarbons occur-

**Corresponding Author:*
Priscillia Egbelehulu,
Department of Physics, University of Abuja, Abuja, Nigeria;
Email: priscilliaegbelehulu@gmail.com

DOI: https://doi.org/10.30564/jgr.v3i3.3540

rence, groundwater investigations, and geothermal potentials [17].

Interpretation of magnetic anomaly pattern leads to geological map productions which gives guidance to exploration procedures [14]. They are also used as tools for reconnaissance survey. Its role has continued to gain relevance in assessing prospective area in recent times as a result of its distinctiveness [4].

Nigeria is furnished with several mineral resources. If duly explored could lead to its industrialization. Countries that are graced with abundant mineral become developed nations [10]. However, a country's greatness is usually the reflection of how her resources are managed [7]. Owing to the fact that Nigeria is endowed with both minerals and manpower competent of harnessing these minerals for industrialization, what is experienced in most cases is that the mineral exploration is usually done by unskilled and unauthorized miners and artesian who uses very crude techniques, lacks the technological know-how and insufficient finance to conduct exploration in a suitable manner. Consequently, they ruin the landscape which in turn affects the environment and its resources such as water, soil and food crops and the health of humans and animals [8]. The scenario is not different from what is obtainable in the study area, as illegal miner and artesian continuously exploits the area Figure 1. Thus the need arises for a research to be carried out to delineate the subsurface structure of the area for proper exploration of mineral. This research work presents the analysis of aeromagnetic data for the intension of recognizing major faults over the study area which is vital in it exploration. Geological information obtained from the data will be a useful guide in the future prospecting.

This work aims at interpreting aeromagnetic data of the study area to delineate the subsurface structures using derivative filters.

Objectives of the study are:

- To identify geologic features such as contact zones, fractures and faults, etc.
- To delineate boundaries of anomalies using derivatives filters.
- To delineate geological structures that might host possible minerals using derivatives filters.

1.1 Location of the Study

The research area is within Abuja, Gwagwalada area council. Bounded by longitude 7°5'15"E and 7°8'45"E and Latitude 8°57'45"N and 9°00'00"N was extracted from aeromagnetic map of sheet 281. The area consists of two broad landforms. These are the medium hill which ranges between 200- 450 m above sea level [11]. Figure 2 and 3 show the location map and topography map respectively. The hills present within the study area are formed by outcropping basement rocks. It has a relatively high temperature with sunshine of the area ranging between 8 - 10 hours daily during the period of January to May. The area records its highest temperature during the dry season at 38 °C. The rain starts by March and ends October [5].

Figure 1. Devastating land scape as a result of artesian mining activities

 DOI: https://doi.org/10.30564/jgr.v3i3.3540

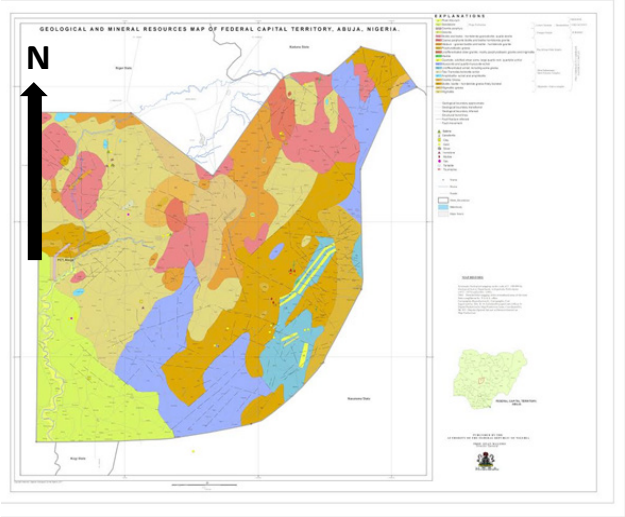

Figure 2. Updated Geological and Mineral Resources Map of FCT (After NGSA, 2017)

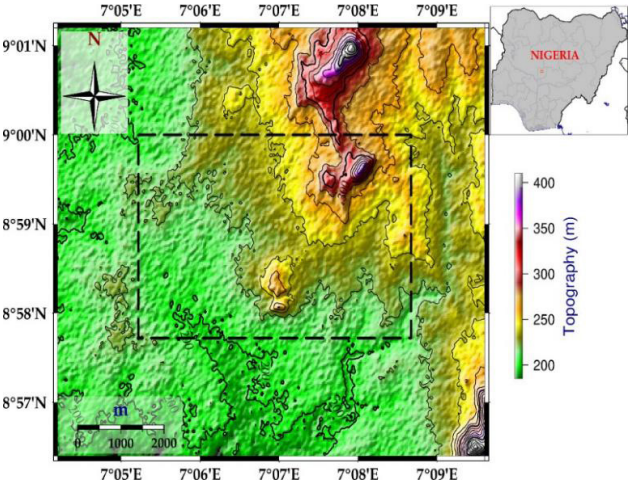

Figure 3. Topography map of study area

2. Geology of the Study Area

Gwagwalada is underlain by the undifferentiated Nigerian basement complex. The region lies within the Precambrian Paleozoic crystalline basement which spans over 50% of the land surface of Nigeria. The basement complex represents the end of two major orogenic cycles [12]. The later of these end products extended from the late Precambrian to lower Paleozoic. They were involved in the extensive remetamorphism and partial mobilization of the underlying basement leading to the development of high grade gnesis, migmatites and older granites. The dominant rock within the study area is banded gneisses. The outcrops are well foliated showing prominent gneissosity with the alternation of bands of mafic and felsic minerals. They are medium-to coarse-grained with large quartz intrusions exploiting joints and weak zones within the rock.

3. Methodology

Aeromagnetic dataset is obtained from Nigerian Geological Survey Agency (NGSA). The surveys were flown having a 100 m flight line spacing and a 500 m tie - line spacing and terrain clearance of 100 m in direction NE-SW, which is perpendicular to the major trend of the geology in the area. The data of the survey were obtained as a total magnetic intensity map.

3.1 Data Processing

Horizontal, vertical, tilt derivative and total horizontal tilt derivative plug was applied over aeromagnetic data of a part of Gwagwalada Abuja to outline area of alteration associated to mineral deposit.

3.2 First and Second Vertical Derivatives

First vertical derivative as well as the second highlight near surface anomalies and is calculated either in the space or frequency domain. They also intensify high-frequency noise. To control this problem, special "tapering" of the frequency response is usually applied. Calculation of the first derivative was initiated by Nabighian in1984, the second derivative filter was used majorly for delineating and estimating depths to the basement which formed the basis of aeromagnetic interpretation [18,3].

3.3 Horizontal Derivatives

Horizontal gradient is usually taken in a particular direction which helps to enhance lateral variation in the magnetic field and diminish its regional trend. This derivate reaches its maximum or minimum value in an area where exhibit a high and contrasting magnetic susceptibility, accentuating discontinuities that are perpendicular to the direction of deviation and revealing clearly faults and edges of the structure. Horizontal gradient is the easiest and simplest way to detect contract location of bodies at depth, having the advantage of minimal sensitivity to noise in the data [13]. M is given as the magnetic field, and the horizontal gradient magnitude (HGM) is thus:

$$HGM = \sqrt{\left(\frac{\partial M}{\partial x}\right)^2 + \left(\frac{\partial M}{\partial y}\right)^2}$$

3.4 Tilt Derivatives

The Tilt derivative is used to determine the boundary of source anomaly. It is used to determine shallow depth as well as deeper depth because of its less sensitivity to

DOI: https://doi.org/10.30564/jgr.v3i3.3540

source depth. Tilt is a function of the ratio of vertical and horizontal derivative of the field's magnetic intensity. However, it does not contain any information of the geomagnetic field strength nor the causative bodies' susceptibility. The peak is located over the center and the zero over the edges of the source.

The total horizontal tilt derivative equalizes signal from near surface and deep seated sources. Its notable feature is it produces amplitude maxima over source edges, gives suitable resolution also is less dependent on the depth of the structures. This application is done basically to reduce the data to a simpler form such that the edges and center of the causative bodies are easily determined. Edge detection of a magnetic structure is one of the most important task in the interpretation of magnetic data [16].

4. Results and Discussion

To delineate the lineaments and structures, the total magnetic intensity (TMI) grid is reduced to the equator (Figure 4) (Figure 5). This ensures that the magnetic anomaly is directly positioned on the body causing them since the direction of magnetization varies. On the RTE map, the magnetic signature is enhanced and trends NE - SW.

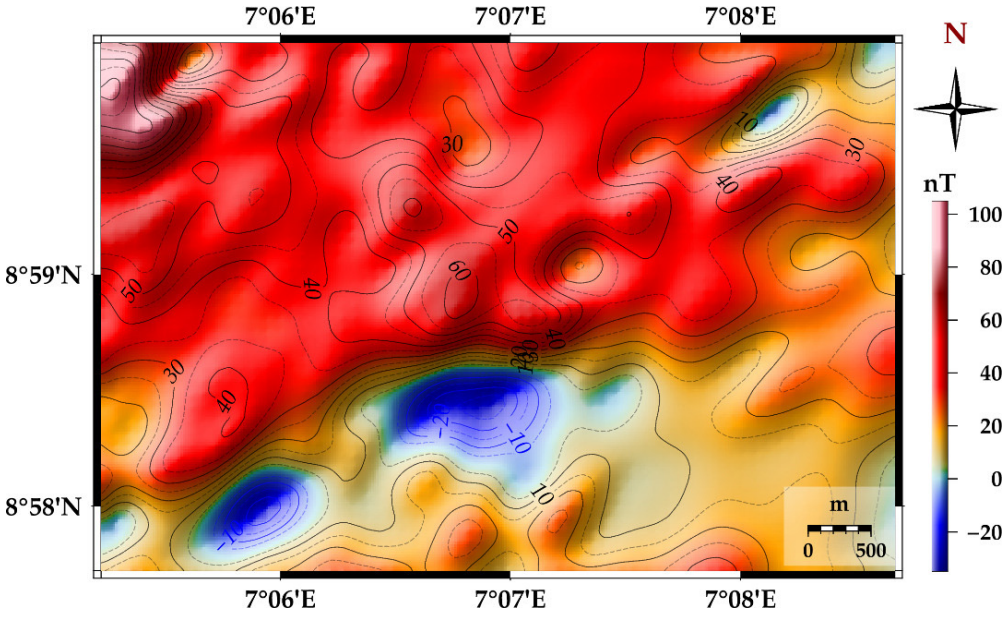

Figure 4. TMI of the study area

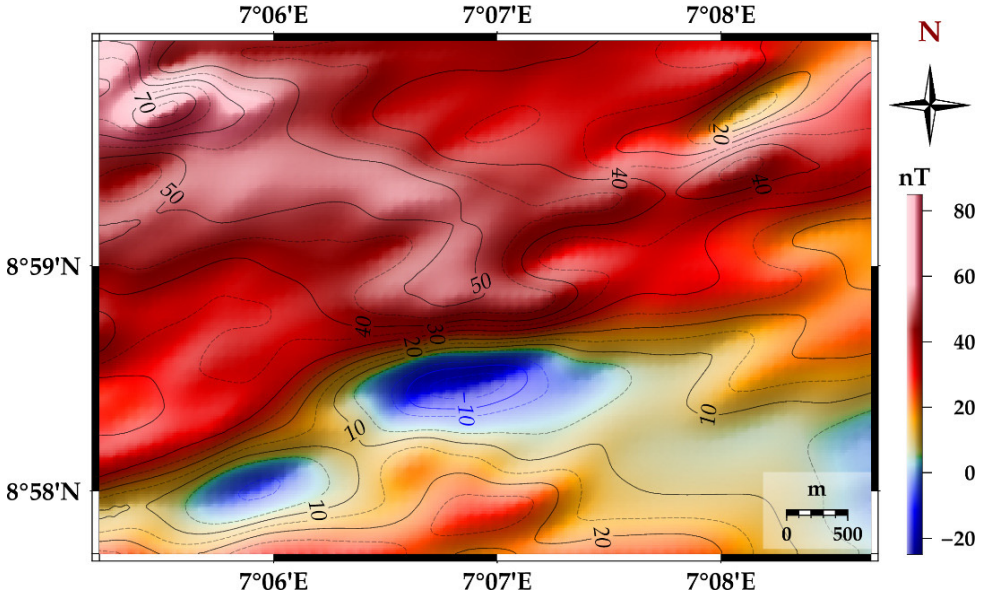

Figure 5. TMI Reduced to Equator

 DOI: https://doi.org/10.30564/jgr.v3i3.3540

Application of the first and second Vertical Derivative for Structural Analysis

The first vertical derivative (FVD) in Figure 6 enhances shallow structures and suppresses the effect of deep-seated geologic bodies. This enhances anomalies over bodies proving a clearer image of the causative structures. The area is marked with magnetic anomaly highs and lows which is attributed to slight variation in depth. High frequency signature noticed at the NE region of the area reveal a near surface depth to magnetic source. This is expected owing to the extrusive landform in the area and typical to Basement complex terrain. The major or predominant structure trend NE-SW. The rock type at the northeastern region is identified as granite gneiss.

The second vertical derivative (SVD) Figure 7 accentuated the structure observed on the FVD. Dominant structures are delineated on the SVD. It accentuates local features and emoves the influence of large anomalies.

The essence of this enhancement is for the zero value to be closely followed by sub-vertical edges of intra-basement blocks of the magnetic data or the edges of basement disturbances or faults. It is particularly helpful in highlighting line noise. The trend of these structures (lineament) correlate with the Pan- Africa structure (lineament) that trends NE - SW.

Interpretation of Structures identified from Horizontal Gradient

Horizontal Gradient (HGRAD) derivative enhances discontinuities such as fault and contact features in the

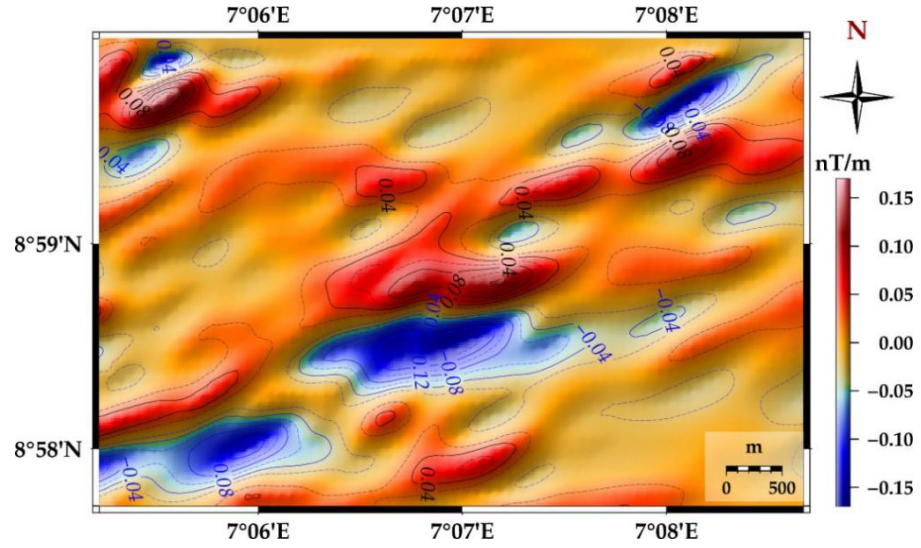

Figure 6. First Vertical Derivative Map

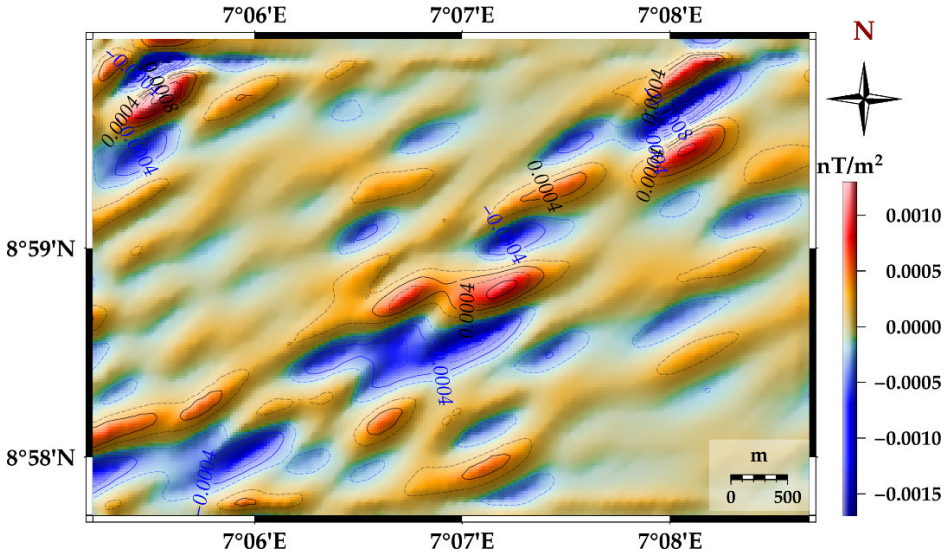

Figure 7. Second Vertical Derivative

DOI: https://doi.org/10.30564/jgr.v3i3.3540

data. It complement to the vertical derivative enhancements. It gives a more exact location for faults than the FVD.

To consider the main fault direction, two maps of horizontal gradient were generated each processed on the RTE map. The first along WE (H_x) direction which highlight the system of faults in the direction of almost NS (Figure 8) with its magnetic intensity. The other enhances the structures in the direction of almost WE (Figure 9) along the direction NS (H_y).

Application of Tilt Derivative and Horizontal Tilt Derivative (TAHG) Analysis and Result

The tilt derivative filter was applied to RTE map to determine the boundary of the source anomaly. Since it is less sensitive to the depth of the source, it was applied to resolve shallow and deep source and to look at faults and contact features Figure 10. The peak of the tilt angle amplitude is located over the center and its zeros over the edges of the source body. Tilt derivatives usually produce

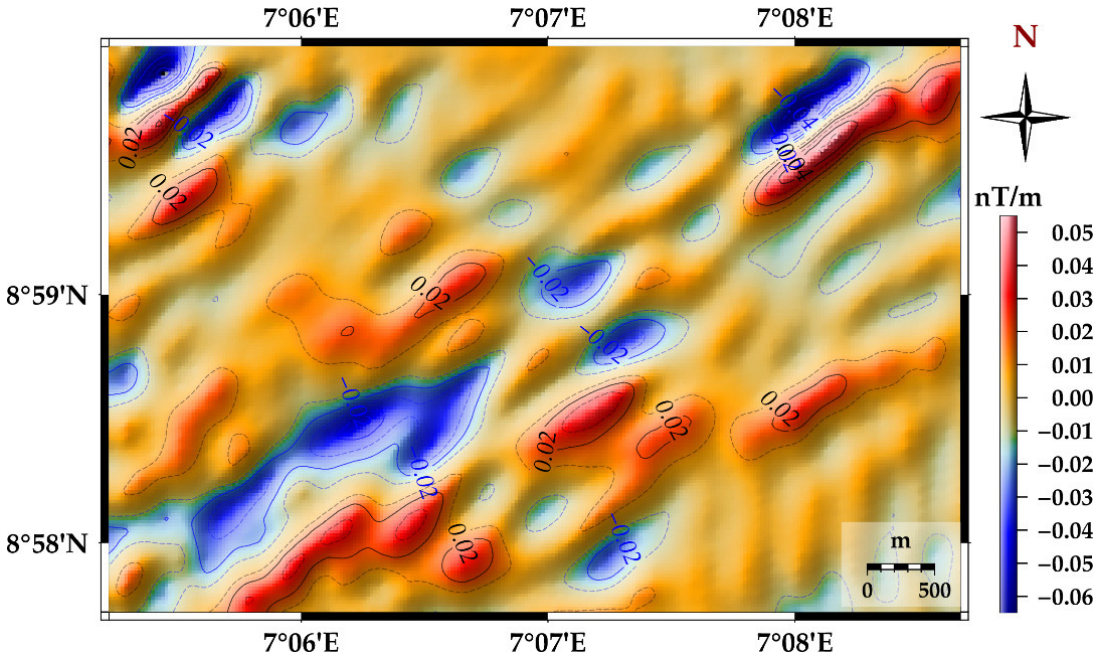

Figure 8. Horizontal Derivative in X-Direction

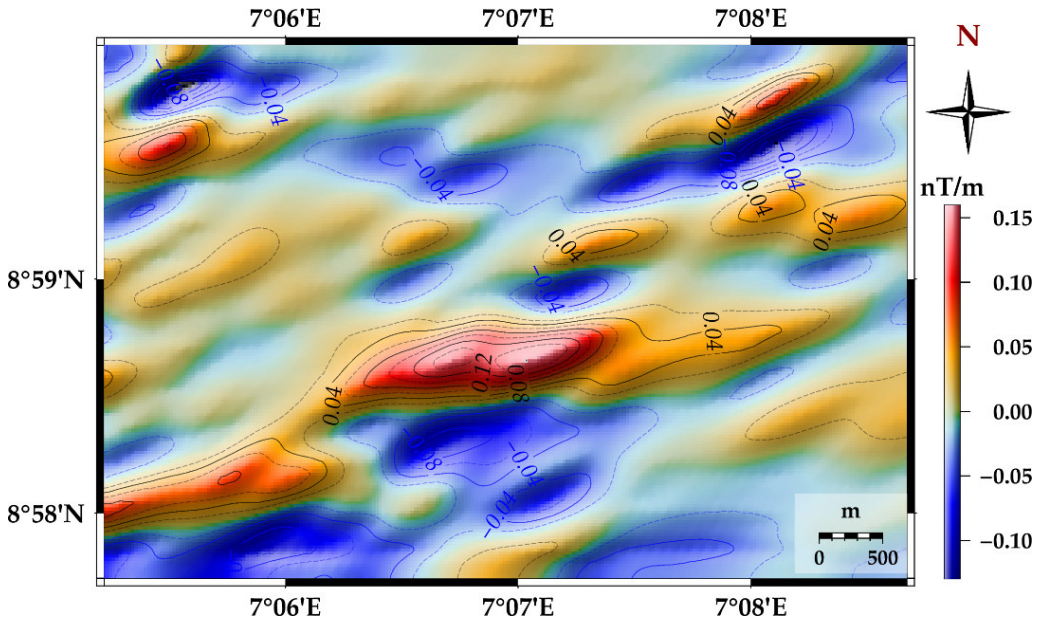

Figure 9. Horizontal Gradient in Y-direction

 DOI: https://doi.org/10.30564/jgr.v3i3.3540

more accurate location for faults than the FVD. The major causative bodies trends from NE- SW. This maximum value of the tilt angle enhances location of the body edges to form a sharp and delicate peak.

The horizontal gradient of tilt (TAHG) applied to the RTE enormalize signals obtained from the shallow and deep seated sources Figure 11. It produces mavxima over the source edges, gives suitable resolution also it is less dependent on the depth of the structures.

5. Conclusions

Analysis from the first vertical derivation (FVD) and second vertical derivative (SVD) showed the enhancement of dominant structure. It enhances shallow structures and suppresses deep-seated geologic bodies. Structures were seen to trend NE- SW. Horizontal gradient were taken at X-direction and Y-direction. This enhanced discontinuities such as faults and contact feature, it compliments results obtained from the vertical derivatives. The Tilt derivative (TD) was used to attain the exact position of fault. TD and TAHG were applied to resolve shallow and deep source and to look at faults and contact feature. The main fault in the study area had the peak of the tilt angle amplitude and could be located within longitude 7°05'00"N, 7°08'30"N and latitude 8°58'00", 8°59'00''. These faults are possible host for mineralization. TAHG showed the edges of the main fault having its peak at the edges.

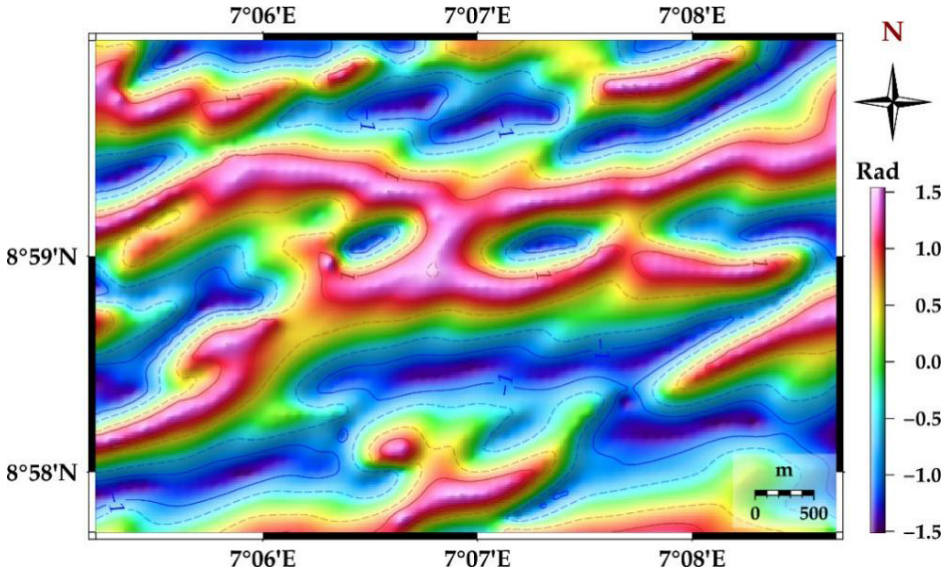

Figure 10. Tilt Derivative of the Study Area

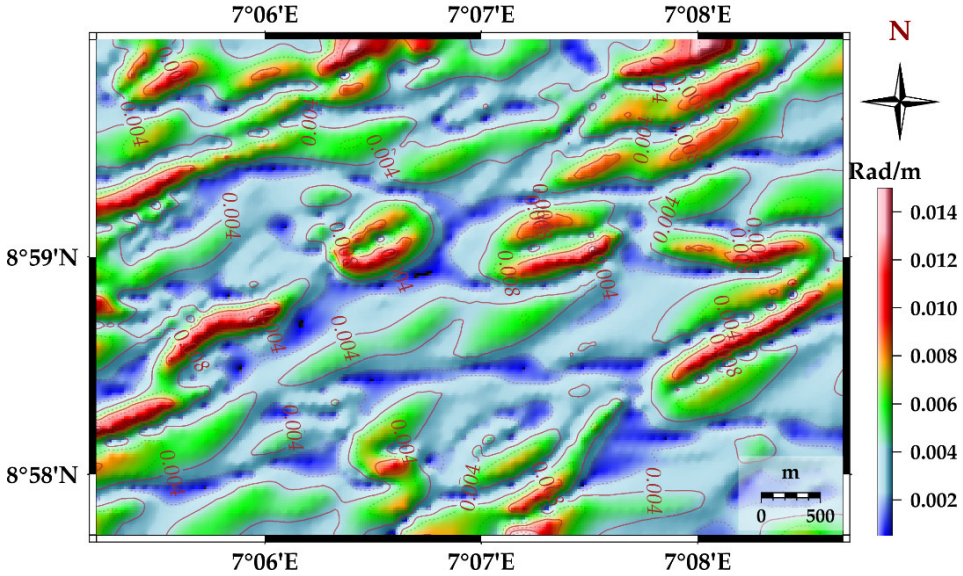

Figure 11. Horizontal Gradient of Tilt Derivative

DOI: https://doi.org/10.30564/jgr.v3i3.3540

References

[1] Adagunodo, T.A., Sunmonu, L.A & Adeniji, A.A. an Overview of Magnetic Method in Mineral Exploration [J]. *Journal of Global Ecology and Environment* (2015), 3(1): 13 - 28.

[2] Adetona, A.A. and Mallam. A. Investigating the Structures within the lower and upper Anambra Basins, Nigeria, Using First Vertical Derivative, Analytical Signal and (CET) Center for Exploration Targeting Plug - in [J]. *Earth Science* (2013), 2(5): 104 - 112.

[3] Andreasen, G.E., and Zietz, I. Magnetic Fields for A 4 X 6 Prismatic Model [J] U. S. Geological Survey Professional Paper 666, (1969).

[4] Barbosa V.C, Silva J.B, Medeiros W.E. Stability analysis and improvement of structural index estimation in Euler deconvolution. Geophysics (1999), 64(1):48-60.

[5] Dawam, P. D. The geography of Abuja federal capital territory (2000). Famous.

[6] Elkhateeb, O.S. Delineation Potential Gold Mineralization Zone in a Part of Central Eastern Desert, Egypt Using Airborne Magnetic and Radiometric data [J]. *NRIAG Journal of Astronomy and Geophysics* (2018)*,* 55 - 70.

[7] Gotan, B.J. Solid Minerals Exploration in Plateau State (Legislation, Difficulties and Framework Involved) [C]. A Paper Presented at A Semina by Nigeria Shippers Council, Jos Nigeria (2004).

[8] Gyang, J.D., Nanle, N. and Chollom, S.G. An Overview of Mineral Resources Development in Nigeria: Problems and Prospects [J]. Continental Journal Sustainable Development (2010), 1, 23 - 31.

[9] Jesperson. A. Aeromagnetic Interpretation of Globe-Miami Copper District, Gila and Pinal Counties, Arizona. Geology Survey Research [R], U.S Geological Survey of Canada, Professional Paper D (1964), 70 - 75.

[10] Okpanachi, U.M. Economics of the Solid Minerals Market [c]. Paper Presented at the Nigeria Shippers Council Seminar on "Solid Mineral Exploration and Exploitation", Jos, Nigeria (2004).

[11] Olugboye, M. O. "Report on the Preliminary Hydrogeological Investigation of FCT Abuja [R]." *Federal Department of water Resources* 4 (1977).

[12] Oyawoye M.O. The geology of the Nigerian Basement Complex—a survey of our present knowledge of them. Journal of Mining Geology and Metal. (1964), 1(2pp87-103):80-91.

[13] Philips, J.D. Processing and Interpretation of Aeromagnetic Data for the Santa Crus Basin - Patahonia Mountains Area South - Central Arizona [R]. U.S Geological Survey Open- file (1998). Arizona 02- 98.

[14] Reeves. C. Aeromagnetic Surveys principles, practice and interpretation. Published by Geosoft (2005), 3 - 5.

[15] Robert, J.H. Application of Magnetic and Electromagnetic Methods to Locate Buried Metal [R]. U.S Department of Interior, U.S Geological Survey, Open - File Report (2003), 03 - 317.

[16] Shahverdi M, Czaderski C, Motavalli M. Iron-based shape memory alloys for prestressed near-surface mounted strengthening of reinforced concrete beams [J]. Construction and Building Materials (2016), 112, 28-38.

[17] Ugwu, S.A., Nwankwo, C.N., Umeanoh, D.C. Investigation of Subsurface Structures for the Evaluation of Hydrocarbon Potential Using Aeromagnetic Data from Mmaku and its Envrons, South - East Nigeria [J]. Journal of Scientific and Engineering Research (2017). 4(9), 152 - 164.

[18] Vacquier, V., Steenland, N.C., Henderson, R.G. and Zietz, I. Interpretation of aeromagnetic maps: Geological Society of America, Memoir (1951), 47.

 DOI: https://doi.org/10.30564/jgr.v3i3.3540

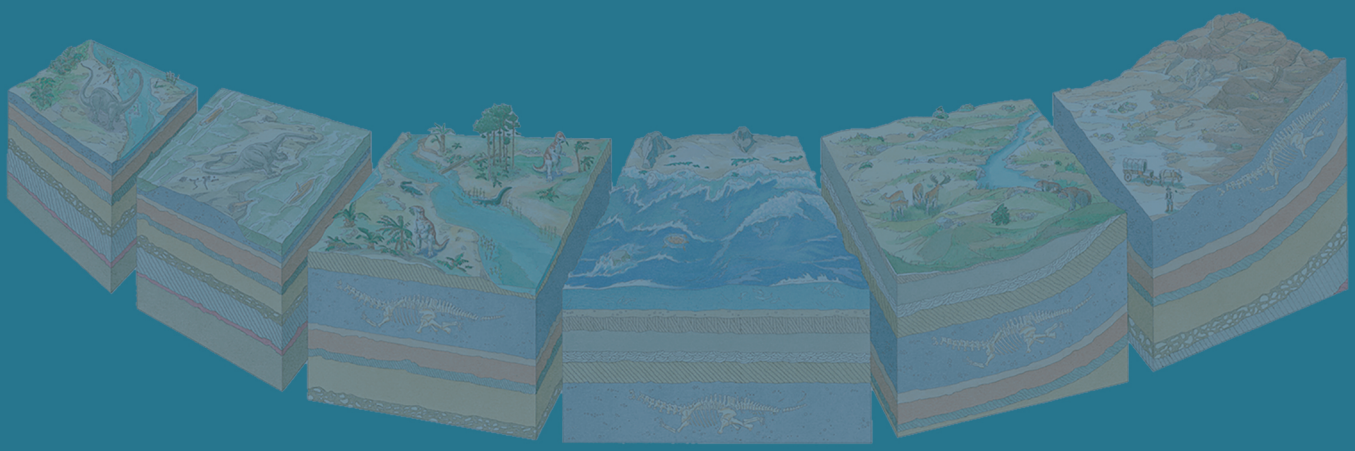

BILINGUAL
PUBLISHING CO.
Pioneer of Global Academics Since 1984

Tel:+65 65881289
E-mail: contact@bilpublishing.com
Website:ojs.bilpublishing.com

ISSN 2630-4961
03
9 772630 496218